

Subcellular trafficking of proteolipid protein (PLP/DM20) and novel mechanisms of ER retention in Pelizaeus-Merzbacher disease

PhD Thesis

in partial fulfilment of the requirements
for the degree “Doctor of Philosophy (PhD)/Dr. rer. nat.”
in the Neuroscience Program
at the Georg August University Göttingen,
Faculty of Biology

submitted by

Ajit Singh Dhaunchak

born in

Chandigarh, India

29. May 2006

DECLARATION

I hereby declare that I prepared the Ph.D. thesis “**Subcellular trafficking of proteolipid protein (PLP/DM20) and novel mechanisms of ER retention in Pelizaeus-Merzbacher disease**” on my own and with no other sources and aids than quoted. I gratefully acknowledge specific help by Dr. Eva-Maria Krämer (standardization of transfection protocols), Mrs. Annette Fahrenholz (immuno-histochemistry of murine spinal cord), Mrs. Gudrun Fricke-Bode (primary oligodendrocyte cultures), and Mrs. Ulli Bode (selection of ES cells). Dr. Hauke Werner contributed equally to the experimental treatment of rumpshaker mice with Turmeric. Two introductory figures were composed of images kindly provided by Christian Humml, Dr. Petra Hirrlinger, Dr. Gesine Saher, Foteini Orfaniotou, Dr. Wiebke Möbius, and Susanne Quintes.

Ajit Singh Dhaunchak

Göttingen, 29. May 2006

ACKNOWLEDGEMENT

I am sincerely grateful to Prof. Klaus-Armin Nave who not only gave me an opportunity to work on such an amazing project under terrific conditions but also granted a high degree of freedom during the work. During these years I have learned a lot from him and I want to learn a lot more.

I am indebted to Prof. Ari Helenius, Prof. Reinhard Jahn and Prof. Harald Neumann for their advice and discussions. I am grateful to entire PLP and friends group, especially Dr. Mikael Simons and Katarina Trajkovic for comments, discussions and support.

I owe many thanks to Dr. Markus H Schwab, Dr. Sandra Goebbels and especially to Dr. Kanwar Vikas Singh Rana who kindled an interest of molecular neurobiology in me and helped me during initial phase of my PhD.

Many thanks to Mrs. Endo Gabriele for always keeping me away from bureaucratic hurdles and creating a friendly atmosphere in the whole department. I would also like to thank the co-ordination team from Neuroscience Graduate Program Dr. Steffen Burkhardt, Dr. Simone Cardoso de Oliviera, Sandra Drube, Dr. Dorothee Wegener and Prof. Michael Hörner for their support in administrative matters during the last four years.

Special thanks to Dr. Johannes Hirrlinger for his expertise in establishing live cell imaging setup in the department. Ulli Bode for her help in a day to day life in the department. I would also like to thank Ingo and an entire CNS myelin group, Hauke, Gesine, Celia, Anke, Susanne, Thorsten and not to mention the warm atmosphere maintained by younger generation PhD students of the north wing including Amit, Schanila, Foteini, Alex and Jan. I am grateful to Patricia and others for taking a close look on my thesis and posters. Many thanks to people who provided with images for composite of two introductory figures, acknowledged in the declaration. I am also grateful to Hajo Horn, Rolf Merker and Markus Born for their help in rescuing me from day to day PC crashes.

I owe special thanks to my dearest friends Neelabh Shankar, Dr. Kanwar Vikas Singh Rana and Anshul Awasthi for always being there for me. I would like to thank my dear friend Rajesh for watching my favourite Hindi movie along for at least fifty times.

My deepest gratitude goes to my loving Parents and to Katja for always being beside me and for their unconditional love and support.

TABLE OF CONTENTS

LIST OF FIGURES.....	VII
1 SUMMARY	1
2 INTRODUCTION	3
2.1 General Introduction.....	4
2.2 Myelin	5
2.3 Human <i>PLP</i> 1 and mouse <i>Plp1</i> gene transcripts	8
2.4 PLP conservation during evolution and topology in myelin membranes	10
2.5 Mutations associated with <i>Plp</i> gene	12
2.6 Sorting of membrane proteins and mechanisms of ER retention	13
2.7 Oligodendrocytes are polarized cells.....	14
2.8 A therapeutic approach toward a mouse model of PMD.....	18
3 MATERIAL AND METHODS.....	19
3.1 Material Used	20
3.1.1 Kits, chemicals and protocol source	20
3.1.2 Solutions and buffers	20
3.1.2.1 Molecular biology buffers.....	20
3.1.2.2 Protein biochemistry buffers	21
3.1.2.3 Immunocytochemistry buffers	24
3.1.3 Bacterial and cell culture media	25
3.1.3.1 LB-Medium.....	25
3.1.3.2 Buffers and media for Cell Culture	26
3.1.4 Bacterial strains and cell lines used	27
3.1.5 Plasmids.....	28
3.1.6 Antibodies and Enzymes	28
3.1.6.1 Antibodies	28
3.1.6.2 Enzyme	29
3.1.7 DNA and Protein Markers	29
3.1.8 Oligonucleotides.....	29
3.2 Methods.....	30
3.2.1 Molecular biological techniques.....	30
3.2.1.1 Maintenance of bacterial glycerol stocks	30
3.2.1.2 Transformation of bacteria	30
3.2.1.3 Plasmid isolation of <i>E. coli</i>	30
3.2.1.4 Enzymatic modification and manipulation of DNA	31
3.2.1.5 Generation of PLP-myc, PLP-EGFP , truncated and myc replacement chimeras	33
3.2.1.6 Site-directed mutagenesis of DNA	34
3.2.1.7 Generation of the PLP-EGFP transgenic “Knock-in” mice.....	37

3.2.2	Protein-biochemical methods	39
3.2.2.1	SDS-poly-acrylamide gel electrophoresis	39
3.2.2.2	Western Blot-analysis	39
3.2.2.3	Lysis of COS-7 and oli-neu cells.....	40
3.2.2.4	Protein biotinylation.....	40
3.2.2.5	Oxidation and reduction assay	40
3.2.2.6	Co-immunoprecipitation	41
3.2.2.7	S35 labeling of proteins and radioimmunoassay	41
3.2.3	Cell culture	41
3.2.3.1	COS-7 and OLN93 cell culture.....	41
3.2.3.2	Oli-neu cell culture.....	42
3.2.3.3	Hybridoma cell culture.....	42
3.2.3.4	Transient transfection of COS-7 and oli-neu cells.....	42
3.2.3.5	Stable transfection of oli-neu cells	43
3.2.4	Immunocytochemistry	43
3.2.4.1	Immunocytochemistry of living cells.....	43
3.2.4.2	Immunocytochemistry of fixed cells.....	43
3.2.5	Confocal analysis.....	44
4	RESULTS	45
4.1	Cysteine mediated cross links cause Pelizaeus-Merzbacher Disease	46
4.1.1	Video microscopy of EGFP-tagged PLP in oligodendrocytes.....	47
4.1.2	Trafficking differences between mutant PLP and DM20 isoforms	50
4.1.3	The role of disulfide bridges in PLP folding	54
4.1.4	Genetic uncoupling of protein misfolding and ER retention	56
4.1.5	ER retention of mutant PLP/DM20 and its rescue by removal of cysteines.....	58
4.1.6	Misfolded PLP forms abnormal dimers and unspecific aggregates.....	63
4.1.7	ER retention of PLP/DM20 chimeras can be rescued by removal of cysteines.....	67
4.2	Quality control of transmembrane domain assembly in PLP	70
4.2.1	Spastic Paraplegia 2 (SPG2) a mild form of PMD	71
4.2.2	Truncated PLP transmembranes are retained in the ER	71
4.2.3	N or C termini deletions did not alter PLP localization.....	73
4.2.4	Perturbations proximal to TM3 retain both PLP and DM20 in the ER	74
4.2.5	Self assembly of transmembrane domains.....	74
4.2.6	Truncated transmembranes associate with calnexin	75
4.3	Conformation sensitive and compartment specific epitope: evidence that PLP matures within the ER.....	78
4.3.1	Wildtype PLP masks 3F4 epitope during its exit from ER.....	79
4.3.2	Adult CNS myelin presents a complete overlapping avidity to 3F4 and A431	82
4.3.3	A novel 16kDa PLP proteolytic cleavage product.....	84
4.4	From transfected oligodendrocytes to PLP-EGFP expressing transgenic “knock-in” mice.....	86

4.4.1	PLP accumulates in endosomes/lysosomes (E/L).....	87
4.4.2	Association of PLP with cholesterol.....	87
4.4.3	Directed trafficking of rapidly moving PLP-EGFP ⁺ endo/lysosomes in primary oligodendrocytes.....	89
4.4.4	Generation of an <i>in vivo</i> tool to study myelination, demyelination and remyelination	94
4.5	A therapeutic approach towards a mouse model of Pelizaeus-Merzbacher disease; treatment of rumpshaker mice with Turmeric	96
4.5.1	Curcumin is an active constituent of Turmeric.....	97
4.5.2	Curcumin treatment of stable cell line expressing PLP ^{msd} -EGFP	97
4.5.3	Treatment of rumpshaker mice with Turmeric	98
5	DISCUSSION.....	100
5.1	Quality Control of Polytopic Membrane Proteins.....	101
5.1.1	Luminal quality control in PLP/DM20 trafficking: an implication to various membrane/secretory protein related diseases.....	101
5.1.2	Self assembly of PLP/DM20 tetraspans	105
5.2	Conformation sensitive epitope of PLP and polarized oligodendrocytes.....	107
5.2.1	3F4 and 010 label mutually exclusive compartments of premyelinating oligodendrocytes ..	107
5.2.2	Oligodendrocytes are polarized cells.....	108
5.3	Treatment of Rumpshaker mice with Turmeric.....	110
6	REFERENCES.....	111
Appendix A: Abbreviations.....		121
Appendix B: Publications.....		123

LIST OF FIGURES

Figure 1: Cells of the central nervous system.....	4
Figure 2: Myelin ultrastructure and major myelin proteins.....	6
Figure 3: Nodal, paranodal, juxtaparanodal and internodal organization in CNS and PNS.....	7
Figure 4: Topology of PLP/DM20 in myelin membranes.....	9
Figure 5: Conservation of PLP among different species.....	11
Figure 6: Protein sorting and domain organization in polarized cells.....	15
Figure 7: Structure of PLP/DM20 and mutations associated with Pelizaeus-Merzbacher disease.....	48
Figure 8: Subcellular distribution of PLP ^{wt} and PLP ^{msd} fused to EGFP, in oli-neu cells.....	49
Figure 9: ER retention in oli-neu cells distinguishes PMD-associated isoforms of PLP, DM20, and chimeras.....	51
Figure 10: Kyte and Doolittle hydrophathy plot of PLP, DM20 and DM20 ^{LSAT-HPDK}	53
Figure 11: Length and position of TM3 determine ER retention or release of mutant DM20.....	54
Figure 12: The function of extracellular disulfide-bridges in PLP folding and cell surface expression.....	55
Figure 13: PLP cysteine mutants that reach the cell surface also accumulate in endo/lysosomes.....	57
Figure 14: Uncoupling of protein folding, ER exit, and the wild-type conformation of PLP.....	58
Figure 15: Unpaired Cys ²⁰⁰ causes ER retention and dimerization of a PMD mutant PLP ^{C219Y}	59
Figure 16: PMD-causing PLP mutations can be rescued by the replacement of cysteines.....	62
Figure 17: PMD-causing PLP mutations rescued by the replacement of cysteines.....	63
Figure 18: Cysteine-mediated PLP crosslinks.....	64
Figure 19: Cysteine-mediated PLP crosslinks in COS-7 cells.....	66
Figure 20: ER lectins associate with mutant and wt PLP with a same affinity.....	67
Figure 21: Outer disulfide bond governs the local and global folding of PLP/DM20 chimera.....	68
Figure 22: All truncated PLPs are retained in the ER, when expressed individually.....	72
Figure 23: Neither N and C termini nor IC2 but TM assembly monitors surface expression of PLP.....	73
Figure 24: Prerequisite for an exit from the ER is proper alignment and masking of TMs in the bilayer.....	76
Figure 25: Truncated PLPs associate with calnexin with an equal affinity.....	77
Figure 26: Oligomeric PLP masks 3F4 epitope at the cell surface.....	80
Figure 27: Maturation of PLP completes in pre-myelin E/Ls whereas PLP ^{C00,219S} matures at the cell surface.....	81

Figure 28: Identical avidity of 3F4 and A431 antibody towards MDL and IPL embedded PLP epitopes	83
Figure 29: A novel 16kDa myelin PLP proteolytic cleavage product.....	84
Figure 30: Association of PLP with cholesterol.....	88
Figure 31: Co-immunoprecipitation from oli-neu stably expressing PLP ^{wt} -EGFP and PLP ^{msd} -EGFP	89
Figure 32: cAMP treatment induces process outgrowth and redistributes PLP to the cell surface	90
Figure 33: Highly mobile and directed endo/lysosomes in primary oligodendrocytes.....	92
Figure 34: Strategy for targeted homologous recombination of <i>Plp</i> gene in mouse ES cells.....	95
Figure 35: Treatment of PLP ^{msd} -EGFP expressing cells with curcumin	98
Figure 36: Survival of rumpshaker mice treated with turmeric.....	99
Figure 37: Proposed mechanism of ER retention.....	102

1 SUMMARY

Missense mutations that predict the misfolding of membrane proteins have been associated with a number of neurogenetic diseases. However, it is not known how apparently minor changes in the amino acid sequence of an extracellular loop or a transmembrane domain lead to complete ER retention with complex loss- and gain-of-function effects. I have chosen PLP/DM20, a highly conserved and abundant tetraspan myelin protein, associated with Pelizaeus-Merzbacher disease (PMD), as a model system. By expressing wildtype and mutant PLP isoforms in glial cells, surprising molecular properties became apparent, including the ability to self-assemble from two truncated PLP polypeptides, and to form conformation sensitive epitope that become masked as the protein matures in the ER. With respect to human disease, it was possible to identify a novel molecular mechanism by which missense mutations cause ER retention of misfolded PLP. Unexpectedly, pairs of cysteines within an extracellular loop of PLP/DM20 play a critical role. Multiple disease-causing mutations require the presence of cysteines such that misfolded PLP/DM20 is efficiently retained in the ER. Replacing cysteines by serine completely prevents ER retention and restores normal trafficking of mutant PLP/DM20. This demonstrates a novel pathological mechanism by which missense mutations greatly reduce the efficiency of intramolecular disulfide bridging. When exposed by misfolding to the ER lumen, unpaired cysteines engage in alternative oxidations that lead to abnormal intermolecular crosslinks. Since extracellular cysteines are a feature of many membrane proteins, this novel pathomechanism is likely to contribute to a diverse group of genetic diseases. To monitor the expression and subcellular trafficking of PLP *in vivo*, a transgenic “knock-in” mouse is being generated that will express a PLP-EGFP fusion protein under control of the endogenous promoter.

In an attempt to develop a cure for Pelizaeus-Merzbacher disease (PMD), we treated a genuine animal model (rumpshaker mice) with Turmeric. The active constituent of this herbal drug (Curcumin) is a non-toxic Ca^{2+} -adenosine triphosphatase pump inhibitor, and known to release membrane proteins from ER retention. In a pilot experiment, we extended the lifespan of rumpshaker mice from 20 to 60 days. These promising data suggest that a therapeutic strategy should be developed for PMD, using turmeric and our *in vitro* and *in vivo* models.

2 INTRODUCTION

2.1 General Introduction

Neuron to glia communication is essential for axonal impulse conduction, synaptic transmission and information processing. Glial cells support and nourish neurons throughout life. They also facilitate neurons in communication and information processing, hence are required for normal functioning of the nervous system. There are three types of glial cells in the central nervous system (CNS) - oligodendrocytes, astrocytes and microglia (Figure 1).

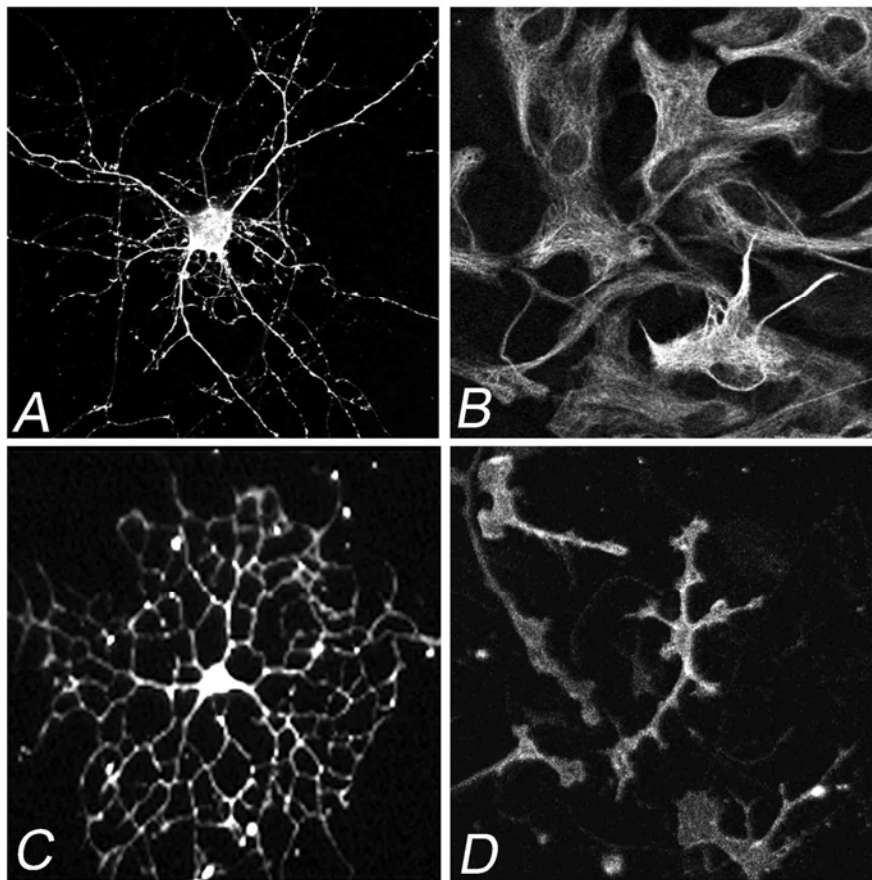


Figure 1: Cells of the central nervous system

Cultured cells of the central nervous system (CNS) stained for cell type specific markers.

A) Neurons stained for dendritic microtubule-associated protein MAP2.

B) Astrocytes stained for glial fibrillary acidic protein (GFAP).

C) Oligodendrocytes stained for 2'3'-cyclic nucleotide 3'-phosphodiesterase (CNP).

D) Microglia stained for cell surface glycoprotein (MAC1).

Oligodendrocytes wrap layers of myelin membrane around axons to insulate them for impulse conduction. Characteristics of myelin and polarized morphology of oligodendrocytes is discussed in more detail in latter sections of introduction.

Astrocytes, which are closely associated with neurons and ensheath synaptic junctions, associate with the nodes of Ranvier, and respond to disease and injury by clearing cellular debris, secreting trophic factors and forming scars. Some astrocytes stretch from blood capillaries to neurons, transporting ions and other substances to sustain neurons and to regulate the extracellular environment (Girault and Peles, 2002; Nedergaard et al., 2003; Pfrieger, 2002; Ransom et al., 2003). A subtype of astrocytes namely “radial glia” span the entire width of the brain from the ventricles to the pial surface during fetal development, providing scaffolding along which neurons migrate (Ever and Gaiano, 2005).

Microglia, the only cells of the CNS that are not derived from ectodermal precursors, are derived from bone marrow monocyte precursors (Kaur et al., 2001). Like their counterparts in the hematopoietic system, microglia in the CNS, respond to an injury or disease by engulfing cellular debris and triggering inflammatory responses. The microglial cells are highly active in their presumed resting state, and continually survey their microenvironment with extremely motile processes and protrusions (Nimmerjahn et al., 2005).

2.2 Myelin

Functional integration of the vertebrate nervous system's complex cytoarchitecture requires rapid nerve impulse conduction. During evolution, this has been achieved through the development of myelin-forming glia. In the CNS, oligodendroglial extend multiple processes to myelinate a short segment (known as internode) of several axons (Figure 2). In the peripheral nervous system (PNS), a single highly versatile cell, Schwann cell, performs all the functions of the CNS oligodendrocytes (forming myelin) and astrocytes (ensheathing synaptic junctions, and bundling small-diameter axons together). The majority of the cytoplasm is extruded, leaving highly compact multi-lamellar myelin (Figure 2), which is composed of approximately 80 % lipids (by dry weight) and rest 20 % proteins (Figure 2). This structure efficiently isolates the axon to enable fast, saltatory conduction, by concentration of voltage-gated sodium (Na⁺) channels at the nodes of

Ranvier (Figure 3) (Pedraza et al., 2001). Membrane compaction leads to a defined periodicity of myelin [which differs in the PNS ($190 \pm 7 \text{ \AA}$) and in the CNS ($170 \pm 7 \text{ \AA}$) myelin]. As a result of membrane compaction a major dense line (MDL) inter-separated by two intra period lines (IPL) is formed. The IPL is a resultant of compaction of two opposing outer membranes (Figure 2).

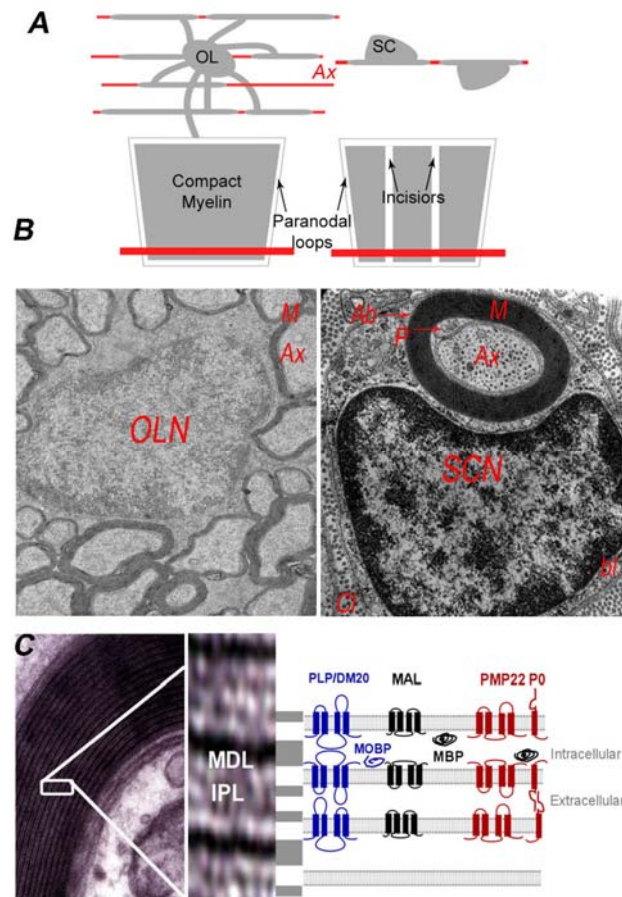


Figure 2: Myelin ultrastructure and major myelin proteins

A) In CNS, a single Oligodendrocyte (OL) myelinate a short stretch of multiple axons whereas in PNS a single Schwann cell (SC) myelinates a short stretch of a single axon. Axons are drawn in red and OL/SC processes and cell body in grey.

B) Ultrastructure of CNS and PNS myelin. Oligodendrocyte (nucleus, OLN) myelinate many axons (Ax), all these axons might (or might not) share their myelin from a single oligodendrocytes. Transverse section of a Schwann cell (nucleus, SCN) spirally wrapping whorls of myelin membranes around an axon. The myelin spiral is bounded by inner (periaxonal, P) and outer (abaxonal, Ab) mesaxons. In PNS, basal lamina (bl) surrounds the entire abaxonal surface, and extracellular collagen fibrils (cl) separate adjacent fibers. Unlike PNS, no visible extracellular matrix separates myelinated fibres in the CNS.

C) Schematics of myelin periodicity. Processes from oligodendrocytes or Schwann cells wrap around axons and cytoplasmic membrane leaflets fuse to form major dense line (MDL), while extracellular leaflets of adjacent lamellae become closely apposed to form the intraperiod lines (IPL). Orientation of major myelin proteins within a membrane bilayer are shown here; proteins found in CNS as well as in PNS myelin (black), proteins exclusive to PNS (magenta) and CNS (blue).

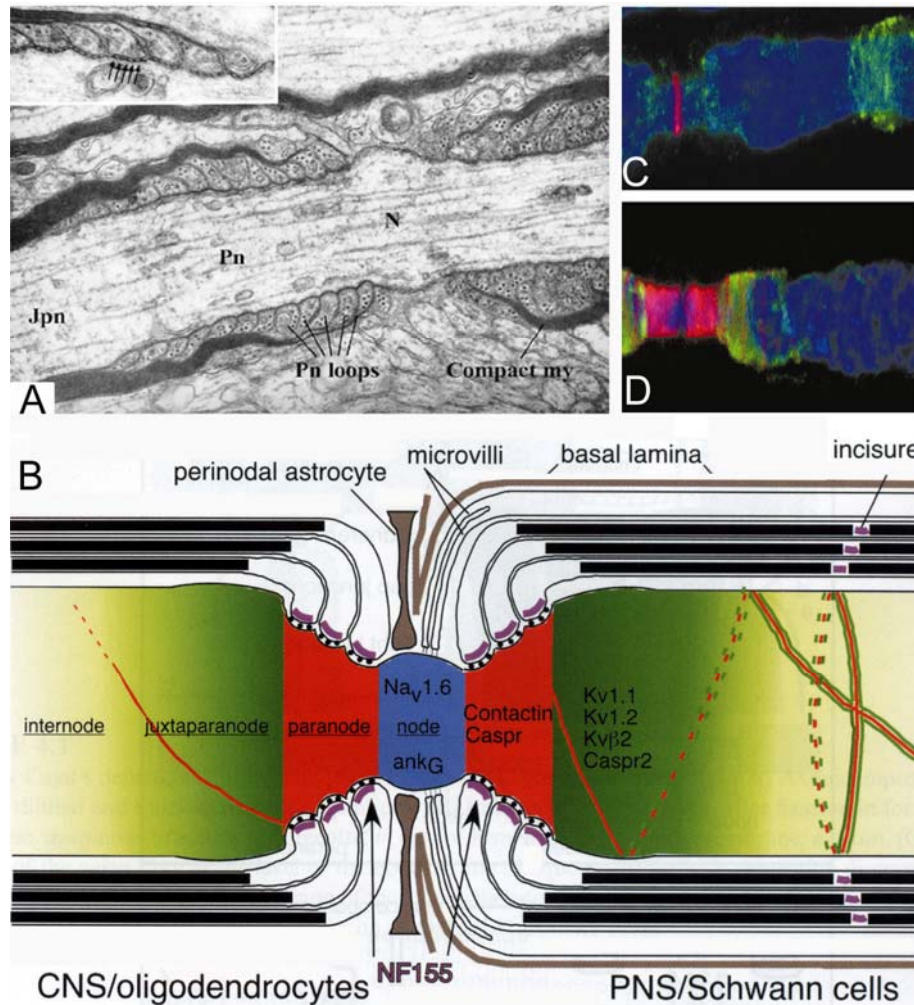


Figure 3: Nodal, paranodal, juxtapanodal and internodal organization in CNS and PNS

A) The axoglial apparatus consists of the node of Ranvier (N), recognized as the bare axonal segment, flanked by paranodal (Pn) loops, formed by the terminal expansions of myelinating (My) cells, and the juxtapanode (Jpn), which is located distal to the paranodal domain. The inset demonstrates the electron-dense “septa” (arrows) of the axoglial junction, whose functions may include intercellular adhesion, as well as molecular sieving.

B) Schematic depicting CNS and PNS myelin sheaths (meeting at a node) surrounding a single myelinated axon. The relative intensity of the red and green indicates the relative abundance of the indicated proteins. The node comprises mainly of clustered sodium channel subunits and their interacting partners. The glial paranodal loops engage in two types of epithelial-like junctions: tight and adherens junctions (for details see Figure 6). OSP/claudin-11 is a constituent of the tight junctions in the CNS, and E-cadherin mediates adhesion at the adherens junctions between the paranodal loops in the PNS. The proteins of the axoglial junction include caspr/paranodin, F3/contactin in the axon, and neurofascin 155 in myelinating glia. The juxtapanodal zone contains the potassium channel subunits Kv1.1, Kv1.2, and Kvβ2, and putative interacting proteins, such as caspr2.

C) The alignment of proteins subdomains in relation to morphological features of the axoglial apparatus in the PNS demonstrates that sodium channels (red) are restricted to the node of Ranvier and are flanked by the caspr paranodal domain (red in **D**). Potassium channels (green in **D**) are localized distal to the caspr “collar” in the juxtapanodal region. Schmidt-Lanterman incisures contain the myelin associated glycoprotein (green in the second panel). Adapted and modified from (Lazzarini RA, 2003; Pedraza et al., 2001).

The compact structure of CNS myelin is maintained by two major proteins, the cytoplasmic myelin basic protein (MBP) and the transmembrane proteolipid protein (PLP), which together comprise approximately 80 % of the total myelin proteins (Lees and Brostoff, 1984). In mammalian PNS, instead of PLP, protein zero (P0) a type I integral membrane glycoprotein of immunoglobulin gene super family, represents >70 % of the total myelin protein (Lemke and Axel, 1985). In contrast, Myelin associated glycoprotein (MAG) is selectively enriched in periaxonal myelin membrane of CNS internode and to a small stretch of inner tongue process membrane (Sternberger et al., 1979; Trapp, 1988). In addition, isolated myelin contains a number of minor protein components whose functions are obscure. These include 2'3'-cyclic nucleotide 3'-phosphodiesterase (CNP) (Tsukada and Suda, 1980), oligodendrocyte myelin glycoprotein (OMG), myelin oligodendrocyte basic protein (MOBP), myelin oligodendrocyte glycoprotein (MOG), oligodendrocyte specific protein (OSP/claudin-11) (Gow et al., 1999), sirtuin 2 and members of the tetraspan-protein family tetraspanins (Birling et al., 1999; Ishibashi et al., 2004; Tiwari-Woodruff et al., 2004).

The CNS myelin is known to inhibit neurite outgrowth after a CNS insult. The underlying mechanisms that account for this regeneration failure in the adult CNS as compared to PNS are poorly understood. The role of CNS myelin specific proteins OMG and NogoA apart from MAG underwent an extensive investigation (Domeniconi et al., 2002; Hwang et al., 1992; Liu et al., 1996).

2.3 Human *PLP 1* and mouse *Plp1* gene transcripts

The X-linked 15.97 kb *Plp1* gene is encoded by 7 exons. The alternative splicing of PLP precursor RNA yields a minor isoform known as DM20 (Nave et al., 1987). DM20 is identical to PLP, except for a 35 amino acid segment, encoded by the 5 prime end of exon 3, that is absent in DM20 (Figure 4) (Nave et al., 1987). It has not been clearly established whether the two isoforms have separate functions in vivo. *Plp1* knockout mice, which lack both isoforms, have defects in the intraperiod line (IPL) of myelin (Boison and Stoffel, 1994; Klugmann et al., 1997; Rosenbluth et al., 1996) and also develop an axonopathy (Griffiths et al., 1998). *Plp1* knockout mice complemented with transgenes expressing only one isoform remain abnormal, whereas when both isoforms are present, the abnormal

phenotype is prevented (Griffiths et al., 1998). Recently, a new exon of the *Plp1* gene in mice has been identified between exons 1 and 2, which is spliced into PLP and DM20 mRNAs, creating a new translation initiation site (Bongarzone et al., 1999). This generates PLP and DM20 proteins with a 12 amino acid leader sequence that apparently targets them to oligodendrocyte cell bodies rather than to myelin membranes (Bongarzone et al., 2001). However, as no homologous exon has been detected in the human genomic sequence, the functional significance of this murine exon is unclear. Small amounts of both *Plp1* gene products are synthesized by Schwann cells in the PNS, with DM20 being an abundant isoform. It is still unclear whether these proteins are incorporated into the compact PNS myelin. Message for soma restricted and classical DM20 and PLP, is also present in thymus (Pribyl et al., 1996), heart (Campagnoni et al., 1992), motor neurons and muscles (Feng et al., 2003; Jacobs et al., 2004) and in lymphoid tissues (Feng et al., 2003; Voskuhl, 1998).

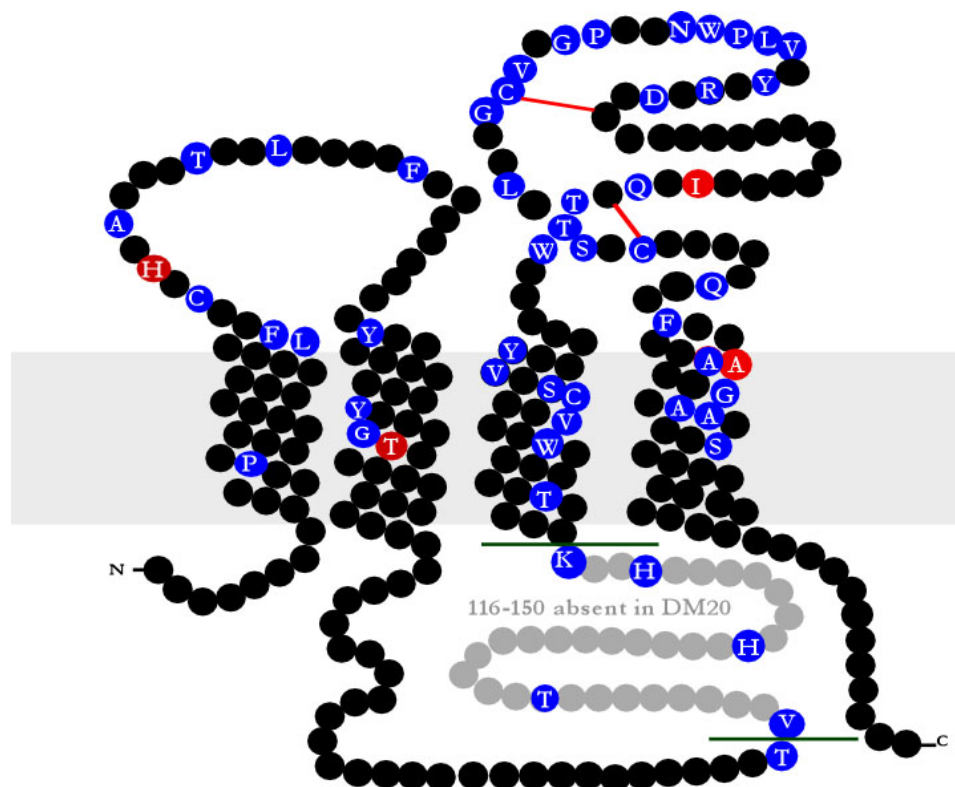


Figure 4: Topology of PLP/DM20 in myelin membranes

PLP and DM20 share the same primary structure except a short 35 amino acid stretch (116-150 in filled grey circle), that is absent in DM20. Blue filled circles are amino acids substitutions associated PMD or SPG2 patients, whereas filled red circle highlight naturally occurring animal models of the PMD. Disulfide bonds in extracellular loop 2 (EC2) are joined by red lines and are critical for PLP folding (for details see section 4.1.3 and Figure 12).

2.4 PLP conservation during evolution and topology in myelin membranes

The amino acid sequence of PLP is highly conserved among mammals: human and murine PLP are identical, and show greater than 99 % homology with PLP from avian, bovine and canine (Figure 5). PLP from amphibians also shows a high degree of homology (>85 %) with mammalian PLP. PLP and DM20 are part of the “DM” family of molecules, which includes the neuronal M6 glycoproteins in mammals, and DM20-like molecules in sharks and rays. Members of this family not only share a high degree of sequence homology, particularly in their transmembrane regions and positions of cysteines, but also contain other conserved domain sequences.

During myelination, DM20 is selectively excluded from the compacted myelin and enriched on the surface of oligodendrocytes, whereas PLP is associated predominantly with the myelin sheath (Trapp et al., 1997). Western blotting of myelin from adult animals identifies both isoforms in the myelin fractions. However, the lack of a specific antibody against DM20 has prevented the unequivocal localization of each isoform by immunocytochemistry. Transfection in heterologous cells infers that PLP and DM20 can be incorporated into the cell membrane independently (Gow et al., 1994; Gow and Lazzarini, 1996; Thomson et al., 1997). Transfection in the cells of oligodendroglial lineage; oli-neu (Jung et al., 1995) and OLN93 (Richter-Landsberg and Heinrich, 1996) reveals that, apart expression at the cell surface, PLP and DM20 accumulate in lamp1-positive endosomal/lysosomal(E/L) compartment.

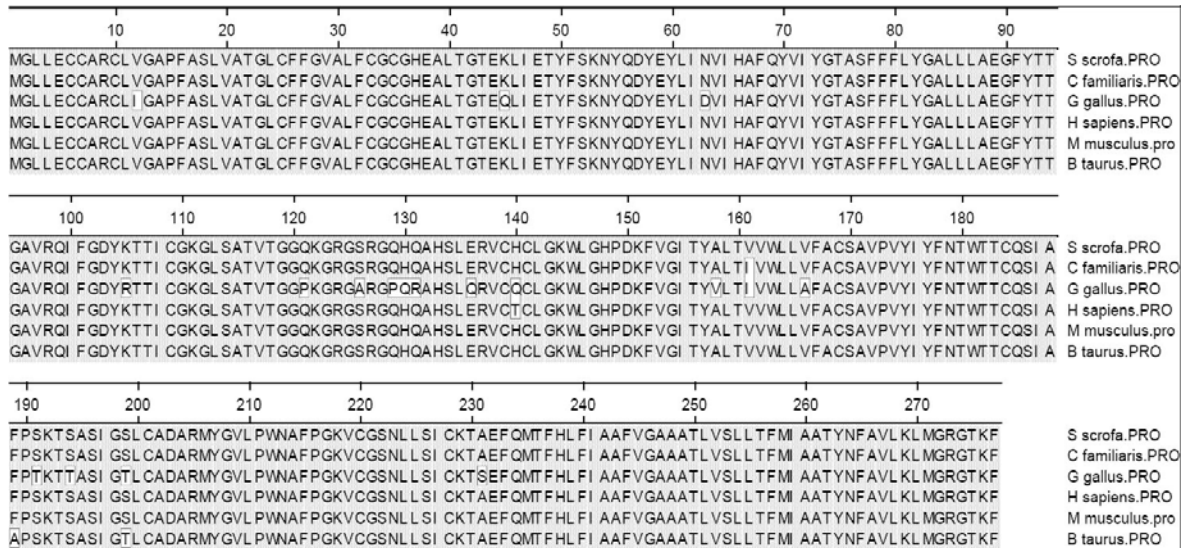


Figure 5: Conservation of PLP among different species

Clustal W alignment (DNA-star MegAlign 6.0), shaded residues are identical. Amino acid sequence of *H. sapiens* PLP shows high homology with *M. musculus*, *S. scrofa*, *G. gallus*, *C. familiaris* and *B. taurus* PLP. Unlike amino acid sequence from mouse, amphibian PLP shows less homology with human PLP (homology not shown).

Several topological models of PLP orientation in membrane bilayer has been proposed based on mathematical modeling, chemical labeling, limited protease digestion, and immuno-labeling (Inouye and Kirschner, 1994; Konola et al., 1992; Popot et al., 1991; Stoffel et al., 1989; Weimbs and Stoffel, 1994). It is established now, that PLP has four transmembrane (TM) domains and two extracellular loop regions (EC1 and EC2) that interact with the opposing membrane in compact myelin (Popot et al., 1991; Stoffel et al., 1989). Both N- and C-termini of PLP protrude into the cytosol (Figure 4). Since, myelin can be purified by sucrose gradient centrifugation and PLP is one of the most abundant membrane proteins, even post-translational modifications of PLP have been studied in detail. By mapping tryptic peptides at reducing and non-reducing conditions, the location of two extracellular disulfide bridges (C183-C227 and C200-C219) within EC2 have been determined (Shaw et al., 1989; Weimbs and Stoffel, 1992).

2.5 Mutations associated with *Plp* gene

Numerous point mutations of the X-linked *PLP1* gene cause Pelizaeus-Merzbacher Disease (PMD; OMIM # 312080) or Spastic Paraplegia type 2 (SPG2; OMIM #312920) in humans, and dysmyelination in corresponding mouse models (Nave and Boespflug-Tanguy, 1996). A large range of mutations involving the *PLP1* gene in humans lead to varying phenotypic severity. A comparison of mutations suggests that SPG2 is a degenerative disease and primarily the PLP "loss-of-function" phenotype. In contrast, PMD is an early developmental disorder and severe leukodystrophy, caused by oligodendrocyte death (Gow et al., 1998; Seitelberger, 1995; Werner et al., 1998). A large number of PMD mutations are substitutions in EC2 (for a comprehensive list of *PLP1* mutations see - <http://www.med.wayne.edu/neurology/ClinicalPrograms/Pelizaeus-Merzbacher/plp.html>).

Mutation in human *PLP1* gene result in variable phenotypic consequences ranging from a life expectancy of an early infancy to those that live bedridden for several decades. The most common abnormalities associated with *PLP1* gene are duplication and triplication, which results in severe early-onset form of PMD. Complete loss of the *PLP1* gene, or mutations leading to almost complete truncation of the protein, result in a milder clinical phenotype than most other mutations. Similarly, in mice there is a variable degree of phenotype from those that die between P20–P34 to those that can live almost indefinitely. The most severely affected mutants include the jimpy mouse (PLP^{jp4j}) and its allele PLP^{jpsd} , and the myelin-deficient (*md*) rat. Moderately affected mutants include the shaking pup (PLP^{shp}) and the paralytic tremor (PLP^{pt}) rabbit, and mildly affected the rumpshaker (PLP^{jprsh}) mouse (Griffiths et al., 1990; Schneider et al., 1992). In addition to these naturally occurring models, imitation of human *PLP1* gene duplication, by transgenic autosomal overexpression of *Plp1* gene result in dose dependent dysmyelinating phenotype in mouse (Readhead et al., 1994). These animals provide ideal tools in which to examine the effects of abnormal or missing PLP on myelin formation and maintenance.

2.6 Sorting of membrane proteins and mechanisms of ER retention

Membrane proteins are targeted to the ER by their signal sequence and are co-translationally inserted into the membrane. In the oxidative environment of the ER, numerous chaperones catalyze the proper folding of the growing polypeptide (Mothes et al., 1997). Before exiting the ER, they are screened by a quality control system that retains unfolded or misfolded proteins and marks them for degradation (Ellgaard and Helenius, 2003; Ellgaard et al., 1999). Some membrane proteins, including ion channels and connexins, are also assembled into homo- and hetero-oligomers in the ER (Hurtley and Helenius, 1989) and can exit only when properly assembled. Monomeric or incompletely assembled subunits are retained by stable interactions with ER resident chaperones (Kleizen and Braakman, 2004).

Mutant proteins that are retained in the ER can induce the unfolded protein response (UPR) that includes ER growth and transcriptional activation of genes encoding chaperones (Patil and Walter, 2001; Rutkowski and Kaufman, 2004). In mammalian cells, the UPR can also trigger apoptosis (Federovitch et al., 2005; Harding et al., 2002). Not surprisingly, in many diseases cell death has been associated with mutant membrane proteins that are thought to be "misfolded" based on sequence analysis. However, the essential features of protein misfolding are often unknown. Whereas mutations that alter a transmembrane (TM) domain cause stable interactions with the ER-resident chaperon calnexin (Swanton et al., 2003), ER retention remains unexplained for the majority of disease-causing substitutions that map into EC loop regions of polytopic membrane proteins.

Many of the structural changes in PLP appear modest, and the underlying cause of oligodendrocyte death is not obvious. Overexpression of mutant PLP in transfected COS-7 cells has suggested misfolding and ER retention as a likely cause (Gow et al., 1994; Jung et al., 1996). However, what defines "misfolding" for an oligodendrocyte (prior to ER retention) remains unclear. Moreover, because of oligodendrocyte death, PLP retention cannot be adequately studied in *in vivo* systems. Here, we have partially solved this problem by using immortalized oligodendrocytes to study PLP trafficking and retention.

The biggest puzzle in PLP biology has been the observation that several substitutions in EC2 cause the retention of PLP, but not the corresponding DM20 mutant (Gow and

Lazzarini, 1996), although PLP and DM20 differ by the length of the cytoplasmic loop. We have hypothesized that the differential behavior of PLP and DM20 may hold a clue as to the underlying retention mechanism. Here, we show that cysteine residues in EC2 are not only essential for protein folding, but also for ER retention of PLP with PMD-associated substitutions. We suggest a disease mechanism for membrane proteins, by which missense mutations alter the EC domain structure such that the formation of intramolecular disulfide bridges becomes inefficient. In the oxidative environment of the ER, unpaired cysteines form instead abnormal protein dimers and unspecific protein crosslinks, that cause ER retention and possibly cell death.

2.7 Oligodendrocytes are polarized cells

Polarized membrane assembly is an intricate process, requiring a coordinated synthesis, transport and sorting of proteins and lipids (Figure 6). During last decade, significant advances were made in defining sorting motifs for apical and basal-lateral protein sorting, describing the sorting machinery in the trans-golgi network (TGN) and plasma membrane (PM) of simple polarized cells. MDCK cells have extensively been used for polarized trafficking studies. Another system that underwent an intensive investigation for polarized trafficking, to dendrites and axons, is Neuronal. Trafficking studies of CNS myelin proteins in MDCK cells (Kroepfl and Gardinier, 2001) have yielded valuable insight into how myelin biogenesis might take place. Myelin forming Schwann cells also share some feature of MDCK cells (Figure 6). Oligodendrocytes, compared to both cell types are much more complicated and must possess a unique trafficking and signaling pathway to sort myelin proteins to various myelin growth cones.

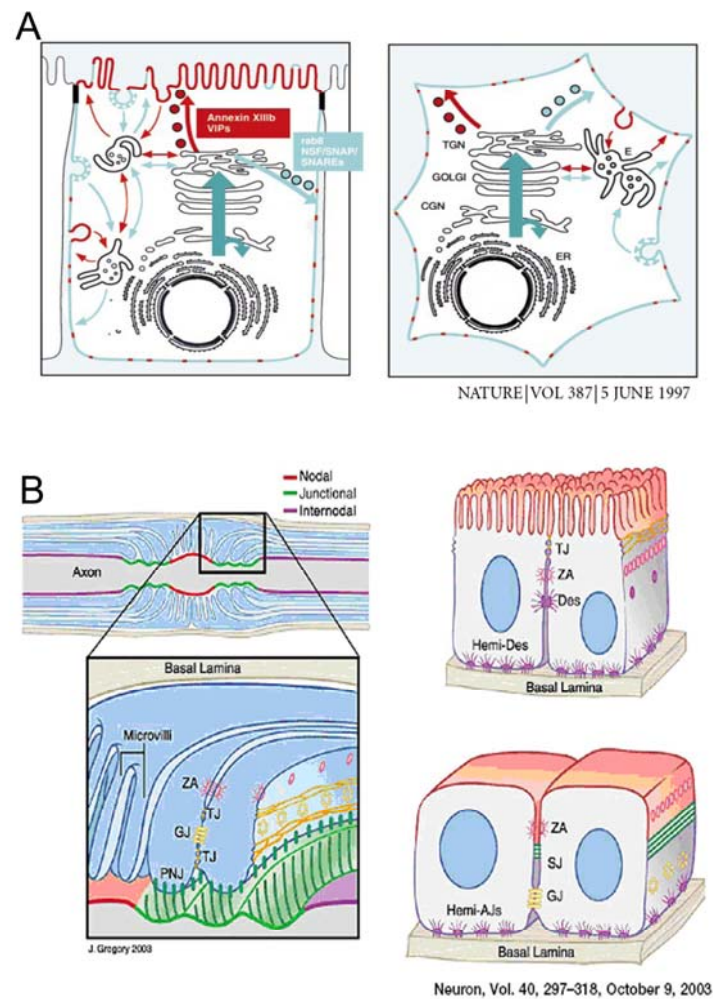


Figure 6: Protein sorting and domain organization in polarized cells

A) Postulated mechanisms of post-golgi circuits in MDCK cells (left) and fibroblasts (right). Sorting in the raft circuit (in red) is based on sphingolipid-cholesterol microdomains. Proteins like vesicular integral membrane protein (VIP) and annexins associate and act as stabilizers for other proteins (Fiedler et al., 1994). Alternatively (in blue), cells employ sorting signals in the cytoplasmic tails and binding at proteins. In the blue circuit NSF-SNAP-SNARE-Rab system is used for vesicular docking and fusion (Fiedler et al., 1995).

B) Schematic organization of the nodal region of myelinating glia (in PNS) is compared to simplified organization of chordate (upper right) and invertebrate epithelial (lower right) cells. The nodal region (red) is masked by Schwann cell microvilli in PNS (astrocytes processes in CNS). The paranodal region is a site of extensive junction formation. It serves as a barrier between the extracellular space at the node and the periaxonal space in the internode. This also separates nodal membrane proteins from the juxtaparanodal proteins. Paranodal loops form extensive autotypic junctions that are radially and circumferentially arrayed: These include tight junctions (TJ) that provide a presumptive paracellular seal between the periaxonal space and the loops, gap junctions (GJ) that permit direct communication between loops, and adherens junctions (AJ) that promote loop to loop attachment. The apical membrane of epithelia is rendered in red, and the lateral domain, a site of homotypic cell interactions, is rendered in purple. A diffusion barrier between membrane domains is provided by tight junctions in chordates; septate junctions in invertebrates (green), which are orthologous to the paranodal junctions, are interposed between domains. [A and B are adapted from (Simons and Ikonen, 1997) (Salzer, 2003)]

How do the CNS myelin internodes and myelin processes expand? Although, there has been substantial progress in our understanding of the factors that determine glial cell fate, much less is known about the cellular mechanisms that determine how the myelin sheath is extended and stabilized around axons. As Oligodendrocytes enter terminal differentiation and contact neurons, they begin to produce myelin membranes at a remarkable rate ($>104 \mu\text{m}^2$ myelin membrane surface area/cell/day; (Pfeiffer et al., 1993)). During myelination, oligodendrocytes must decide how many times each growing process needs to be wrapped around a segment of an axon. By following biochemical clue displayed by each axon, oligodendrocytes must integrate each signal and respond by delivering proteins and lipids to each growing process, accordingly. These biochemical clues or signals also help oligodendrocytes to discriminate between: glial and neuronal processes, dendrites and axons. Do glial cells rely on biochemical clue, once the myelination is completed, is still a major questions of the field. Understanding how myelinating glia and neurons co-operate to achieve this feat is a challenging and important problem. Current concepts of lipid rafts, which propose the existence of microdomains in membranes, might help to explain how proteins and lipids are delivered to the growing membrane (Figure 6 A). However, such concepts might be less useful for understanding how the myelin macrodomain, with its distinct protein and lipid content, is stably segregated from the plasma membrane of the myelin-forming glial cell. Cholesterol is a major constituent and a rate limiting step in myelination. Transgenic mice with oligodendrocytes that lack an ability to synthesize cholesterol show a delay in myelination that seems to be at least partially compensated by cholesterol uptake (Saher et al., 2005). Lipids are probably targeted to the growing process as a consequence of their interactions with particular proteins (Horvath et al., 1990; Sankaram et al., 1991). Solving the puzzle about lipid, leads to another puzzle i.e, how proteins are segregated into growing myelin tongue. Most likely this occurs as a result of a combination of factors, such as the specific targeting of proteins during their biosynthesis, cis-association with other proteins and finally by trans-adhesive associations during compaction and axon–glia interaction.

Studies have therefore focused on how oligodendrocytes (OLs) synthesize MBP and PLP and incorporate them into the growing myelin sheath. The discovery that myelin basic protein (MBP) is synthesized in the growing myelin process (Colman et al., 1982; Trapp et al., 1988) on free ribosomes was a major step forwards in understanding of how proteins

might be delivered to the myelin membrane. This was one of the first demonstrations of localized mRNA translation in a eukaryotic cell, and indicated that MBP is incorporated into the growing myelinating process at sites that are quite distant from the oligodendrocyte cell body.

In our study, we have investigated vesicular trafficking to myelin compartment by generating stable oligodendrocyte cell line expressing PLP^{wt}-EGFP. We also transfected primary oligodendrocytes (OLs) to compare trafficking polarization between precursor and mature cells. When expressed in cultured OLs, PLP resides in a compartment with characteristics of a late endosome/lysosome (LE/L) compartment. Co-culture with neurons (or cAMP treatment) lead to an increase of PLP on the PM and a disappearance from the LE/L (Trajkovic et al., 2006).

Do neurons give instructions to glial cells? Oligodendrocyte precursor cells (OPCs) in the CNS migrate into developing white matter where they differentiate into postmitotic OLs and produce the myelin sheath. The differentiation of OPCs in terms of changes in gene expression and in morphology has been studied extensively *in vitro* and *in vivo* (Pfeiffer et al., 1993). Because OPCs differentiate normally in axon-free culture and express myelin components, a role for neurons was not immediately apparent. OPCs and newly born OLs require astrocyte-derived factors such as PDGF, but OLs become dependent on axonal signals later. Axonal signaling to OLs occurs on at least two levels (Barres and Raff, 1999; Coman et al., 2005). Electrical activity mediated by extrasynaptic release of adenosine (Stevens et al., 2002) is required for proliferation of OPCs. Additionally, contact-mediated neuronal signals play important roles in OPC and Schwann cell differentiation and myelination (Corfas et al., 2004). Michailov and colleagues have shown that the levels of neuregulin 1 type III overexpression by axons results in hypermyelination in PNS (Michailov et al., 2004). In a follow up study Salzer and colleagues have shown neuregulin 1 type III also determine the ensheathment fate of axons in the PNS (Taveggia et al., 2005).

2.8 A therapeutic approach toward a mouse model of PMD

Recently, curcumin has been shown to resolve amyloid plaques (*in vivo*) (Lim et al., 2001; Yang et al., 2005) and the drug is capable of crossing the blood brain barrier (Giri et al., 2004; Natarajan and Bright, 2002; Scapagnini et al., 2006; Tomita et al., 2005). Curcumin has been shown to modulate a number of cellular messenger pathways, including NF- κ B and intracellular calcium (Egan et al., 2004; Sarkar and Li, 2004). Curcumin has also been shown to modulate and abrogate protein aggregates/retention of myelin protein zero (*in vitro*) (Khajavi et al., 2005) and other channel proteins CFTR (*in vivo* and *in vitro*) (Egan et al., 2004). At molecular level, curcumin acts as a non toxic and potent Ca^{2+} -ATPase pump inhibitor (Logan-Smith et al., 2001). As many luminal chaperons are Ca^{2+} binding proteins (Nigam et al., 1994; Szperl and Opas, 2005; Trombetta and Parodi, 1992) here we directly tested with an *in vivo* approach whether misfolded PLP is released from the ER or not.

The treatment of rumpshaker mice (a model for Palizaeus-Merzbacher disease) with turmeric (the rhizome powder) resulted in a prolonged lifespan of the mutant mice. These promising data suggest that a therapeutic strategy should be developed for PMD, using turmeric and our *in vitro* and *in vivo* models.

3 MATERIAL AND METHODS

3.1 Material Used

3.1.1 Kits, chemicals and protocol source

All chemicals used were purchased from the Sigma-Aldrich unless stated otherwise. DNA purification kits and other molecular biology kits were purchased from Qiagen, Promega Stratagene and Sigma-Aldrich. Cell culture and general laboratory material from Falcon, Nunc and Eppendorf was used.

Wiley interscience online protocol source for cell biology (http://www.mrw.interscience.wiley.com/cp/cpcb/cpcb_contents_fs.html) and molecular biology (http://www.mrw.interscience.wiley.com/cp/cpmb/cpmb_contents_fs.html) was referred before any new experiments.

3.1.2 Solutions and buffers

3.1.2.1 Molecular biology buffers

DNA-sample buffer (6x)

20 % (w/v) Glycerol in TAE buffer

0.025 % (w/v) Orange G or bromophenol blue

dNTP-stock solutions (100 mM)

25 mM each dATP, dCTP, dGTP, dTTP (Boehringer, Mannheim)

Ethidiumbromide

1 µg/ml for agarose gels in 1xTAE

TAE (50x, 1000ml)

2 M Tris-Acetate, pH 8.0

50 mM EDTA

57.1 ml Glacial acetic acid

Make 1000ml with dH₂O

TE (1x)	
10 mM	Tris-HCl, pH 8.0
1 mM	EDTA

3.1.2.2 Protein biochemistry buffers

Biotinylation and protein labeling

Biotin-maleimide

N-Biotinoyl-N'-(6-maleimidohexanoyl) hydrazide
(membrane permeable)

Stock-200 mM in DMSO

Sulfo-NHS-LC-Biotin (membrane impermeable)

1 mM in DPBS (prepare fresh)

Sulfo-NHS-LC-Biotin (quenching buffer)

1 M Glycine or Lysine in DPBS

DSP

Dithiobis(succinimidyl) propionate

200 mM in DMSO (Cross-linker)

DPBS 1x, cell culture

0.7 mM CaCl₂

2.6 mM KCl

136 mM NaCl

0.5 mM MgCl₂

8.1 mM Na₂HPO₄

1.5 mM KH₂PO₄

Iodoacetamide

200 mM stock in PBS

Promix S³⁵ L-methionine and L-cysteine (Amersham)

7.15 mCi

Lysis buffer I

20 mM	Tris-HCl, pH 7.5
150 mM	NaCl
1 mM	EDTA
0.1 to 0.3 %	SDS
1 mM	PMSF (add before use)

Lysis buffer II

20 mM	Tris-HCl, pH 7.5
150 mM	NaCl
1 mM	EDTA
1 %	Triton X 100
1 mM	PMSF (add before use)

Western Blotting

Blocking Buffer

5 %	non fat dry milk powder in TBS
-----	--------------------------------

Blotting buffer, 1x (pH unadjusted, Western Blotting)

39 mM	Tris-HCl
48 mM	Glycine
10-20 %	Methanol

SDS running buffer (1x)

25 mM	Tris-HCl
192 mM	Glycine
1 % (w/v)	SDS

SDS sample buffer (1x)

25 mM	Tris-HCl, pH 6.8
5 % (v/v)	Glycerol
0.01 % (v/v)	Bromophenol blue
0.2 to 2 % (v/v)	β -ME (add fresh)

SDS sample buffer (5X)

62.5 mM	Tris-HCl, pH 6.8
2 % (w/v)	SDS
20 % (v/v)	Glycerol
0.01 % (v/v)	Bromphenol blue
0.2 to 2% (v/v)	β -ME (add fresh)

SDS separating gel 12.0 % (4 gels of 1.5mm thickness)

13 ml	dH ₂ O
15 ml	30 % Acrylamide BioRad (29.1)
9.4 ml	1.5M Tris-HCl, pH8.8
370 μ l	10 % SDS
125 μ l	10 % APS
30 μ l	TEMED (Biorad)

SDS stacking gel (4 gels)

6.1 ml	dH ₂ O
1.3 ml	30 % Acrylamide BioRad (29.1)
2.5 ml	0.5 M Tris-HCl, pH 6.8
100 μ l	10 % SDS
50 μ l	10 % APS
10 μ l	TEMED

Stripping buffer

50 mM	Tris-HCl, pH 6.8
1 %	SDS
300 mM	β ME

TBS

50 mM	Tris-HCl, pH 7.5
140 mM	NaCl

3.1.2.3 Immunocytochemistry buffers

PBS 1x, cell culture

136 mM	NaCl
2.6 mM	KCl
10 mM	$\text{Na}_2\text{HPO}_4 \cdot 2\text{H}_2\text{O}$
1.4 mM	KH_2PO_4

Set pH to 7.2 with 10 N NaOH; make 1000 ml with H_2O

TBS

25 mM	Tris-HCL, pH 7.5
136 mM	NaCl
2.6 mM	KCl

Fixative

2 %	Paraformaldehyde in PBS/TBS
-----	-----------------------------

Permeabilization buffers

0.1 %	Saponin in TBS/PBS
0.001 %	Triton X 100 in TBS/PBS
0.1 %	Digitonin in TBS/PBS

Blocking Buffer

2 %	BSA (Fraction V)
-----	------------------

0.1 %	Porcine skin gelatine
2 %	Goat serum
0.02 %	Biotin
0.1 %	Saponin
Dissolved in TBS/PBS	

Blocking Buffer (live staining)

3 %	Goat Serum in DPBS
-----	--------------------

Dilution Buffer

2 %	BSA (Fraction V)
0.1 %	Porcine skin gelatine
2 %	Goat serum
0.02 %	Biotin
Dissolved in TBS/PBS	

Mounting Agent

Aqua poly-mount (Polysciences)

3.1.3 Bacterial and cell culture media

Bacterial media were autoclaved and supplemented with antibiotics prior to the use. DMEM for mammalian cell culture was purchased from GIBCO or BioWhittaker.

3.1.3.1 LB-Medium

1 %	Bacto Tryptone
0.5 %	Bacto Yeast extract
1 %	NaCl

Make 1000 ml with H₂O, set pH 7,5 with 10 N NaOH and autoclave.

Before use add antibiotics to the following concentrations;

150 mg/l	Ampicillin (Amp)
50 mg/l	Chloramphenicol (Cm)
25 mg/l	Kanamycin (Kan)

3.1.3.2 Buffers and media for Cell Culture

Curcumin

1 μ M in DMSO

Trypsin-EDTA Solution

Dilute 1:10 in PBS or DMEM

COS-7 medium

DMEM, 1000 mg/l glucose

10 % FBS

1 % Penicillin/Streptomycin

0.1 % Amphotericin (0.1 %)

2 mM L-Glutamine

Live cell Imaging medium

DMEM, High glucose (4500mg/l)

25 mM Hepes

1 % Horse Serum

Without phenol red

Labeling S³⁵ medium

Methionine and cysteine free DMEM

All other regular constituents added

Oli-neu medium (SATO)

DMEM, 4500 mg/l glucose

1 μ g/ml Transferrin

10 μ g/ml Insulin

25 μ g/ml Gentamycin

220 nM Sodium-Selenite

520 nM L-Thyroxine

500 pM Tri-iodo-threonine

100 μ M Putrescine
200 nM Progesterone
Sterile filter and add between 1 to 5 % Horse Serum

OLN93 medium

DMEM, 4500 ml/l glucose
10 % FBS
1 % Penicillin/streptomycin
2 mM L-Glutamine

Hybridoma medium

RPMI 1640 medium

1 to 10 % FBS
1 % Penicillin/streptomycin
2 mM L-Glutamine
1 % Non essential amino acids (100x; Gibco #11140-076)

Electroporation buffer

50 mM K_2HPO_4
20 mM CH_3COOK
20 mM KOH
Adjust pH to 7.4

Freezing Medium for oli-neu and COS-7 cells

70 % DMEM
20 % FCS
10 % DMSO

3.1.4 Bacterial strains and cell lines used

Escherichia coli DH5 α and XL1-Blue

Mammalian cell lines

COS-7	Green monkey kidney
Oli-neu	Rat O2A
OLN93	Rat O2A
Hybridoma clones	010 and 3F4.4C2

3.1.5 Plasmids

pRK5	Amp-r (Modified and described Jung et al, 96)
pGEMT-EASY	Amp-r (Promega)
pEGFPN1	Kan-r (BD Biosciences)
pMSVChygro	Amp-r (BD Biosciences)
pComTRUE	Amp-r (Mod. by Schwab MH from pBluescript KS)

3.1.6 Antibodies and Enzymes**3.1.6.1 Antibodies**

Primary antibodies directed against

The source of all anti-PLP antibodies, except the 3F4 (Greer et al., 1996), is described in (Jung et al., 1996)

Myc	Sigma
Calnexin	Stressgen
Calreticulin	Stressgen
PDI	Stressgen
Lamp1	Pharmagen

Secondary antibodies

Cy TM 5-coupled anti IgG anti-rabbit/mouse	Dianova
Cy TM 3-coupled anti IgG/M anti-mouse	Dianova
Cy TM 3-coupled anti IgG anti-rabbit	Dianova
Cy TM 2-coupled anti IgG anti-rabbit/mouse	Dianova
HRP-conjugated anti-IgG-anti-mouse/rabbit	Dianova

3.1.6.2 Enzyme

Restriction enzymes supplemented with 10x buffer were obtained from New England Biolabs and Fermentas. If specified in datasheet BSA was added to the restriction mixture. Other common molecular biology enzymes were obtained from under mentioned vendors.

CIP (alkaline Phosphatase) (1 U/ μ l)	Roche
Pfu high fidelity DNA polymerase	Stratagene
RedTaq DNA polymerase	Sigma

3.1.7 DNA and Protein Markers

DNA-marker Lambda/HindIII	Promega
DNA-marker PhiX174/HaeIII	Promega
Precision Plus prestained protein standard	BioRad

3.1.8 Oligonucleotides

Oligonucleotides were ordered from the service facility of the Max-Planck-Institute for Experimental Medicine. All oligonucleotides used for site-directed mutagenesis are listed in next section.

3.2 Methods

3.2.1 Molecular biological techniques

3.2.1.1 Maintenance of bacterial glycerol stocks

Genetically modified *E.coli* were stored as glycerol stocks (20 to 30 % glycerol (v/v) in LB medium) at $-80\text{ }^{\circ}\text{C}$. For expansion of glycerol stock, LB medium was inoculated using an inoculation loop or autoclaved toothpicks and incubated overnight at $37\text{ }^{\circ}\text{C}$ on 50 rpm (rotations per minute) on a tilted platform.

3.2.1.2 Transformation of bacteria

To 50 to 100 μl chemical competent *E.coli*, pretreated for 5 minutes with 1.7 μl β -ME either 1 to 50 ng of plasmid DNA or 5 to 10 μl of ligation mixture was added and incubated for 15 minutes on ice. After a heat shock (30 sec, $42\text{ }^{\circ}\text{C}$) and successive incubation on ice (1 minute) *E. coli* were directly plated onto LB plates containing an appropriate resistance. For some ligation bacteria were incubated on $37\text{ }^{\circ}\text{C}$ with 500 μl LB medium prior to plating. Plates were incubated at $37\text{ }^{\circ}\text{C}$ overnight.

3.2.1.3 Plasmid isolation of *E. coli*

Plasmid isolation from 3 ml cultures (Minipreps)

(Qiagen (8 strip vacuum manifold) Mini preparation kit)

3 ml LB media (supplemented with matched antibiotics) were inoculated with a single colony and incubated over night at $37\text{ }^{\circ}\text{C}$ at 50 rpm on a tilted platform. Cultures were transferred into 2 ml Eppendorf tubes and cells were pelleted by centrifugation (3000 rpm, 3 minutes, room temperature). Plasmids were isolated from the bacteria according to the manufactures protocol. The DNA was eluted from the columns by addition of prewarmed ($50\text{ }^{\circ}\text{C}$) 200 μl H_2O Tris-HCl (10 mM, pH 8.0).

Plasmid isolation from 200 ml-cultures (Maxipreps)

(Qiagen Maxiprep kit)

For preparation of large quantities of DNA, the Qiagen Midi/Maxiprep kit was used. The glycerol stock (from analytically tested and sequenced clone) was used to inoculate 3 ml of LB medium (with antibiotic) and incubated at 37 °C on 50 rpm for 4 to 6 hours. The starter culture was then used to inoculate 200 ml of LB medium, incubated overnight at 37 °C, on constant agitation. Cells were pelleted in a SARVOL centrifuge (SLA-1500 rotor at 6,000 x g, 15 minutes, 4 °C) and DNA was isolated as described in the manufactures protocol. Finally, the DNA pellet was resuspended in 500 µl of prewarmed (50 °C) Tris-HCl (10 mM, pH 8.0) and the DNA concentration was determined.

3.2.1.4 Enzymatic modification and manipulation of DNA

Digestion of DNA

For restriction digestion with type II endonucleases, 1 µg DNA was incubated with 5 to 10 units of enzymes for twice as long as recommended time (generally 2 to 3 hours at 37 °C) at required temperatures. For double digests involving enzymes requiring incompatible buffers, the DNA was digested sequentially. The DNA was purified between the two digestions using the Qiagen gel extraction kit. Restriction was terminated either by addition of sample buffer or by heat inactivation.

Dephosphorylation of Plasmid-DNA

After heat inactivation of restriction enzymes, 1 units of Calf Intestine Phosphatase (CIP, Roche) per 100 ng plasmid DNA was added. The reaction was incubated at 37 °C for 30 minutes and terminated by addition of sample buffer. After extraction from the agarose gel, the plasmid DNA was used for ligation.

Ligation of DNA-fragments

Ligation of DNA fragments was performed by mixing 25 to 50 ng vector DNA with a threefold molar excess of insert DNA. 0.5 µl of T4-ligase and 1 µl of 10x ligation buffer (both Promega) were added and the reaction mix was brought to a final volume of 10 µl. The reaction was incubated either for 2 hours at room temperature or overnight at 4 °C. The reaction mixture was used directly for transformation without any further purification.

DNA Gel-electrophoresis

For the separation of DNA fragments ranging from 100 bp to 15 kb agarose gels ranging from 0.7 % to 2.0 % were used. Desired amount of agarose was dissolved in 1xTAE buffer by heating in a microwave. After the agarose had cooled to approximately 60 °C, ethidiumbromide was added (1 µg/ml) and the agarose was poured into horizontal custom made gel tray, combs were placed in the setup and the agarose was allowed to solidify. The gel was immersed in 1xTAE buffer in gel loading chamber, prior to the loading or stored at 4 °C for a maximum of 2 weeks. After loading the samples (containing 10x sample buffer), the gels were run at 120 V constant (or 8 to 10 V/cm length) until the desired separation was achieved. For documentation, snapshots of UV-transilluminated gels were taken.

Extraction of DNA fragments from agarose gels

(Modified from Qiagen Gel Extraction kit protocol)

For isolation and purification of DNA fragments from agarose gels, the excised fragments were heated at for 10 minutes at 55 °C in three volumes of QG buffer. The mix was directly applied to the spin column (from Qiagen kit) centrifuged, washed once with PE buffer, air dried (or centrifuged for 1 minute) and eluted by addition of 30 µl prewarmed (50 °C) H₂O. The DNA-concentration was determined by running 1 to 3 µl of gel purified DNA next to a molecular weight standard, on an agarose gel.

Determination of DNA concentrations

DNA concentrations were estimated spectrophotometrically and by quantitative agarose gels. For determining the concentration of DNA preparations, the eluate or plasmid DNA was diluted 1:100 with water and the solution was pipetted into a 50 µl cuvette. Concentration was determined by measuring the absorbance at 260 nm, 280 nm and 320 nm. A ratio of A₂₆₀/A₂₈₀ between 1.8 and 2 monitored a sufficient purity of the DNA preparation. Running gel purified DNA samples next to a molecular weight standard gave an estimation of the DNA concentration, and was used to check the integrity of DNA prior to a ligation or transformation.

DNA Sequencing

DNA (f.c 100 ng/μl) diluted in H₂O was submitted to the sequence facility at the Max Planck Institute for Experimental Medicine. The obtained sequencing data was analyzed using DNASTar (Lasergene 5, upgraded to 7) software package as well as applications available at the “National Center for Biotechnology Information” (NCBI, <http://www.ncbi.nlm.nih.gov>) and ENSEMBL (<http://www.ensembl.org>).

3.2.1.5 Generation of PLP-myc, PLP-EGFP , truncated and myc replacement chimeras

All PLP modifications were done with PLP-ORF either amplified or excised from pR4 vector (Jung et al., 1996).

PLP-myc

The myc epitope was introduced by PCR. PLP cDNA was amplified using a sense primer with MCS and an antisense primer encoding the myc-epitope. The antisense primer replaces the stop codon TGA with codons encoding a flexible linker (SGP) followed by a myc epitope encoding sequence, a stop codon TGA and a PstI site. The amplified product was subcloned into the same vector (pRK5) using EcoR1/PstI sites.

Primers used

PLP-myc	SENSE	ACATACGATTTAGGTGACACT
	ANTISENSE	AAACTGCAGCTATCACAGGTCTTCTTCGCTTATCAGCTTC TGTTCCGGACCGCTGAACTTGGTGCCCTCG

PLP-EGFP

Enhanced green fluorescence protein (EGFP) tag was fused to the 3' end of PLP-ORF by gene sewing/fusion PCR. The 3' overhang of the antisense primer for PLP (without the stop TGA, otherwise same as above) shared a homology with 3' overhang with the sense primer from EGFP (without an initiation codon ATG). Individually amplified PLP and EGFP cDNA were purified and the sense primer from the PLP and the antisense from EGFP were used for sewing both products. The 3' homologous overhang of PLP with 5'

overhang of EGFP served as a bridge to sew the two genes. The final product was cloned into the vector pEGFP-N1 utilizing EcoRI/NotI sites.

Primers used

PLP	SENSE	ACATACGATTTAGGTGACACT
	ANTISENSE	CGGACCGCTCTGCAGCAGGTCTTCTTCGCTTATCAGCTTC TGTTCCGGACCGCTGAACTTGGTGCCTCG
EGFP	SENSE	CAGAGCGGTCCGGTGAGCAAGGGCGAG
	ANTISENSE	AGGGGGAGGTGTGGGAGGTT

Truncated and myc replacement chimeras

Truncated PLPs encoding the first half of PLP/DM20 were generated by using an antisense primer encoding a stop codon. For truncated PLPs encoding the second half of the protein, sense primer encoding methionine/or specific signal peptide for translation initiation was used. Myc replacement was introduced by gene sewing PCR as described above.

3.2.1.6 Site-directed mutagenesis of DNA

To generate site directed mutagenesis of PLPcDNA, we used a high-fidelity cloned or native Pfu DNA polymerase for amplification and subsequent digestion with DpnI, followed by transformation into chemical competent bacteria.

Primer designing

Sense and antisense primers (24-32 oligonucleotides) were manually designed with a required change in the exact middle of the primer. To achieve a melting point between 50 to 65 °C the length of the primers was varied accordingly. Designed primers were proofread using Lasergene's "EditSeq and Seqman" software packages. All primers were synthesized in the (facility) provided by the Max-Planck-Institute. The oligonucleotide stocks (50 pM) received were immediately diluted to 10 pM in PCR grade H₂O.

Primers used for site directed mutagenesis

PLP ^{C183S}	SENSE	ACCTGGACCACCTCTCAGTCTATTGCC
	ANTISENSE	ACCTGGACCACCTCTCAGTCTATTGCC

PLP ^{C200S}	SENSE	ATAGGCAGTCTCTCCGCTGATGCCAGA
	ANTISENSE	TCTGGCATCAGCGGAGAGACTGC
PLP ^{C219S}	SENSE	CCTGGCAAGGTTTCTGGCTCCAACCTT
	ANTISENSE	AAGGTTGGAGCCAGAAACCTTGCCAGG
PLP ^{C227S}	SENSE	CTTCTGTCCATCTCCAAAACAGCCGAG
	ANTISENSE	CTCGGCTGTTTTGGAGATGGACAGAAG
PLP ^{C219Y}	SENSE	CCTGGCAAGGTTTATGGCTCCAACCTT
	ANTISENSE	AAGGTTGGAGCCATAAACCTTGCCAGG
PLP ^{D202N}	SENSE	AGTCTCTGCGCTAATGCCAGAATGT
	ANTISENSE	ACATTCTGGCATTAGCGCAGAGACT
PLP ^{V208D}	SENSE	AGAATGTATGGTATCTCCCATGGAATG
	ANTISENSE	CATTCCATGGGAGATCACCATACATTCT
PLP ^{L209H}	SENSE	ATGTATGGTGTTCACCCATGGAATGCTT
	ANTISENSE	AAGCATTCCATGGGTGAACACCATACAT
PLP ^{W211R}	SENSE	GGTGTCTCCACGGAATGCTTCCCTG
	ANTISENSE	CAGGGAAAGCATTCCGTGGGAGAACACC
PLP ^{P215S}	SENSE	GGAATGCTTTCTCTGGCAAGGTT
	ANTISENSE	AACCTTGCCAGAGAAAGCATTCC
PLP ^{L223P}	SENSE	TGGCTCAACCCTCTGTCCATCT
	ANTISENSE	AGATGGACAGAGGGTTGGAGCCA
DM20 ^{T115K}	SENSE	AAGGGCTGAGCGCAAAGTTTGTGGGCATCACC
	ANTISENSE	GGTGATGCCACAAAACCTTTCGCTCAGGCCCTT
DM20 ^{LSAT-HPDK}	SENSE	GGACATCCCGACAAGTTTGTGGGCATC
	ANTISENSE	CTTGTCGGGATGTCCCTGCCGCAGATGGTGGT

PCR (using Pfu DNA polymerase)

All site-directed mutagenesis were performed in a 50 µl reaction mixture, in duplicates.

0.1 to 5 ng Template (pGEMT/pRK5/pEGFP-NI all, containing PLP cDNA)
 10 pM Sense primer

10 pM	Antisense primer
100 pM	dNTPs (25 mM each)
10 x	Pfu-polymerase
2 Units	Pfu-polymerase (cloned or native)

For both pRK5 and pEGFPNI (containing PLPcDNA) the amplification of 7 minutes and for pGEM-T amplification of 3 minutes were performed.

PCR steps used for the whole plasmid amplification:

1. 95 °C Denaturation (5 minutes)
2. 55 °C Annealing (1 minutes)
3. 72 °C Amplification (5 to 7 minutes)
4. 95 °C Denaturation (45 seconds)
5. 72 °C Amplification (10 minutes)
6. 4 °C Pause

A loop was inserted between cycle 5 and 3. The amplification was carried for 18 cycles.

PCR purification and DpnI digestion of amplified DNA

DpnI recognizes the methylated target sequence: 5-GmATC-3 (where the A residue is methylated) to selectively digest template DNA (all common strains of *E. coli* exhibit *Dam*-methylation at the sequence 5-GATC-3).

As all site directed mutagenesis were done in duplicates, one amplified set was separated on agarose gel, extracted and then treated with DpnI. The other PCR amplified DNA was treated directly with DpnI after amplification. After 1 hour of digestion with DpnI, 10 to 25 µl of DNA was used for transformation. After selection of matched antibiotics, 4 clones were picked, verified by restriction analysis and sequenced.

3.2.1.7 Generation of the PLP-EGFP transgenic “Knock-in” mice

DNA construct for homologous recombination and screening recombination via PCR

Short arm for homologous recombination and EGFP fusion.

For the modification of the *Plp* gene, the cos901 cosmid was used. EGFP-ORF was fused to *Plp* exon7 replacing the termination codon by gene sewing PCR as described above. Transcription of this recombined locus would yield normal transcripts from exon 1 to 7, in addition exon 7 now also encoded from 5' to 3' SGP-myc-Pst1-SGP-EGFP-Stop.

The PCR amplified short arm, for homologous recombination was cloned into pComTrue vector after fusion with EGFP-ORF (fusion PCR, see above) using XhoI/AgeI sites. XhoI/AgeI sites were introduced by sense/antisense primers annealing at 5' end of homologous region and 3' end of EGFP-ORF respectively. The short arm read as follow from 5' to 3' end: XhoI - intron 5 (523 bases onwards) - exon 6 – Intron 6 - exon 7 (69 bases) –spacers – EGFP – AgeI site. Note that the spacers correspond to SGP-myc-SGP-PstI as shown above.

EGFP-ORF and *Plp* homologous regions were amplified by PCR using Pfu DNA polymerase. The purified produced were fused by another round of PCR, with overhangs serving as a bridge to sew both products. The final PCR product was cloned into the pGEMT-EASY vector, excised after sequencing and subcloned into pCom-True vector using the XhoI/AgeI site.

Long Arm for homologous recombination

The 4.6 kb downstream of the exon 7, including the entire 3' UTR region of *Plp* gene served as a long arm for homologous recombination in embryonic stem (ES) cells. The long arm, flanked by SacII sites, was also PCR amplified and cloned directly into pCom-True vector.

Control PCR for screening homologously recombined ES cells

To screen homologously recombined ES cells using control PCR. A set of primers was tested on a control plasmid mixed with genomic ES DNA from non-transfected cells. The control plasmid bears an upstream sequence of the short arm and to distinguish the PCR product from the recombination product, 400 bps of irrelevant DNA were cloned into the

short arm. The control plasmid yielded a product of about 1900 bps whereas the homologously recombined ES yielded a product of 1492 bps with the same primers.

The PCR reaction was made as described above with following modifications:

Outer PCR (primers used 8210 and 8223)

ES cells DNA (template)	5 μ l
MgCl ₂	1.0 μ l

Inner PCR (primers used 8210 and 8224)

Outer PCR product (template)	1 μ l
MgCl ₂	1.0 μ l

PCR for detection of the homologous recombination (Nested PCR)

- | | | |
|-----|---------|------------------------------|
| 1. | 95 °C | 5 minutes |
| 2. | 95 °C | 45 seconds |
| 3. | 57 °C | 45 seconds |
| 4. | 72 °C | 2 minutes (to step 2, 19) |
| 5. | 4 °C | Pause |
| 6. | 95 °C | 5 minutes |
| 7. | 95 °C | 45 seconds |
| 8. | 57.3 °C | 45 seconds |
| 9. | 72 °C | 1.49 minutes (to step 2, 31) |
| 10. | 4 °C | Pause |

In the outer PCR the loop was inserted between step 4 and 2. After 19 cycles of amplification, 1 μ l of PCR product was added to a fresh premix containing the inner primers.

3.2.2 Protein-biochemical methods

3.2.2.1 SDS-poly-acrylamide gel electrophoresis

The Separation of proteins was performed by means of the discontinuous SDS polyacrylamide gel electrophoresis (SDS-PAGE) using the Mini-Protean 3 system (BioRad). A separating gel of desired thickness and percentage of acrylamide was layered with H₂O saturated iso-butyl alcohol. Before casting a stacking gel, the residual alcohol was removed and the future interface between the two gels was rinsed twice with dH₂O. The polymerized gels were stored in humid filter paper for a maximum of 7 days. The chamber and gels were assembled as described by the manufactures protocol. 5 µl of prestained Precision-plus (BioRad) was loaded on each gel as a molecular weight standard and to monitor electroblotting. A maximum of 40 µl sample was loaded in a single pocket and the gels were run on a constant current of 30 mA per gel, with a maximum voltage of 150 V. Gels were subjected to Western blotting, once the bromophenol blue reached the lower end of the gel.

3.2.2.2 Western Blot-analysis

Electrophoretic transfer

Proteins were transferred from the SDS-gel onto a PVDF membrane (Amersham/Millipore, pore size 0.45 µm) using the Invitrogen blotting apparatus. PVDF membranes were incubated in transfer buffer for 5-15 minutes, after activation in methanol for 30 seconds. Blotting paper and blotting pads presoaked in transfer buffer were assembled according to the manufacturer's protocol. Note that the blotting buffer used differs from the manufacturers recommended. Proteins were transferred at a constant voltage of 38 V and a maximum current of 275 mA, for 1 hour at RT for a 1.5 mm gel (and 45 minutes at RT for 0.75 mm gels).

Immunological detection of proteins on PVDF membranes

After electrophoretic transfer, the membranes were rinsed briefly in TBS and blocked for at least 1 hour at RT in blocking buffer (5 % non-fat dry milk in TBS). Primary antibody diluted in blocking buffer was applied for at least 1 hour at RT (or overnight at 4 °C). After four washes in TBS-T (0.05 % Tween 20 in TBS), HRP-conjugated secondary antibodies

were applied for at least 1 hour, followed by four washes with TBS-T. Membranes were exposed using the Enhanced Chemiluminescence Detection kit (PerkinElmer).

Densitometry evaluation of band intensity

For the quantification of the western blots only non-saturated developed western blots were used and scanned as 8 bit, 256 gray scale images (at 1200 dpi's on an EPSON F-3200 scanner). Scanned images were first transformed to 512 by 512 pixels, using Photoshop 7.0.1, and exported as TIF-files. Intensities of individual bands were quantified with the BioRad freeware 'Quantity-one' software, after registration.

3.2.2.3 Lysis of COS-7 and oli-neu cells

Cells were harvested in Lysis Buffer I (Cell Surface Biotinylation), Lysis Buffer II (co-immunoprecipitation) or 1x SDS sample buffer (for monitoring the oxidation-reduction state of PLPs), 24 to 36 hours after transfection. Before addition of lysis buffer, the free SH groups were blocked by incubation membrane with permeable Iodoacetamide (10 to 20 mM) at 4 °C for 10 minutes, in dark.

3.2.2.4 Protein biotinylation

Surface biotinylation was carried out between 24 to 36 hours after transfection and cells were washed twice with ice-cold DPBS. Surface proteins were biotinylated by incubating cells with 0.3 mg/ml Sulfo-NHS-LC-biotin (Pierce) in DPBS for 30 seconds at 4 °C. the Biotinylation was terminated by two washes with 20 mM glycine in DPBS at 4 °C for 30 seconds, each. The Biotinylated cells were then lysed directly in Lysis buffer I, and the biotinylated proteins were precipitated with streptavidin-coupled agarose beads (Pierce) at RT for 3 hours. Agarose beads were pelleted by centrifugation and washed five times with lysis buffer II at RT. Precipitated proteins were solubilized by addition of 4x LDS-sample buffer to the agarose beads. Proteins were separated by SDS-PAGE and immunoblotted against the C terminus of the myc epitope.

3.2.2.5 Oxidation and reduction assay

Cells were washed twice with DPBS were incubated with a free cysteine blocking moiety of a low (Iodoacetamide) or a high (biotin maleimide) molecular weight. Cells were either harvested in lysis buffer-I or 1x SDS loading dye. For reducing conditions 300 mM β -ME

(between 0.2 to 2 % v/v) were used in 5x loading dye, and for non reducing gels the sample was run without addition of β -ME. Proteins were electroblotted with the above described protocol.

3.2.2.6 Co-immunoprecipitation

Cells grown in 6 well plates were harvested 24 to 36 hours after transfection or induction. Cells were rinsed twice with DPBS, incubated with 10 to 20 mM iodoacetamide in DPBS for 15 minutes at 4 °C, rinsed twice with PBS and solubilized with lysis buffer II. Samples were incubated on ice for 30 minutes with intermittent vortexing and then centrifuged at 13000 g for 10 minutes to remove the insoluble material. The supernatant was pre-cleared by incubation with Protein-A/G-agarose beads in lysis buffer-II containing 1 % BSA. The antibodies were added to the supernatant for at least 4 hours to overnight at 4 °C. At least 3 to 4 hours before the pull-down, 35 μ l of Protein-A/G agarose were added to each Co-IP. After 4 to 5 washes with lysis buffer-II, followed by a centrifugation at 6000 g after each, the agarose beads were finally rinsed in PBS before analysis on SDS-PAGE.

3.2.2.7 S³⁵ labeling of proteins and radioimmunoassay

For S³⁵ labeling of proteins, the normal media of growing cells was replaced with a methionine/cysteine free media supplemented with 250 μ C of Promix (Amersham). After 24 to 72 hours of labeling, cells were washed twice with DPBS and proceeded as above (Co-IP), note here utmost care was taken for the disposal of the radioactive waste. After SDS-PAGE, gels were dried on a vacuum dryer and document on Kodak X-MAT (OMAR) radiographic films and with phosphoimager.

3.2.3 Cell culture

3.2.3.1 COS-7 and OLN93 cell culture

COS-7 and OLN93 cells were maintained on untreated tissue-culture dishes (Falcon) in Dulbecco's modified Eagle's medium (DMEM) and 10 % fetal bovine serum (FBS). Cells were grown at 37 °C in a 5 % CO₂ atmosphere, and the medium was changed every third day. For passaging cells, confluent plates were washed once with PBS, followed by a short trypsinization with 0.05 % trypsin-EDTA (Sigma).

3.2.3.2 Oli-neu cell culture

Oli-neu cells (kindly provided by J. Trotter) were maintained in SATO medium containing 1 to 5 % horse serum (HS) on PLL coated tissue culture dishes (Falcon). Cells were grown at 37 °C in a 5 % CO₂ atmosphere. For passaging, confluent plates were washed once with medium, followed by a short trypsinization with 0.005 % trypsin-EDTA.

3.2.3.3 Hybridoma cell culture

Hybridoma cells were culture on untreated tissue culture dishes (Falcon). Before harvesting hybridoma supernatant, the cells were spilt at very high dilutions and allowed to grow for about one to two weeks. The supernatant was cleared from cellular debris by centrifugation at 3500 rpm for 20 minutes. The hybridoma supernatant was aliquoted and stored untreated at -20° C.

3.2.3.4 Transient transfection of COS-7 and oli-neu cells

COS-7 cells were washed with PBS, trypsinized (or scraped mechanically), pelleted and resuspended in electroporation buffer (supplemented freshly with 25 mM Mg₂SO₄). Plasmids were used at 10 µg/300 µl cell suspension (4×10^6 cells/ml) for electroporation in a Biorad Gene Pulser (350 V and 450 µF). The average efficiency achieved using above parameters varied between 80 to 95 %.

Oli-neu cells were either transfected with Fugene 6 (Roche) for immunocytochemical or by electroporation for biochemical analysis. Fugene (1 µl) and DNA (1 µg) both diluted in DMEM without serum were mixed and allowed to stand at RT for 10 minutes, before addition to the cells. The average efficiency of transfection in oli-neu cells varied between 5 to 10 %. For biochemical analysis the suspension of oli-neu cells (5×10^6 cells/ml) suspended in DMEM without serum, after scrapping from culture dishes and centrifugation, was electroporated at 250 V/950 µF (BioRad Gene Pulser). Plasmids were used at 15 to 30 µg/400 µl cell suspension. The average efficiency of transfection using electroporation was about 15 to 25 %.

3.2.3.5 Stable transfection of oli-neu cells

To establish stable cell lines expressing PLP^{wt}-GFP and PLP^{msd}-EGFP, first a killing curve for oli-neu cells in response to increasing concentrations of Hygromycin B (Roche, Cat no 843555) was established. Absolute killing was achieved at a concentration of 500 µg/ml of Hygromycin B. Oli-neu cells were co-transfected with StuI linearized PLP-EGFPNI and AflIII linearized pMSCV-hygro (clonotech) in a ratio of 10:1 of linearized plasmids. Cells were allowed to express hygromycin phosphotransferase and 24 hours post transfection, SATO media was supplemented with 500 µg/ml Hygromycin B. Media was changed once after 10 days to wash off the dying cells. Approximately 3 to 4 weeks after transfection, PLP-EGFP expressing clones were picked on an inverted Leica-DMIRBE fluorescence microscope. Clones were diluted and seeded in PLL coated 96 well-plates (Falcon) at a dilution of one single cell per two wells. Cells from a well with single colony were expanded and maintained as a PLP^{wt}-GFP or PLP^{msd}-EGFP expressing monoclonal cell lines.

3.2.4 Immunocytochemistry

3.2.4.1 Immunocytochemistry of living cells

Live staining of cells with antibody 3F4 was performed at 4 °C on water/ice slurry (unless stated otherwise). Cells grown on PLL-coated coverslips (24 well plates) were washed once with ice-cold DMEM and primary antibodies diluted in ice-cold DMEM were applied directly onto the cells for 10 minutes. Cells were washed twice with DPBS and fixed with 2 % PFA for 10 minutes. Cells were shifted to RT during fixation. After two additional washes in DPBS, Cy3-conjugated secondary antibodies diluted in DMEM were applied for at least 30 minutes. Cells were washed twice in DPBS, rinsed in ddH₂O, and mounted. Live staining of cells with antibody O10 was performed as previously described (Jung et al., 1996).

3.2.4.2 Immunocytochemistry of fixed cells

Immunostainings were carried out 18 to 24 hours after transfection. All steps were performed at RT, unless stated otherwise. Cells grown on PLL-coated coverslips were washed once with TBS and fixed for 5 minutes in 2 % PFA. Cell were then washed twice

for 10 minutes in TBS, permeabilized with 0.01 % saponin in TBS (for 1-10 minutes) and blocked in blocking buffer for at least 30 minutes. Primary antibodies diluted in blocking buffer were applied for at least 1 hour at room temperature or overnight at 4 °C. After three washes in TBS (10 minutes each), fluorochrome-conjugated secondary antibodies were applied for at least 45 minutes. After three washes with TBS (10 minutes each), cells were rinsed in distilled water, and mounted in Aqua-Poly/Mount (Polysciences, Warrington, PA) on glass slides.

3.2.5 Confocal analysis.

Fluorescent images were captured on a confocal microscope (LSM 510; Carl Zeiss MicroImaging, Inc.) with a 63x oil plan-Apochromat objective (NA 1.4; Carl Zeiss MicroImaging, Inc.). For time-lapse live cell imaging, coverslips with cells were mounted into a live cell imaging chamber and observed in a low auto-fluorescence imaging medium at 37 °C. The temperature was controlled by means of a digital system (Tempcontrol 37-2; PeCon) or a custom-built perfusion system. For final analysis, captured LSM images were exported as TIF images. Documentation and processing of TIF images were done with Photoshop 7.0.1.

4 RESULTS

4.1 Cysteine mediated cross links cause Pelizaeus-Merzbacher Disease

4.1.1 Video microscopy of EGFP-tagged PLP in oligodendrocytes

Studying PLP in transfected COS-7 cells suffers from possible artifacts of overexpression in a non-glial cell type. We have therefore used primary oligodendrocytes and an oligodendroglial cell line [oli-neu (Jung et al., 1995)], in addition to COS-7, to compare mutant and wildtype PLP. For visualization, we tagged PLP with either the myc epitope or the enhanced green fluorescent protein, separated from the C-terminus by a flexible linker (Figure 7). In all these experiments, wildtype PLP (PLP^{wt}, including the tagged isoforms) exhibited surface expression (Figure 8). In oli-neu cells, PLP^{wt} reached the cell surface within 8 hours after transfection (movie 1 in attached compact disc). Within 24hours, PLP^{wt} accumulated in LAMP1-positive late endosomes (movie 2 in attached compact disc). In contrast, a mutant PLP isoform derived from myelin synthesis-deficient mice (PLP^{msd}, A242V substitution; a natural model for the connatal form of PMD) is retained in the ER of oligodendrocytes (movies 3 and 4 in attached compact disc), in agreement with previous data (Gow et al., 1998). In the following, we will refer to the reticular pattern of intracellular PLP expression as ER retained (Figure 8).

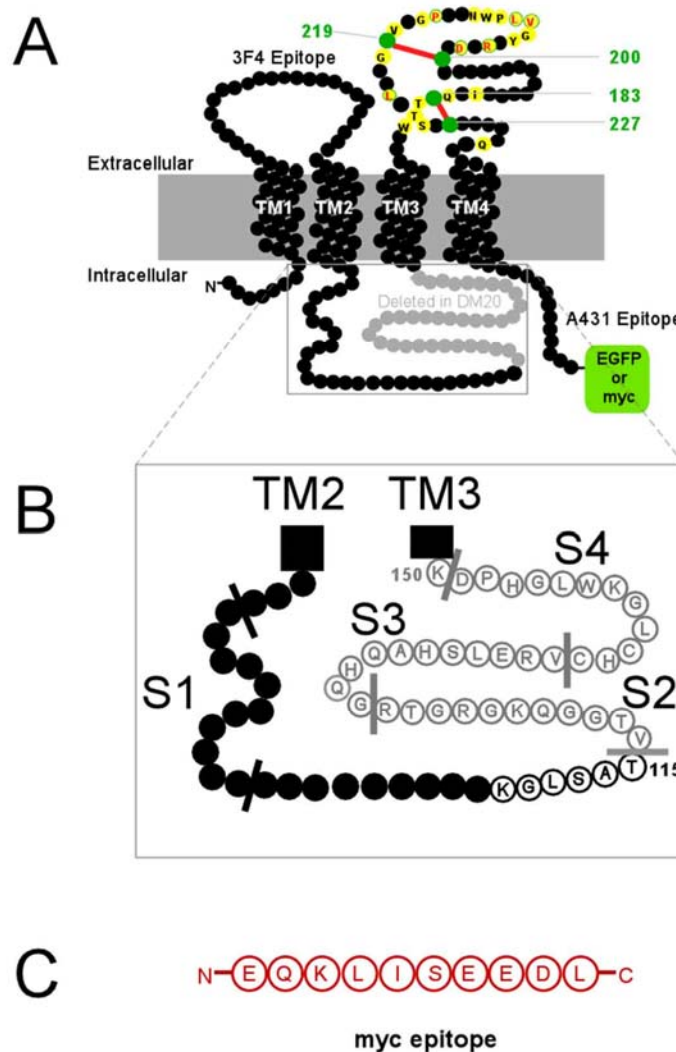


Figure 7: Structure of PLP/DM20 and mutations associated with Pelizaeus-Merzbacher disease

A) Two-dimensional model of PLP (276 residues as black beads) and its splice isoform DM20, lacking 35 residues (marked in grey) from an intracellular loop. The orientation of four transmembrane domains (TM1-4) positions both N- and C-terminus into the cytoplasm. Within the second extracellular domain (EC2), the position of 4 cysteine residues (in green) for two disulfide-bridges (in red) is indicated. Also indicated are C-terminal epitope tags used in this study (EGFP or myc) and the approximate positions of extracellular (3F4) and intracellular (A431) antibody binding sites common to PLP and DM20. Positions of amino acids in EC2 that are substituted in patients with Pelizaeus-Merzbacher disease are marked in yellow. Those that have been studied in detail here carry the single letter code of the wildtype sequence, labeled in red.

B) Schematic view of the intracellular loop of PLP/DM20, flanked by TM2 and TM3, and including a PLP-specific sequence (open grey circles). The positions of 4 segments (S1-S4) are indicated, each of which has been replaced individually with the myc-epitope tag (in C), giving rise to different PLP "chimeras" (S1-S4). These constructs were used to test for the presence of an ER retention signal in PLP (for details see text).

C) Amino acid sequence of the myc-tag peptide used to replace intracellular PLP segments S1-S4 (in B).

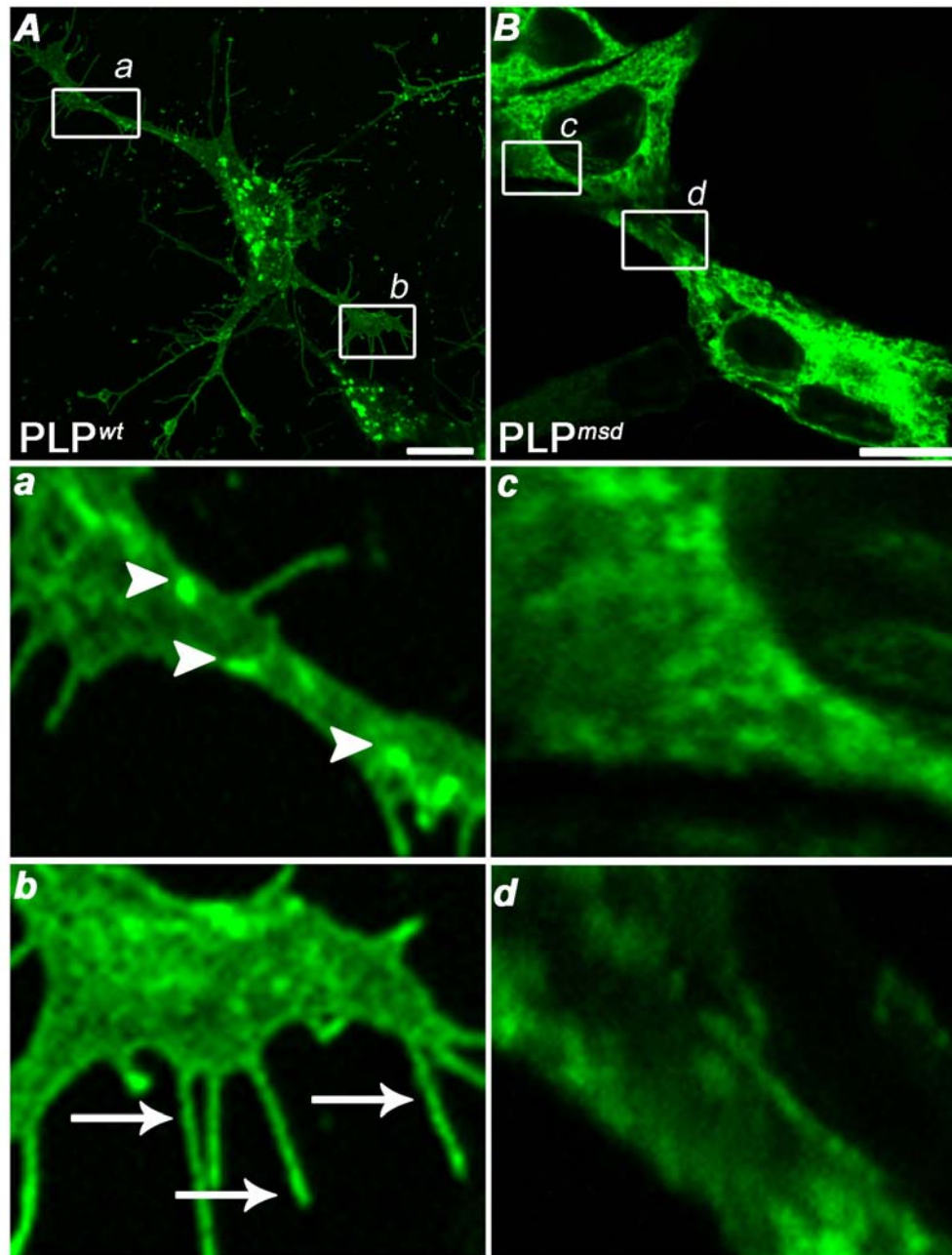


Figure 8: Subcellular distribution of PLP^{wt} and PLP^{msd} fused to EGFP, in oli-neu cells

A) When expressed, PLP^{wt} exits the ER and reaches the cell surface. Glial cells protrude numerous filopodial processes and PLP^{wt} accumulates in endosomal/lysosomal compartment. Magnifications (a, b) of boxed area in A, are magnified glial processes showing endosomes accumulation (arrow head) and filopodial protrusions (arrow). Scale bar: 10 μ m.

B) PLP^{msd} (A242V substitution) is retained in the ER of oli-neu cells. Glial cells lack any visible processes. There is a reticular distribution of EGFP fluorescence, with no accumulation in endosomal compartment. Magnifications (c, d) of boxed area in B, are magnification in a close proximity to the cell surface. Note that there is complete absence of fine microspikes. Scale bar: 10 μ m.

4.1.2 Trafficking differences between mutant PLP and DM20 isoforms

PLP and DM20 with substitutions in transmembrane domains (such as PLP^{msd}) are both retained in the ER (Gow et al., 1994; Jung et al., 1996). In contrast, there is an unexplained difference in trafficking of some PLP and DM20 isoforms if they carry the same substitution in EC2 (Gow et al., 1997; Gow and Lazzarini, 1996). Also in oli-neu cells, some EC2 mutants of PLP (PLP^{D202N}, PLP^{L209H}, PLP^{P215S}) were ER retained (Figure 9 and data not shown) whereas the corresponding mutations in DM20 were cell surface expressed and accumulated in late endosomes (Figure 9 A). In these experiments, surface expression was confirmed by live staining with the monoclonal antibody 3F4 (Greer et al., 1996) directed against an extracellular PLP epitope (Figure 7).

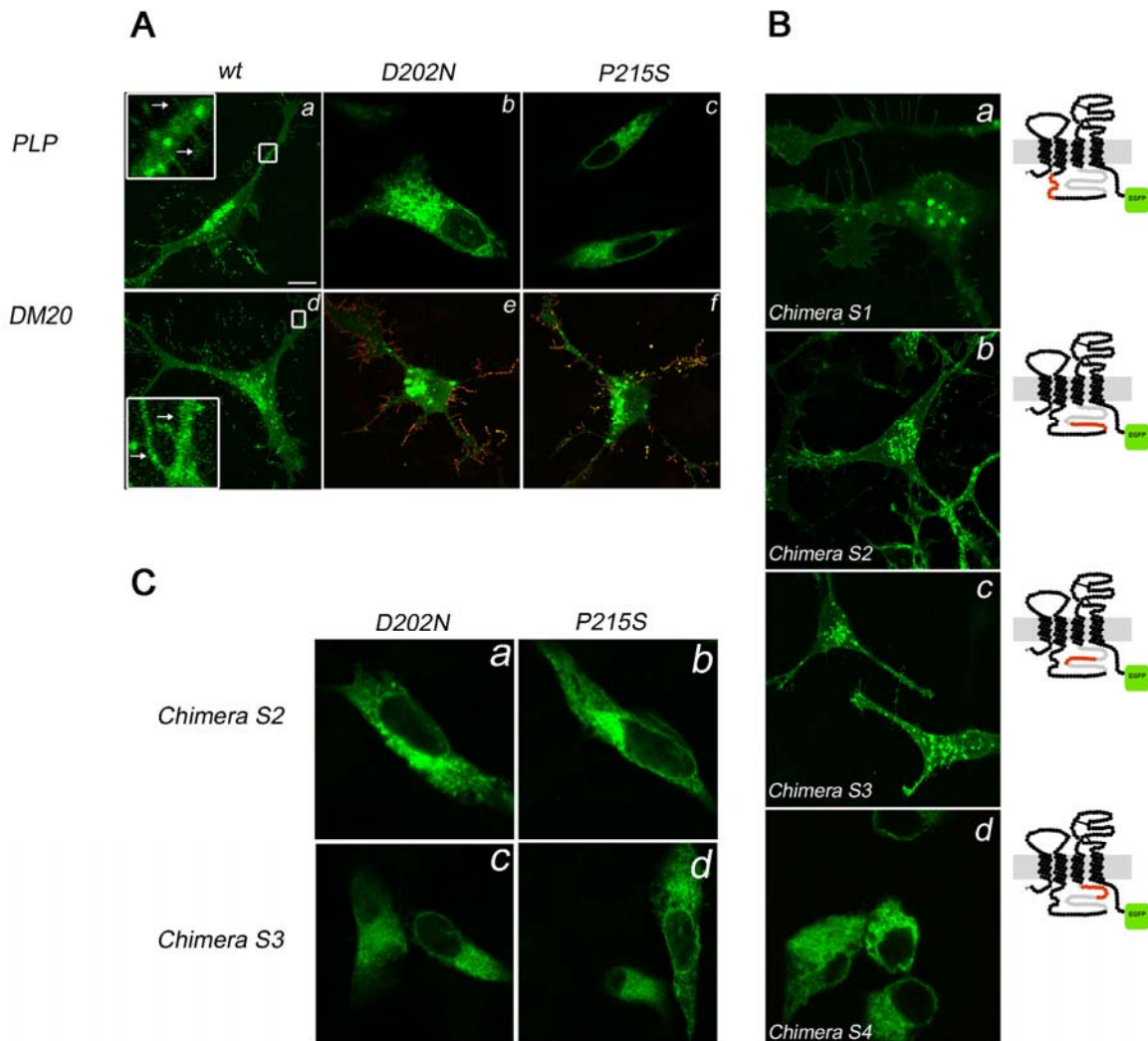


Figure 9: ER retention in oli-neu cells distinguishes PMD-associated isoforms of PLP, DM20, and chimeras

A) Wildtype PLP and DM20, here fused to a C-terminal EGFP, exit the ER and reach the cell membrane (a, d), as shown by confocal imaging revealing distal transport vesicles in glial processes and membrane-associated fluorescent microspikes (arrow in magnified inset). Specific PMD substitutions that map into EC2 (D202N, P215S; amino acid positions refer to the sequence of PLP) cause ER retention of mutant PLP (b, c) but not of mutant DM20 (e, f). This could be confirmed by DM20 live-staining (in red) with monoclonal antibody 3F4 (e, f). The intracellular EGFP signal marks either a late endosomal compartment (a, d, e, f) or the reticular ER when PLP is retained (b, c). Scale bar: 10 μm (A to C)

B) In search for a PLP-specific ER retention signal, PLP-myc chimeras S1-S4 were expressed that lacked different segments (S1-S4 in Figure 7) of the PLP-specific intracellular loop (schematically indicated on the right). In the absence of any further modification, chimeras S1-S3 were able to exit the ER of oli-neu cells, reaching a late endosomal compartment (a-c). Chimera S4 was by itself ER-retained, suggesting that no retention signal had been removed.

C) Importantly, in combination with PMD mutations mapping into EC2 (D202N and P215S), also chimeras S2 (a, b) and chimera S3 (c, d) were ER-retained. This suggests the absence of any retention signal in the PLP-specific cytoplasmic loop that could explain the differential ER retention of mutant PLP and DM20 (A).

PLP and DM20 differ in their cytoplasmic loop, whereas the tested PMD mutations map into EC2 (Figure 7), which appears contradictory. Theoretically, PLP could harbor a retention signal in the PLP-specific loop that is missing in DM20. To test this, we generated 4 chimeric constructs in which the myc epitope replaced equally short segments (S1 to S4) in the intracellular loop of PLP (Figure 7). In the absence of any PMD mutation, 3 out of the 4 chimeras tested trafficked to the oligodendrocyte surface, similar to PLP^{wt} (Figure 9B panel a-c). Chimera S1, replaced for a segment common to both PLP and DM20, was unlikely to include a PLP-specific retention signal. On the other hand, replacement of S4 resulted by itself in ER retention. We therefore tested PLP chimeras S2 and S3 in combination with PMD-causing mutations in EC2 (PLP^{D202N} and PLP^{P215S}). Remarkably, none of these mutant PLP chimeras trafficked like mutant DM20. All were retained in the ER (Figure 9 C). Thus, the intracellular loop of PLP does not harbor essential ER retention signals that could explain the trafficking differences between EC2 mutations of PLP and DM20.

By Kyte-Doolittle analysis of DM20, the N-terminus of TM3 exhibits an extended hydrophobicity of 5 residues compared to the TM3 region of PLP (Figure 7 and Figure 10), owing to the absence of charged amino acids in DM20 (Nave et al., 1987). We therefore hypothesized that TM3 of DM20 (but not of PLP) can shift its position within the lipid bilayer by more than one helical turn when required for protein folding. For DM20, this flexibility might compensate minor mutation-induced constraints that impair normal folding of EC2. Such a compensatory shift of TM3 could potentially explain why specific mutant forms of DM20 (but not of PLP) can pass the quality control of the ER. When the polar amino acid (T) that flanks TM3 in DM20 was replaced with a basic residue (K), this modified TM3 was "shorter" and cell surface expressed (Figure 11 A). Importantly, when mutations in EC2 were added, the DM20^{T115K} variants showed substantial ER retention (Figure 11 B, C), in strong support of our model. Similarly, when we replaced all 4 residues (LSAT¹¹⁵) that precede TM3 in DM20 by the corresponding 4 residues of PLP (HPDK¹⁵⁰), the DM20^{HPDK} protein behaved like DM20^{wt} (Figure 10 and Figure 11). However, introducing additional mutations (i.e. D202N, L209H and P215S) also here caused this DM20 to be strictly retained in the ER (Figure 11 E and F). Thus, the motif 'HPDK' in the PLP-specific loop serves as a stop-transfer-signal for TM3 (Figure 10),

limiting its ability to move in the lipid bilayer and to compensate for (mutation-induced) minor misfoldings of EC2.

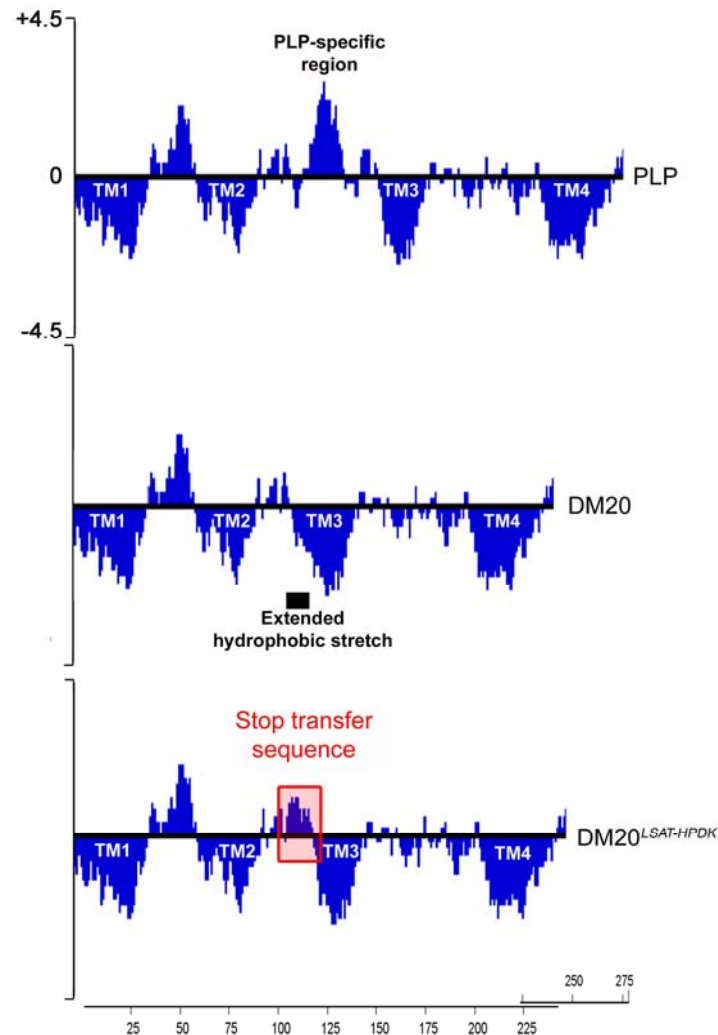


Figure 10: Kyte and Doolittle hydropathy plot of PLP, DM20 and DM20^{LSAT-HPDK}

Kyte and Doolittle hydropathy plot of PLP, DM20 and DM20^{LSAT-HPDK} chimera, scale bar: same for all as in PLP. Hydrophilicities plotted with a window of 11 amino acid residues, negative hydrophilicity reveals a highly hydrophobic stretch. Both PLP and DM20 share four highly hydrophobic transmembrane stretches. PLP specific region imparts a highly hydrophilic nature to intracellular loop (IC). In contrast, DM20 bears an extended hydrophobic stretch, which allows TM3 to glide a single alpha helical turn up or down to reorient EC2 during local misfolding. This gliding phenomenon can be completely reversed by simply reversing the positive hydrophobicity of DM20 specific region to a positive hydrophilicity by replacing amino acid residues LSAT to HPDK. This DM20 not only display hydrophilic characters like PLP but also traffics like PLP^{wt} in transfected cells

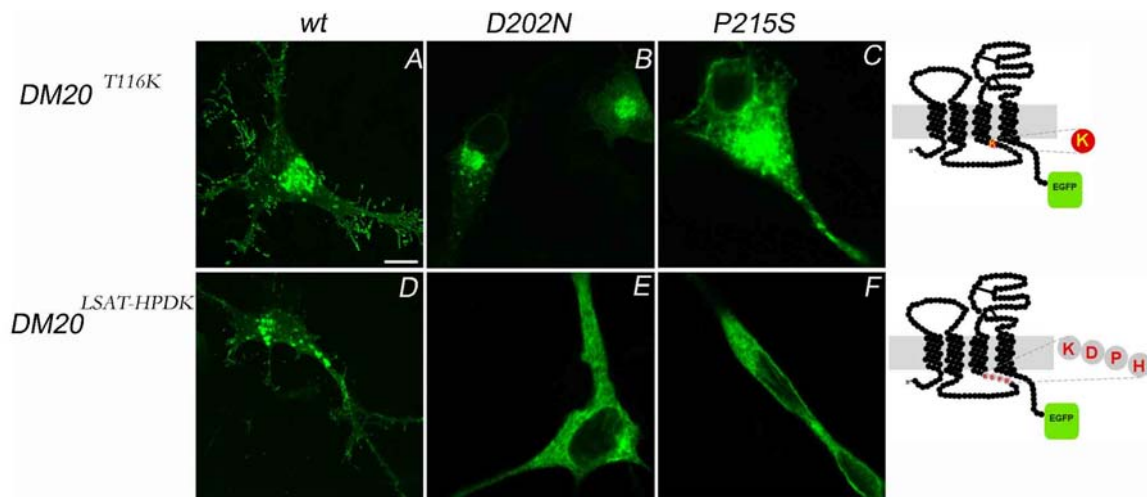


Figure 11: Length and position of TM3 determine ER retention or release of mutant DM20

The third TM domain of DM20 is potentially longer than in PLP, due to a stretch of 4 uncharged residues in DM20 (pos. 112-115) immediately preceding TM3. Replacing the juxta-membrane threonine by a lysine in DM20 (T115K) did not prevent cell surface expression (A), but is likely to reduce transmembrane domain sliding of TM3. Importantly, T115K partially impaired transport of two PMD mutant isoforms (B, C). An even greater effect on DM20 retention had the substitution of 4 consecutive residues (HPDK¹⁵⁰: the predicted TM3 "stop transfer" signal in PLP at the equivalent position in DM20 (LSAT¹¹⁵) (Figure 10). Also this modification (depicted on the right) allowed DM20 to traffic normally (D) but caused complete ER-retention when combined with mutations D202N (E) or P215 (F). Together, this strongly suggests that a subtle transmembrane domain sliding of TM3 allows DM20 (but not PLP) to properly fold the globular EC2 domain in the ER lumen, despite its PMD-causing substitution. Scale bar: 10 μ m.

4.1.3 The role of disulfide bridges in PLP folding

How can minor misfoldings within EC2 have so dramatically different consequences in PLP and DM20? As depicted in (Figure 7 A), four cysteine residues form bridges C¹⁸³-C²²⁷ and C²⁰⁰-C²¹⁹ (Shaw et al., 1989; Weimbs and Stoffel, 1992). To analyze a possible role of these bridges in EC2 folding, we analyzed various cysteine-to-serine and cysteine-to-alanine mutants in transfected oli-neu and COS-7 cells. PLP lacking bridge C¹⁸³-C²²⁷ was strictly retained in the ER, similar to PLP^{msd}, as indicated by the reticular immuno-staining of cells that also lacked visible processes (Figure 12 B, right panel). Thus, the membrane-proximal bridge is essential to pass the quality control system of the ER. Unexpectedly, PLP lacking the outer bridge C²⁰⁰-C²¹⁹ was readily detectable on the cell surface (Figure 12, left panel), very similar to wildtype PLP (Figure 12 A, left panel). These oli-neu cells also exhibited a multipolar morphology with numerous filopodial processes (magnified in inset).

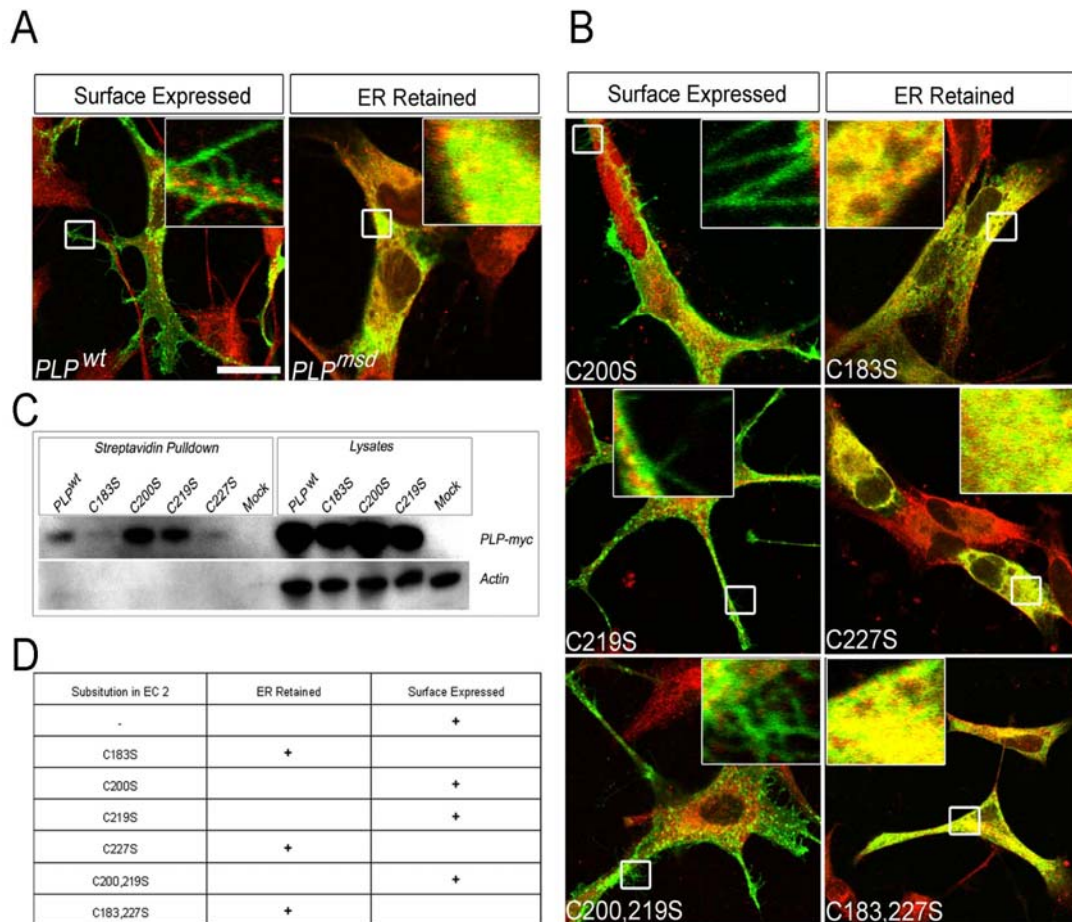


Figure 12: The function of extracellular disulfide-bridges in PLP folding and cell surface expression

A) In transfected, fixed and permeabilized oli-neu cells, mutant PLP-myc (in green) co-localizes with the endogenous chaperone and thiol-disulfide oxidoreductase PDI (in red). Only merged images are shown. **Left:** Wildtype protein (PLP^{wt}) reaches the cell surface, as demonstrated by green fluorescent microspikes at the tip of processes (magnified in inset), **Right:** In contrast, PLP^{msd} (derived from *jimpy-msd* mice) fails to reach the cell surface. There are no labeled microspikes (magnified in inset), but there is substantial overlap between PLP^{msd} and PDI (yellow). Note also the paucity of cellular processes. Scale bar: 20µm

B) From two disulfide bridges in EC2, the “outer” one (Cys²⁰⁰-Cys²¹⁹) is dispensable for folding and cell-surface expression. To test the function of each cysteine bridge (see Fig 1A) for PLP folding and colocalization with PDI (in red), single and double cysteine-to-serine substitutions were engineered for each disulfide bridge. Replacing one or both cysteines of the outer bridge did not interfere with cell surface labeling of PLP (in green), as indicated by fluorescent microspikes (left panels and magnified in insets). In contrast, replacing one or both cysteines of the membrane-proximal bridge (Cys¹⁸³-Cys²²⁷) led to severe misfolding, as visualized by ER retention and colocalization of PLP with PDI (yellow overlay in inset), similar to PLP^{msd} (in A). Only merged images are shown. Thus only the membrane-proximal disulfide bridge is essential to reach normal folding of PLP.

C) To obtain independent biochemical evidence that PLP^{C200S} and PLP^{C219S} (lacking the outer bridge) are cell surface expressed in COS-7 cells, all membrane proteins were biotinylated with membrane impermeable NHS-sulfo-biotin prior to cell lysis, and proteins were pulled down with streptavidin-agarose beads. Only myc-epitope labeled PLP^{wt}, PLP^{C200S}, and PLP^{C219S} could be detected on Western blots (lanes 1, 3, 4). The absence of actin in the first six lanes confirms that only live cells were biotinylated. Total lysates served as positive controls for transfection and loading (mock: transfected with plasmids lacking a cDNA insert).

D) Summary of subcellular distribution of PLP, interpreted from immuno-cytochemistry of oli-neu (A, B) and biochemistry of COS-7 cells (C).

To biochemically confirm the presence of PLP cysteine mutants at the cell surface, we biotinylated all surface proteins of transfected COS-7 cells prior to harvesting, and precipitated the marked proteins with streptavidin-conjugated agarose beads. Subsequent western blot analysis demonstrated that PLP^{wt}, PLP^{C200S}, and PLP^{C219S} were indeed in the pool of biotinylated cell membrane proteins. In contrast, PLP^{C183S} and PLP^{C227S} single mutant isoforms were almost undetectable, confirming their intracellular retention (Figure 12 C and D).

4.1.4 Genetic uncoupling of protein misfolding and ER retention

Overexpression of PLP^{wt} in either COS-7 or in oli-neu cells led to accumulation in late endosomes, as demonstrated by Lamp-1 costaining about 24 hours later (Figure 13 A). Since PLP^{wt} accumulation in late endosomes has been documented for primary oligodendrocytes and in vivo (Trajkovic et al., 2006), we consider this the normal pathway of PLP trafficking. Endosomal cycling of PLP forms a membrane secretory compartment that is important for regulated exocytosis and myelin growth (Trajkovic et al., 2006). Also the single mutants PLP^{C200S}, PLP^{C219S}, and the double mutant PLP^{C200,219S} accumulated in this Lamp1-positive endosomal compartment (Figure 13 C,D and E). In contrast, PLP^{C183S} never reached the surface or colocalized with Lamp1, even 40 hours after transfection (Figure 13 B).

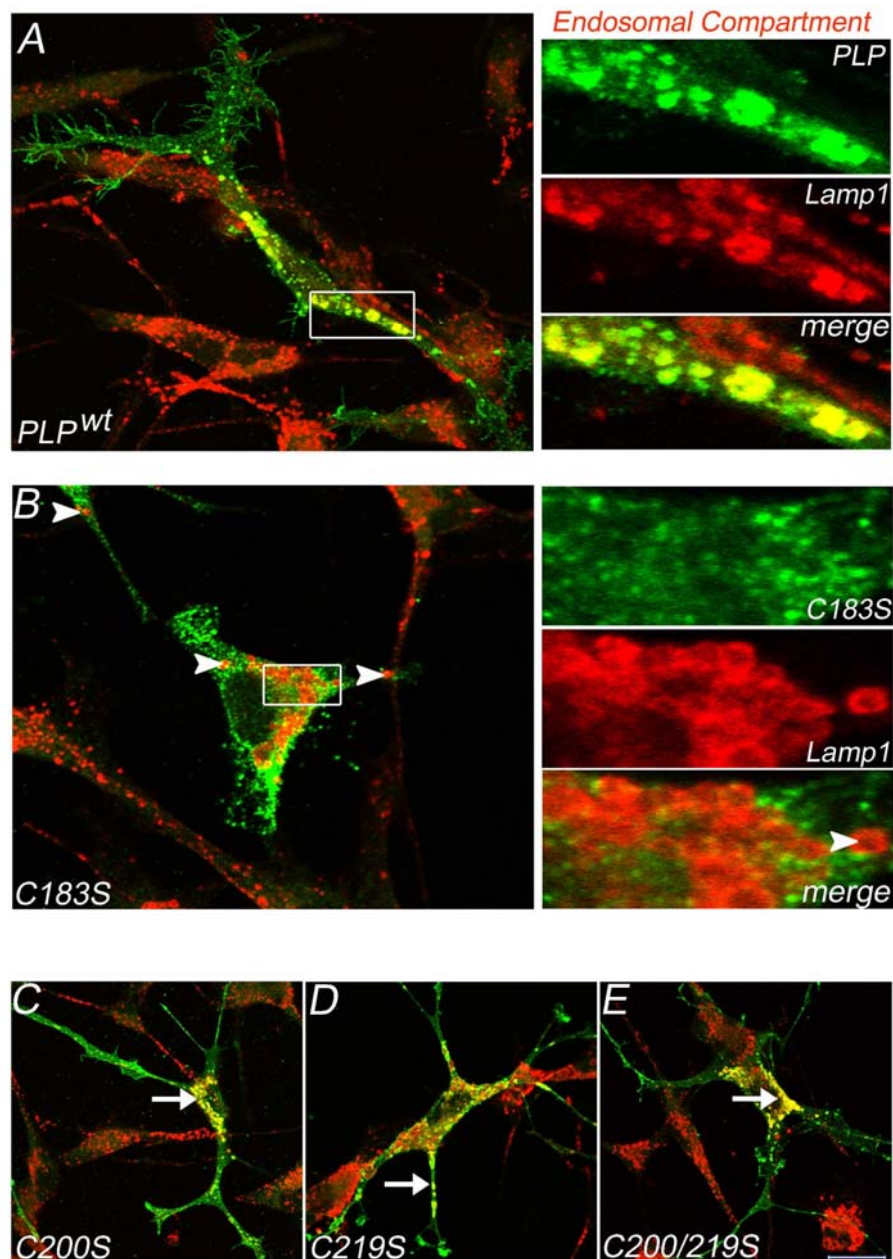


Figure 13: PLP cysteine mutants that reach the cell surface also accumulate in endo/lysosomes

A) 24 hours after transfection of oli-neu cells, wildtype PLP (in green) can be co-localized with Lamp1 (in red) in a late endosomal/lysosomal compartment. Boxed area is magnified on the right.

B) PLP^{C183S}, lacking the essential disulfide bridge in EC2 (C¹⁸³-C²²⁷), fails to reach the Lamp1-positive compartment, strongly suggesting that it requires endosomal reuptake from the cell surface. Boxed area is magnified on the right (arrowhead, lack of PLP-Lamp1 colocalization). Same results were obtained for PLP^{C227S} and PLP^{C183,227S} (not shown).

C-E) By the same criteria, all PLP mutants lacking the distal disulfide bridge, by replacement of one or two cysteines (as indicated), showed normal trafficking and colocalization with Lamp1 (white arrow), similar to wildtype PLP (in A). Scale bar: 20 μ m.

Next, we tested the monoclonal antibody 010, recognizing a conformation-sensitive PLP epitope present in wildtype but not in mutant PLP/DM20 isoforms (Jung et al., 1996). Interestingly, while PLP lacking disulfide bridge C^{200} - C^{219} reached the surface of transfected cells similar to the wildtype protein, it remained an 010-negative "misfolded" mutant (Figure 14). This demonstrates that PLP misfolding and ER-retention can in principal be uncoupled.

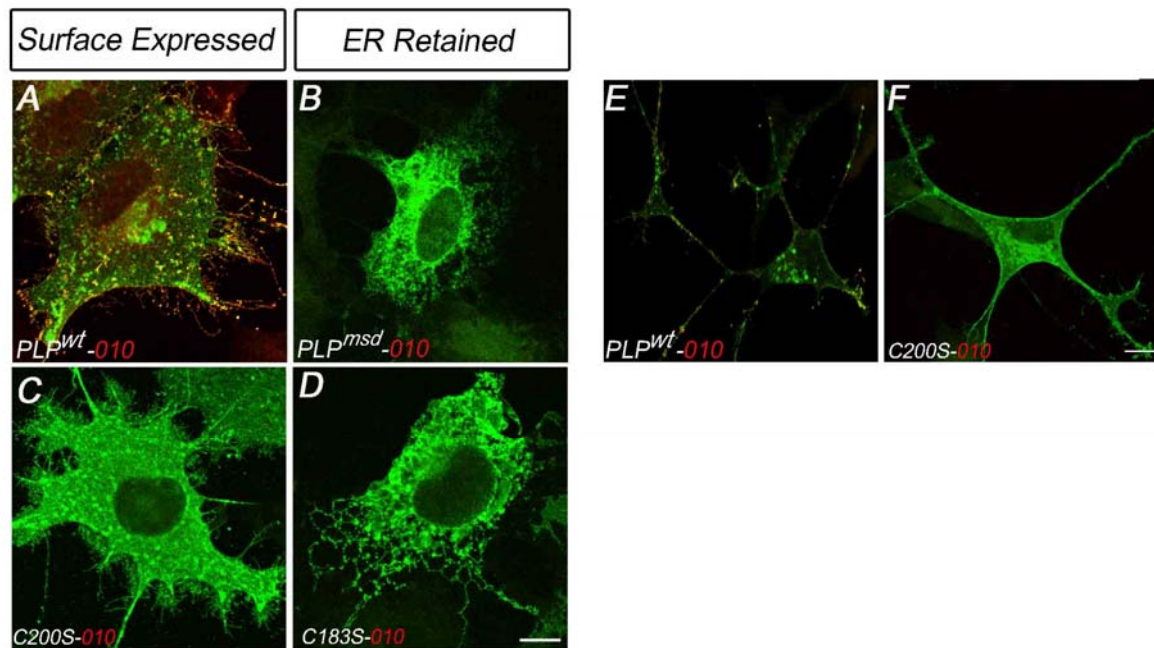


Figure 14: Uncoupling of protein folding, ER exit, and the wild-type conformation of PLP

We used COS-7 (A, B, C and D) and oli-neu (E, F) to monitor the emergence of the conformation-sensitive O10 epitope in PLP cysteine mutants that pass or fail the quality control check in the ER. Following the live-staining of transfected cells with the monoclonal antibody O10 (in red), cells were permeabilized and stained with the C-terminus specific PLP polyclonal antibody A431 (see Figure 7). Unexpectedly, only wildtype PLP exhibited the O10 epitope (A, E). PLP^{C200S} (lacking the distal disulfide bridge) was surface-expressed but O10-negative (C, F), similar to PLP^{C183S} (lacking the essential proximal bridge) and to PLP^{msd} (B, D). These data are in agreement with (but do not prove) that the distal disulfide bridge C^{200} - C^{219} is required to form PLP homo-oligomers that specifically exhibit the O10 epitope. Scale bar: 10 μ m.

4.1.5 ER retention of mutant PLP/DM20 and its rescue by removal of cysteines

PMD point mutations that alter EC2 have a particular severe phenotype in vivo (Nave and Boespflug-Tanguy, 1996), yet their effect on PLP folding and function is not understood. Although the disulfide bridge C^{200} - C^{219} in EC2 was dispensable (Figure 12 B), we found a

natural PMD mutation that involved one of these cysteines (PLP^{C219Y}) (Osaka et al., 1999) and clearly led to ER retention A, B. Since the highly related mutation PLP^{C219S} does not cause ER retention (Figure 12), we hypothesized that the unpaired C²⁰⁰ is sterically exposed when a larger residue (Y²¹⁹) causes local misfolding, and that unpaired C²⁰⁰ is the real cause of ER retention. Indeed, substituting this cysteine in a double-mutant protein (PLP^{C200S,C219Y}) completely rescued the phenotype of oli-neu cells (Figure 15 C and D). Western blot analysis revealed that PLP^{C219Y} (but not PLP^{wt} or the rescued double mutant) formed dimers that were sensitive to reducing agents (Figure 15 E). This strongly suggests that the retention of PLP^{C219Y} is caused by cysteine (C²⁰⁰) oxidation and abnormal crosslinks that prevent normal oligomerization.

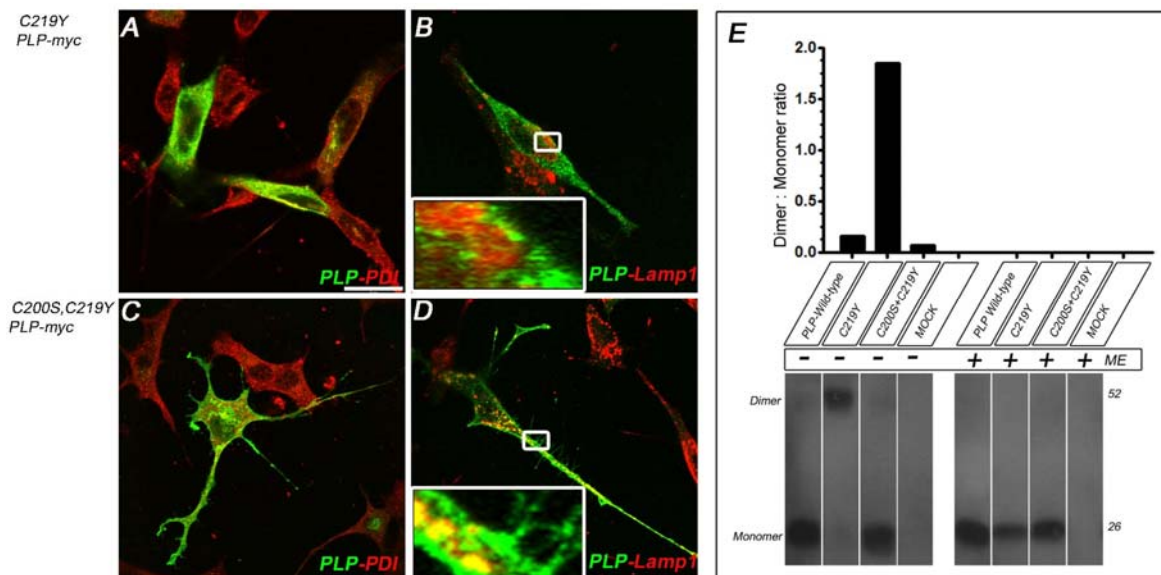
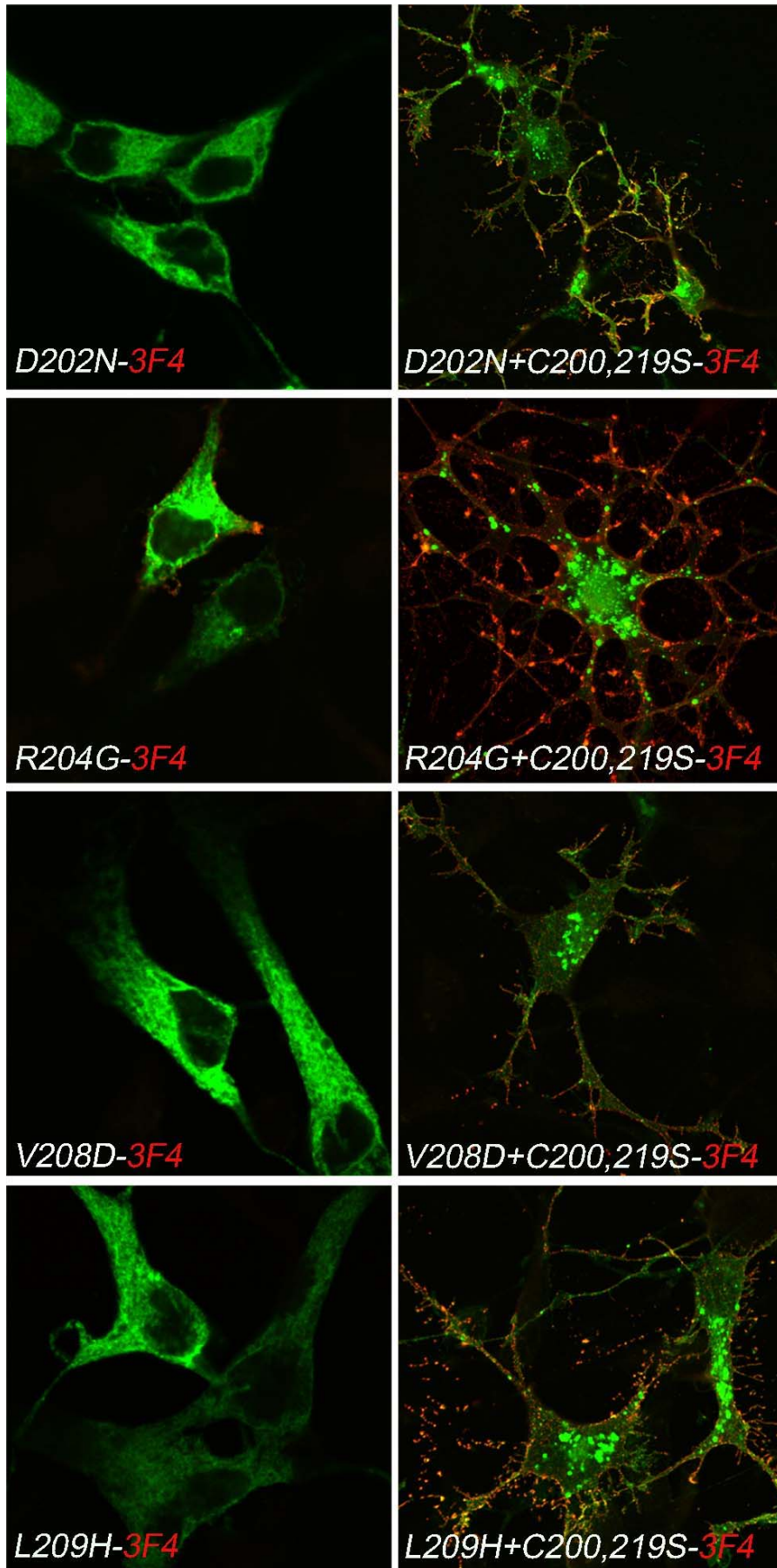


Figure 15: Unpaired Cys²⁰⁰ causes ER retention and dimerization of a PMD mutant PLP^{C219Y}

Oli-neu cells were transfected to express a myc-epitope labeled natural PMD mutant PLP^{C219Y} (A, B) or a "double mutant" PLP^{C219Y,C200S} (C, D). Only merged images are shown. The PMD mutant was retained as visualized 24 hours post transfection by lack of processes and colocalization of PLP (in green) with the ER marker PDI (red in A), but segregation of PLP from the late endosomal/lysosomal marker Lamp1 (red in B and magnified in inset). In contrast, the double mutant PLP behaved like a "wildtype" protein, with reduced colocalization with PDI and the branched morphology of oli-neu cells (in C), and the emergence of green fluorescent microspikes on processes (D and magnified in inset). PLP^{C219Y,C200S} also overlapped with the endosomal marker (yellow area in D). Thus, it is not Y²¹⁹ but an unpaired C²⁰⁰ that emerges as the cause of PMD.

When oli-neu cell extracts were analyzed by semi-quantitative Western blots (E), mutant PLP^{C219Y} revealed predominantly a dimer band, whereas PLP^{wt} and the "rescued" PLP^{C219Y,C200S} were monomeric. In the presence of mercaptoethanol (ME), all forms were monomeric, demonstrating that dimerization of PLP^{C219Y} can be attributed to cysteine oxidation. Scale bar: 10 μ m.

Next we hypothesized that many other PMD point mutations mapping into EC2 could likewise induce minor misfoldings that, while leaving C²⁰⁰ and C²¹⁹ in place, are sufficient to impair the formation of a disulfide bridge. We analyzed several of the PMD-associated mutations, including PLP^{D202N}, PLP^{R204G}, PLP^{V208D}, PLP^{L209H} and PLP^{P215S} (for review see (Nave and Boespflug-Tanguy, 1996)). All mutant PLP isoforms were strictly retained in the ER of oli-neu cells [Figure 16 left column (or COS-7 cells Figure 17, left column)]. However, when combined with a C200S and C219S substitution, the triple-mutant PLP isoforms showed robust surface expression, as shown by live-staining, right column. Taken together, PMD point mutations induce small structural changes in EC2, thereby exposing unpaired cysteines that become responsible for ER retention. Some DM20 mutants are protected from this pathomechanism, because higher flexibility of TM3 facilitates normal folding of EC2, despite the disease-causing substitution.



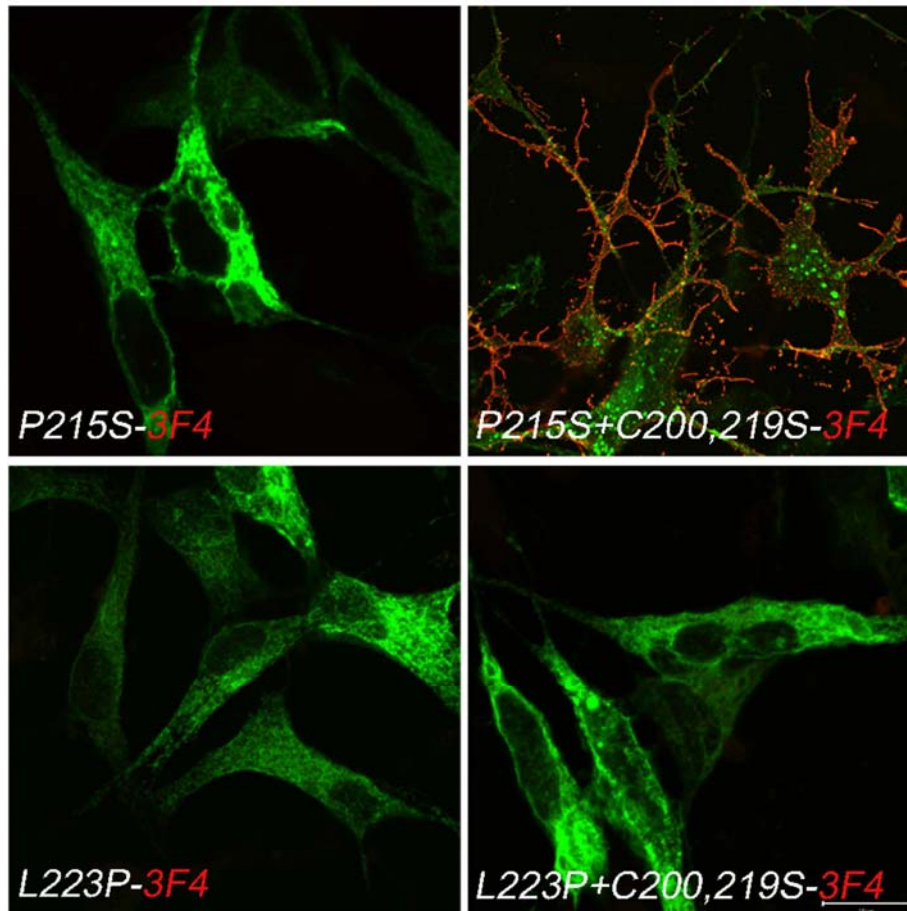


Figure 16: PMD-causing PLP mutations can be rescued by the replacement of cysteines

To distinguish PLP at the cell surface from PLP in intracellular compartments, oli-neu cells that express various EGFP-tagged mutant PLP isoforms (in green) were additionally live-stained for PLP, using the monoclonal 3F4 antibody (in red; see Fig 1A). Only merged images are shown. The same results were obtained with COS-7 cells (Figure 17 and data not shown). We analyzed various natural PMD-causing mutations that map into EC2 (PLP^{D202N}, PLP^{R204G}, PLP^{V208D}, PLP^{L209H}, PLP^{P215S}, PLP^{L223P}) for cell surface expression of PLP in the absence (**left column**) or the presence (**right column**) of additional point mutations that substituted C²⁰⁰ and C²¹⁹ for serine. Remarkably, in absence of C²⁰⁰ and C²¹⁹, the PMD-causing mutants were fully "rescued" from ER retention, and PLP was localized at the cell surface (red label) and in the late endosomal/lysosomal compartment (in green). In the presence of EC2 cysteines, all PMD mutants were 3F4-negative and confined to the ER. Note also the lack of glial processes. This reveals that ER retention of natural disease-causing mutants (not involving cysteine residues themselves) are mediated by the cysteines in EC2. Only one mutant tested (PLP^{L223P}) could not be "rescued", most likely because misfolding induced by a proline perturbs even the second "essential" disulfide bridge (see Figure 12). Scale bar: 10 μm .

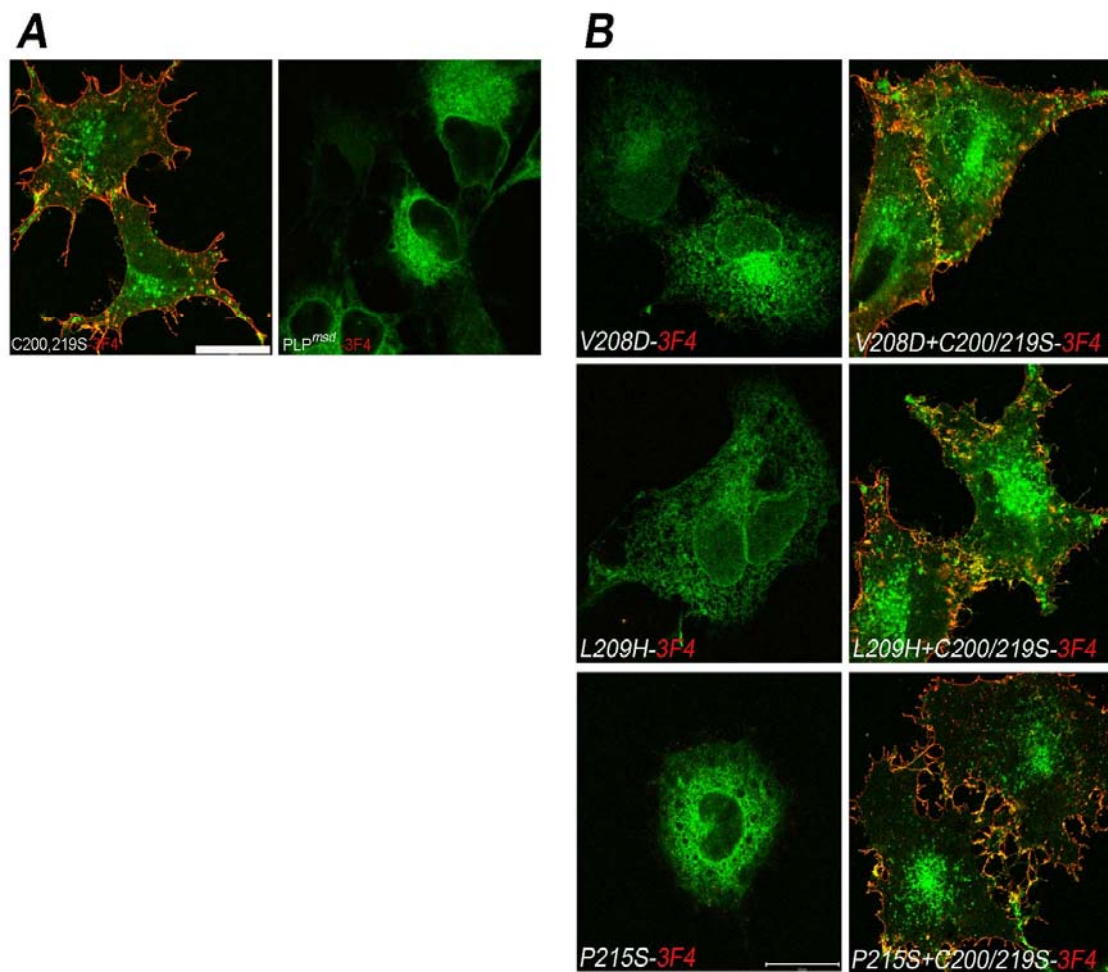


Figure 17: PMD-causing PLP mutations rescued by the replacement of cysteines

A) To distinguish PLP at the cell surface from intracellular compartments, COS-7 cells that express EGFP-tagged mutant PLP isoforms (in green) were additionally live-stained with the monoclonal 3F4 antibody (in red; see (Figure 7)). Only merged images are shown. Left: normal trafficking of PLP lacking the disulfide bridge C^{200} - C^{219} . Right: ER retention of PLP^{msd} . Note the absence of surface staining.

B) We analyzed various natural PMD-causing mutations that map into EC2 (PLP^{V208D} , PLP^{L209H} , PLP^{P215S}) for cell surface expression of PLP in the absence (**left column**) or the presence (**right column**) of additional point mutations that substituted C^{200} and C^{219} for serine. In absence of C^{200} and C^{219} , the PMD-causing mutants were "rescued" from ER retention, and PLP (in green) was also localized at the cell surface (red label) and in a vesicular late endosomal/lysosomal compartment. In the presence of EC2 cysteines, all PMD mutants were 3F4-negative and confined to the reticular ER.

4.1.6 Misfolded PLP forms abnormal dimers and unspecific aggregates

What are the molecular consequences when intramolecular disulfide bridges fail to form? Most likely, the oxidative environment of the ER causes alternative crosslinks that interfere with PLP oligomerization, maturation, and surface expression, as defined by the O10 epitope. To analyze the fate of misfolded PLP, we determined its mobility by

polyacrylamide gel electrophoresis (PAGE) in the presence or absence of reducing agents. When derived from primary oligodendrocytes or transfected oli-neu cells, the majority of PLP^{wt} migrated as a monomer with an apparent MW of 26 kDa, under both reducing and non-reducing conditions (Figure 18 A). In contrast, PMD-causing forms, such as PLP^{D202N} or PLP^{C219Y}, migrated in addition as 52 kDa dimers (Figure 18 B). Importantly, upon addition of mercaptoethanol (ME), these dimers were reduced to monomers, suggesting that they represent cysteine-mediated cross-links. Indeed the "rescued" mutants PLP^{D202N+C200,219S} and PLP^{C219Y+C200S}, that lacked free cysteines in EC2, migrated as monomers also under non-reducing conditions (Figure 18 B).

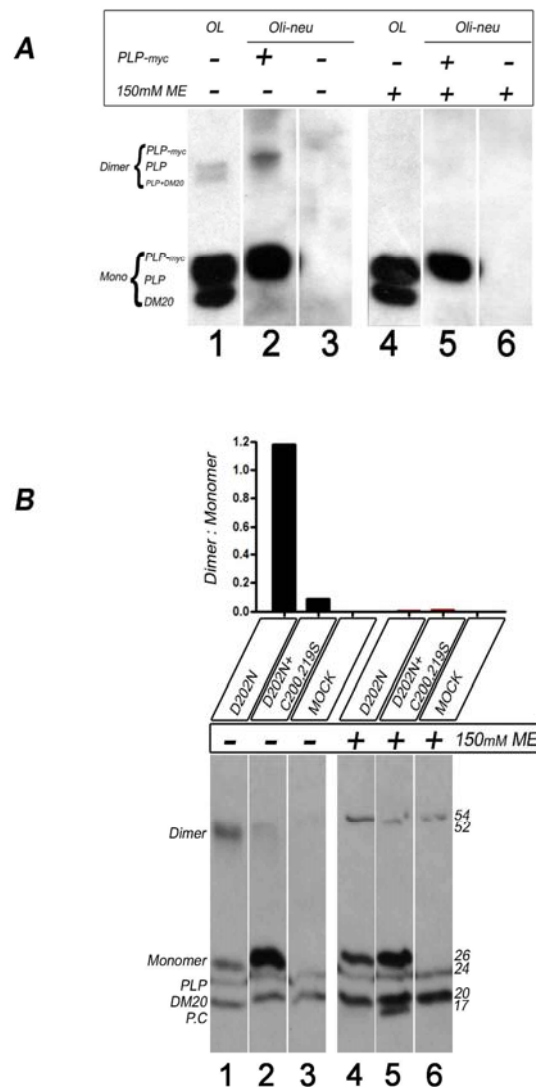


Figure 18: Cysteine-mediated PLP crosslinks

A) SDS-PAGE of cellular extracts from primary oligodendrocytes (OL) and oli-neu cells with immunodetection of PLP/DM20. When analyzed under non-reducing conditions, endogenous PLP/DM20 expression in cultured OL (lane 1) leads to a small percentage of dimerized PLP and DM20, detected by antibody 3F4. Absence of dimers in the presence of mercaptoethanol (ME) suggests they are cysteine-mediated crosslinks. Transfected oli-neu cells, expressing the slightly larger epitope-tagged PLP-myc (lane 2), also exhibit a small percentage of ME-sensitive PLP dimers, detected with an anti-myc antibody.

B) Semiquantitative analysis of PLP dimers in oli-neu cells expressing a natural PMD mutant (PLP^{D202N}). By Western blot analysis of non-reducing gels using antibody 3F4, more than 50 % of the PMD-associated PLP was detectable in a 52 kDa dimeric form (lane 1). When PLP was "rescued" by the additional substitution of C²⁰⁰ and C²¹⁹ for serine (see Figure 15), dimer formation could be largely prevented (lane 2). All the dimers were completely lost in the presence of 150mM mercaptoethanol (lanes 4 and 5). A 54 kDa protein in reducing gels was unspecifically detected by antibody 3F4 and also present in mock-transfected cells (lane 6). Note that this antibody also detected endogenous PLP/DM20 expression. When PLP reaches the cell surface, some PLP cleavage (P.C.) occurs that gives rise to a novel 16 kDa band (lane 5)

When derived from transfected COS-7 cells, even PLP^{wt} formed some dimers, trimers, and possibly higher oligomers or cross-links with other proteins (Figure 19).

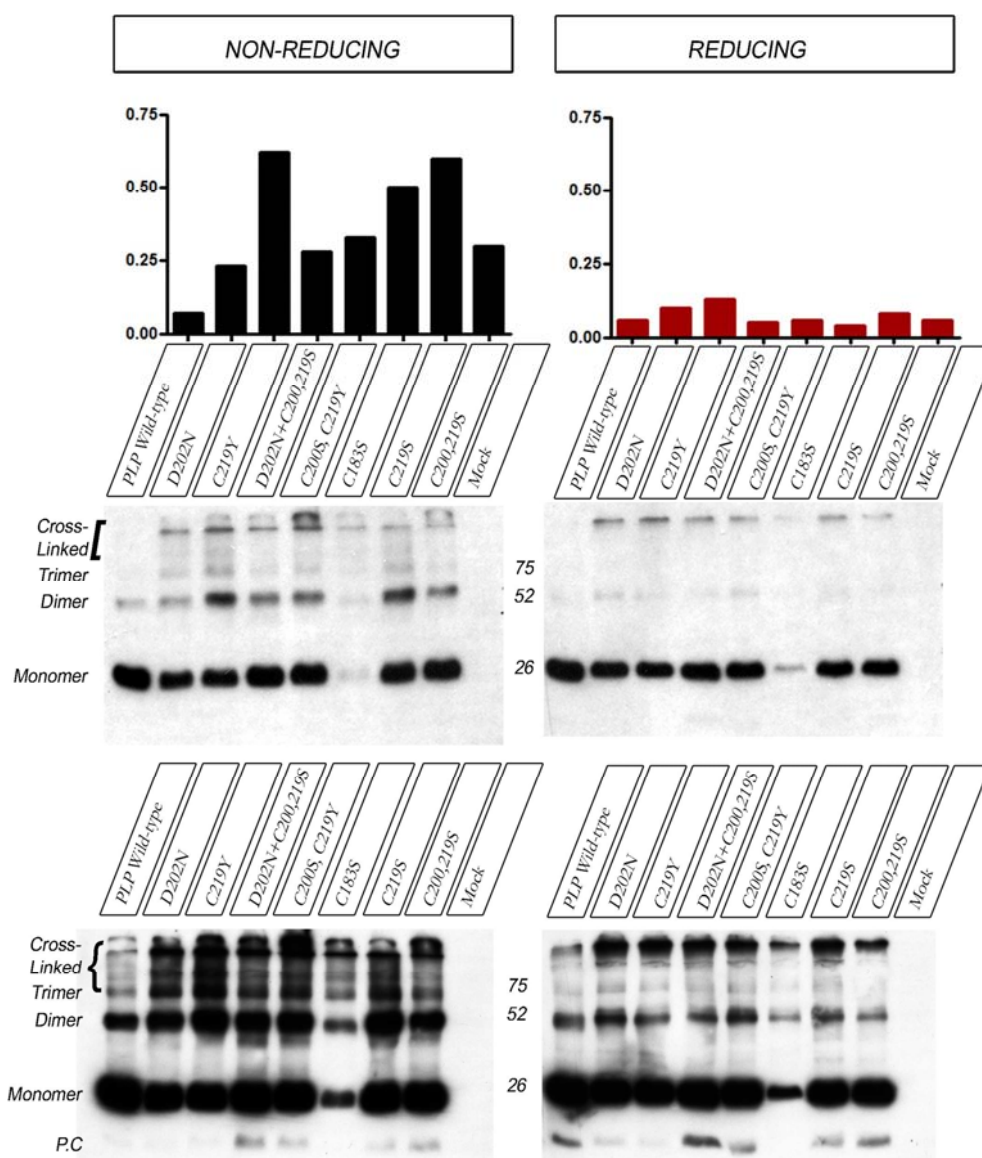


Figure 19: Cysteine-mediated PLP crosslinks in COS-7 cells

Same membranes exposed for different periods. Semiquantitative analysis of PLP dimers in COS-7 cells expressing a natural PMD mutants and PLP^{wt}. SDS-PAGE of cellular extracts from COS-7 with immunodetection of PLP, with 3F4 antibody. When analyzed under non-reducing conditions, mutant PLP forms dimers to a much higher extent as compared to PLP^{wt}. Reduction of dimers in the presence of ME suggests they are cysteine-mediated crosslinks. PMD-associated PLPs (PLP^{D202N} and PLP^{C219Y}) are more abundant in 52 kDa dimeric form, compared to PLP^{wt}. The rescue of PMD PLPs by additional substitution of C²⁰⁰ and C²¹⁹ to serine, dimer formation could be prevented but to a lesser extent as compared to oli-neu cell (Figure 18). In COS-7 cells apart from dimerization/trimerization (75kDa) mutant and wt PLPs crosslink to other proteins. These crosslinks are reducible to large extent to monomers.

Note that in over-exposure shows the cross links can be reduced largely to monomer with addition of 150 mM ME. Also note that PLP is cleaved and a PC product is even released in COS-7 cells giving rise to a novel 16 kDa band.

Wildtype PLP associated with calnexin to same extent as mutants (Figure 20). Under reducing conditions these PLP^{wt} dimers and oligomers could be reduced to monomers, suggesting significant misfolding upon overexpression in COS-7 cells (Figure 19). As expected, the PMD-causing mutants (PLP^{D202N}, PLP^{C219Y}) formed these ME-sensitive aggregates to a much higher degree and the removal of Cys²⁰⁰ and Cys²¹⁹ protected mutant PLP isoforms from aggregation, but to a mild extent (Note that wildtype PLP is also misfolded upon overexpression in COS-7 cells and associates with calnexin and calreticulin).

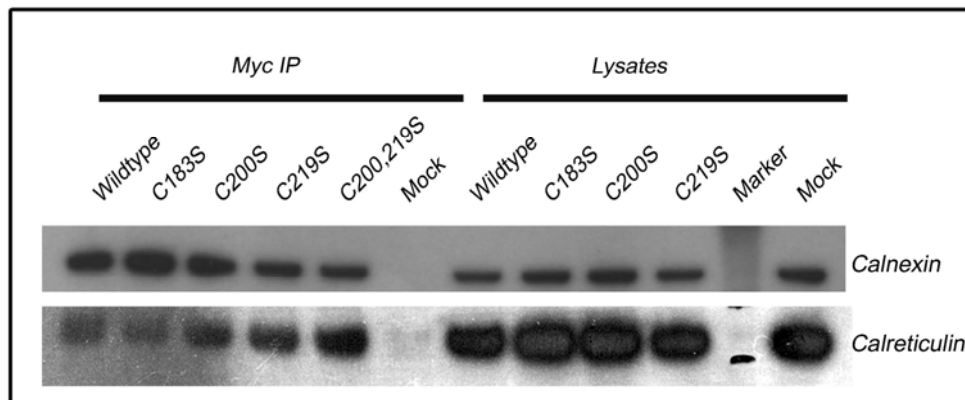


Figure 20: ER lectins associate with mutant and wt PLP with a same affinity

Transiently transfected COS-7 cells were, solubilized and immunoprecipitated with anti-myc antibody. Note that only PLP^{C183S} is a ER retained variant. Coimmunoprecipitated material (lanes 1 to 6) was western blotted with anti-calnexin and anti calreticulin antibodies. Lysates serves as a control and neither calnexin nor calreticulin is up-regulated upon misfolded protein expression in COS-7 cells. Association of PLP appears much stronger to membrane spanning lectin calnexin compared to its soluble homologous calreticulin.

4.1.7 ER retention of PLP/DM20 chimeras can be rescued by removal of cysteines.

Above results (Figure 9 and Figure 11) demonstrate that introduction of PMD causing mutations into PLP or its chimeras cause the retention of PLP because free cysteines have been exposed (by changes in the loop) to the oxidative environment of the ER. Furthermore, even DM20 could also be retained in ER by limiting the hydrophobic stretch of DM20 by replacing LSAT¹¹⁵ with HPDK¹¹⁵ (Figure 10 reverses the positive hydrophobicity to a positive hydrophilicity).

To confirm our hypotheses of TM sliding as well as EC2 local misfolding, we removed the critical disulfide bond (C^{200} - C^{219}) also in the PLP chimeras involving S2, S3 (see Figure 9 and Figure 21) and in $DM20^{T115K}$ and $DM20^{LSAT-HPDK}$ each harboring in addition the PMD-causing substitution P215S. To our surprise, all these "quadruple" mutant proteins reached the surface of transfected glial cells, similar to wildtype PLP^{wt} (Figure 21).

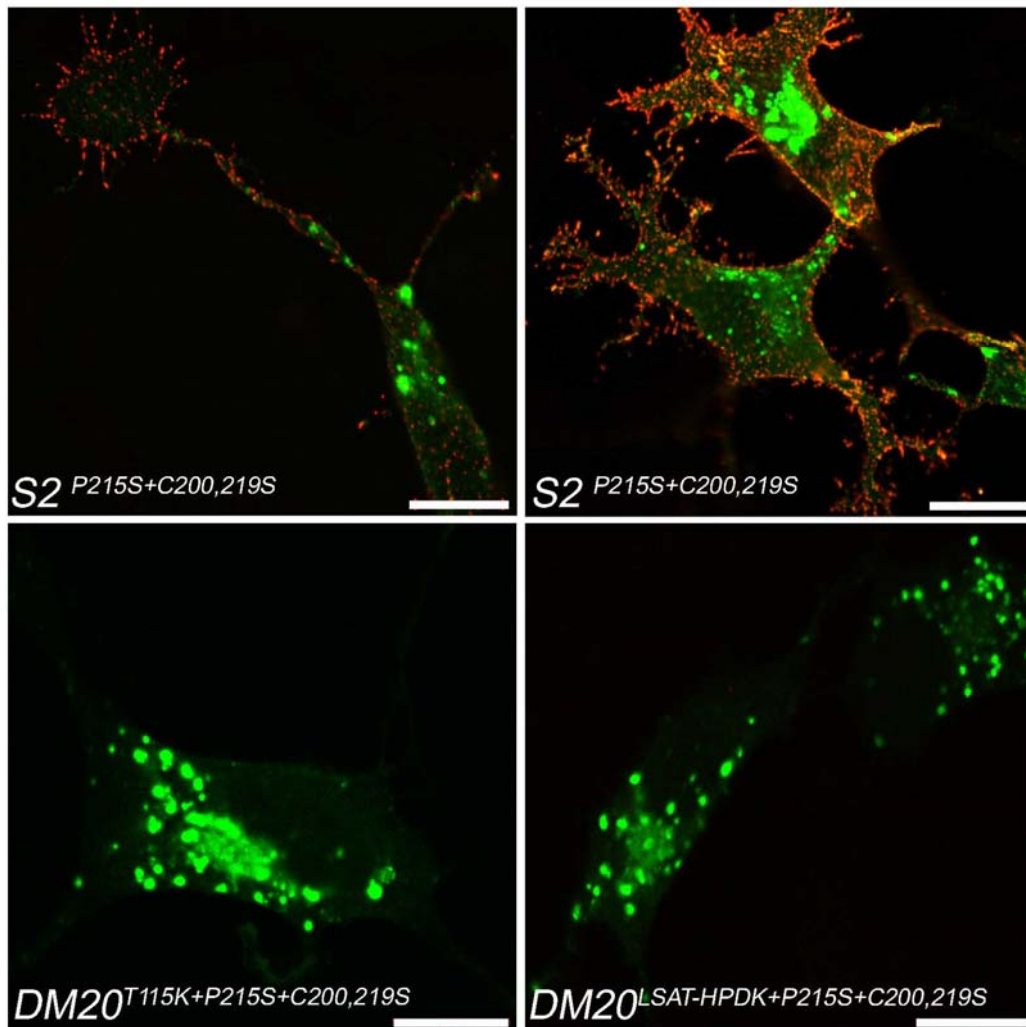


Figure 21: Outer disulfide bond governs the local and global folding of PLP/DM20 chimera

Oli-neu cells transfected with EGFP fusion constructs. Scale bar 10 μ m. PMD mutation bearing chimeras S2, S3, $DM20^{T115K}$ and $DM20^{LSAT-HPDK}$ with removal of outer cysteine pair are not retained in the ER. Interestingly only the PLP quadruple chimera (D2 and S3) show an immunoreactivity to live staining with 3F4. $DM20$ quadruple chimeras selectively accumulate in endo/lysosomal compartment and show no reactivity to 3F4 antibody.

Taken together our data support the following disease model. PMD-causing mutations of a large extracellular loop region in PLP/DM20 induce minor structural changes that compromise efficient formation of normal disulfide bridges, thereby exposing unpaired cysteines to the oxidative environment of the ER. Here competing oxidations generate aberrant dimers of PLP/DM20 that fail to mature (O10⁺, possibly oligomeric forms) and are retained in the ER (inducing UPR and cell death in vivo). Only some DM20 mutants are protected from this pathomechanism, because the flexibility of TM3 allows normal folding in EC2 with the generation of intramolecular disulfide bridges.

4.2 Quality control of transmembrane domain assembly in PLP

4.2.1 Spastic Paraplegia 2 (SPG2) a mild form of PMD

Spastic Paraplegia 2 (SPG2) is a milder form of PMD resulting from mutations affecting the soluble domains or from mutations leading to an abnormal termination of growing polypeptide (Bond et al., 1997; Cailloux et al., 2000; Kobayashi et al., 1996; Saugier-Verber et al., 1994). To study the fate of these truncated PLPs, we engineered PLP cDNA, and constructed truncated PLPs, which encode the first two (TM1,2), first three (TM1,2,3), second two (TM3,4) or only the last (TM4) hydrophobic transmembrane domains, respectively, and use the natural methionine/or specific signal peptide (Kleijnen et al., 1997) for translation initiation. Further to study, how perturbations in soluble domains influence PLP trafficking, we expressed PLPs with myc replacements in intracellular loop (IC), the region between TM2-3. In order to identify any putative retention signal in PLP, we also deleted N and C termini of PLP.

4.2.2 Truncated PLP transmembranes are retained in the ER

PLP cDNAs encoding truncated PLPs were transfected individually into COS-7 (and olivine data not shown) cells. The intracellular distribution of the each truncated molecule was mapped using appropriate antibodies (or EGFP fluorescence). TM1,2 (PLP 1-99-myc tag), TM1,2,3 (N terminus myc tagged, PLP^{impy}), TM1,2,3 (1-236-myc, and 1-183-myc; data not shown), TM3,4 (Met-Gly-135-276 untagged or EGFP) and TM4 (signal peptide MHCI+228-276) all display a reticular pattern of labeling (Figure 22), highly concentrated in the perinuclear region. The reticular pattern strongly resembles the pattern displayed by PLP^{msd} (which served as a control for ER retained PLPs throughout our study, last panel). To ensure proper insertion of TM4, with N luminal and C cytosolic, we added a MHCI signal peptide to N terminus (Kleijnen et al., 1997) and stained methanol fixed and digitonin permeabilized cells (Figure 22 E-inset in greyscale)

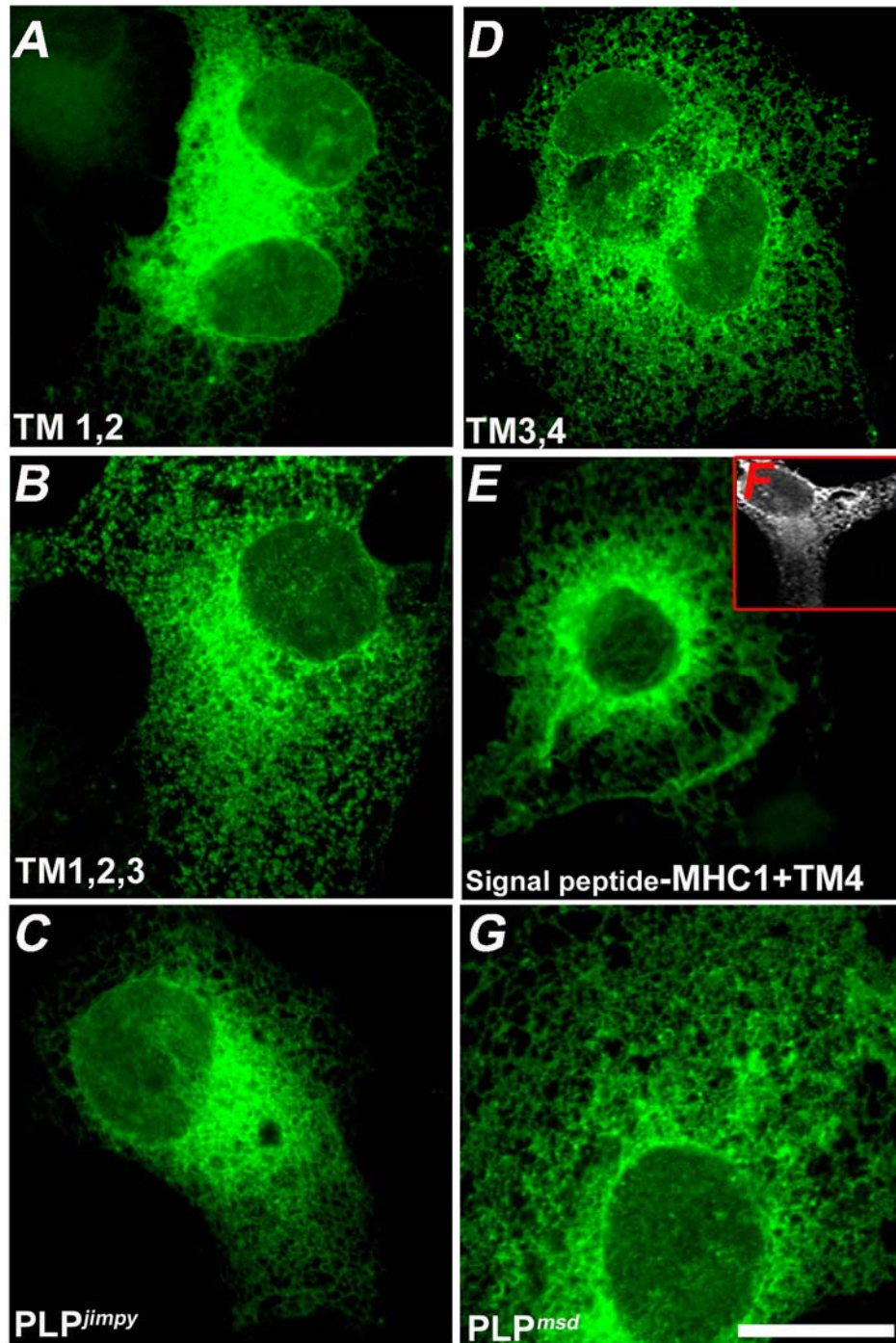


Figure 22: All truncated PLPs are retained in the ER, when expressed individually

Truncated PLPs are retained in the ER of transfected COS-7 cells. Fixed cells permeabilized and stained for C or N terminus myc epitope in left panel and EGFP fluorescence in right panel. Scale bar 10 μm . Truncated PLPs, with a first half of protein regardless of whether exhibiting two or three TMs are strongly retained in the ER, left panel. Interestingly, the second half of the protein whether TM3,4 or TM4 alone were also retained in the ER, exactly like PLP^{msd}. To confirm the proper orientation of TM4, the untagged TM4 was stained using A431 antibody, in fixed cells permeabilized with digitonin (inset in greyscale).

4.2.3 N or C termini deletions did not alter PLP localization.

PLPs lacking N(Δ N) or C(Δ C) termini did not show any change in subcellular distribution of PLP^{wt} or PLP^{msd} in transfected cells. Δ N/or Δ CPLP^{wt} traffics to cell surface and protrude numerous filopodial processes whereas PLP^{msd} was completely retained in the ER, irrespective of N or C termini deletion [Figure 23 and Δ NPLPs studied and discussed in previous work (Dhaunchak, 2003)]. This data infers that N or C termini of PLP do not harbor any retention signal.

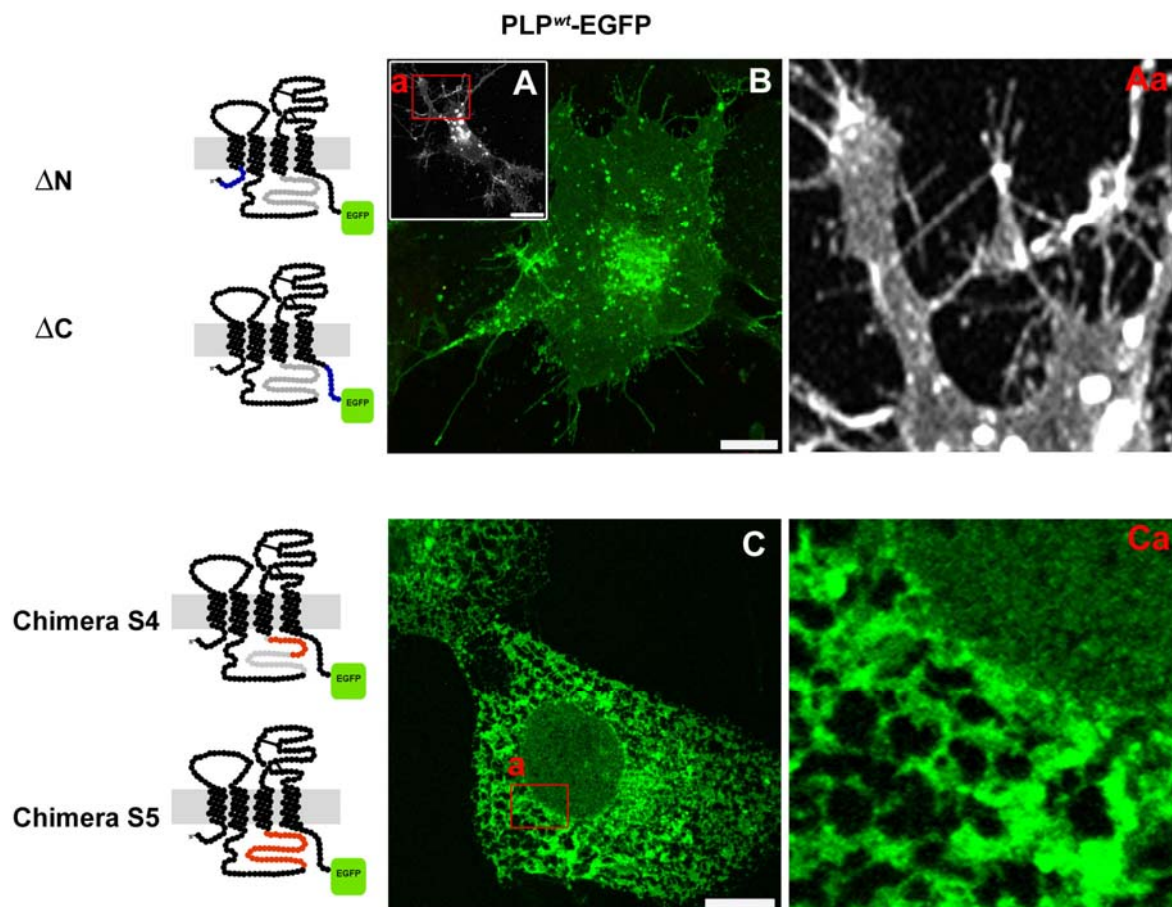


Figure 23: Neither N and C termini nor IC2 but TM assembly monitors surface expression of PLP

PLP topological models on the left highlight the site of deletion (blue) or myc replacement (red). Scale bar annotates 10 μ m from A to C. Oli-neu (**A**, grayscale) and COS-7 (**B**) cells expressing Δ CPLP^{wt}-EGFP show a PLP^{wt} like distribution of EGFP fluorescence. Transfected cells protrude numerous filopodial processes and accumulate PLP in endosomes, shown in **Aa** (blowup of a oli-neu arbor). Δ NPLP^{wt}-EGFP also displayed a similar distribution, data not shown (Dhaunchak, 2003). Chimeric PLPs with a myc replacement proximal to TM3 expression are strongly retained in the ER (**C**). Chimera S4 (**C and blow up in Ca**) shows a reticular distribution extended out to periphery, with no vesiculated structure or filopodial processes.

4.2.4 Perturbations proximal to TM3 retain both PLP and DM20 in the ER

Incorporation of myc tag distal to TM3, replacing a short stretch of 9-10 amino acids, in IC of PLP did not alter the trafficking of PLP to the cell surface or to the endosomal compartment (chimera S1, S2, S3 section 4.1.2). Juxtamembrane incorporation of myc tag, replacing a stretch of amino acids (**139-150**) proximal to TM3 or complete PLP-specific region (**116-150**), strongly retained PLP/DM20 in the ER (Figure 23).

We have shown that disulfide bond 183-227 is critical for overall folding of PLP and DM20, whereas disulfide bond 200-219 monitors the local folding and trafficking of PLP/DM20. These cysteine bridges impart a proper topology and are required for assembly of transmembrane domains to generate a trafficking competent PLP molecule. To test whether, an artificially assembling TM3 and TM4 (by complete removal of EC2 and insertion of autonomously folding domains) we generated a PLP cDNA construct replacing entire EC2 by two HA tags flanked by flexible linkers (from N to C termini- TM3-SGP-HA-SGP-HA-SGP-TM4). The resulting, PLP^{ΔEC2-HA} was completely retained in the ER (data not shown). This observation suggests that either TMs do not assemble properly or an artificial assembly of TMs is inefficient in determining the surface expression and folding of PLP, and this assembly can only be achieved by proper disulfide bonding.

4.2.5 Self assembly of transmembrane domains

Co-transfected COS-7 and oli-neu cells in whom, both TM1,2 and TM3,4 are derived from PLP^{wt} results in surface expression of both halves of the protein. Both truncated proteins assemble to escape the ER quality control and TMs can also be seen in E/L compartment (Figure 24 A and oli-neu data not shown). When TM1,2 and TM3,4 are derived from PLP^{msd}, they fail to exit the ER (Figure 24 A) which strongly infers that the single Ala²⁴² to Val substitution impairs the TM assembly of both halves. An attempt to rescue PLP^{jimpy}, by co-transfection of construct encoding TM4 resulted in complete ER retention of both proteins (not shown). The frameshift mutation introduces 9 cysteines (instead of 4 in PLP^{wt}) in the EC2 of PLP^{jimpy} polypeptide. The exposure of these cysteines to the oxidative environment of ER might also add to the cause of ER retention and impaired trafficking of other proteins. Co-transfection of PLP constructs encoding TM1,2,3 (1-236-myc) and TM4 (with signal peptide) also resulted in a complete retention of both isoforms (Figure 24 C).

This data are in a complete agreement with our above observation (Figure 12 and section 4.1.3) that disulfide bond 183-227 is critical for proper alignment of TM3 and TM4.

4.2.6 Truncated transmembranes associate with calnexin

All PLPs including truncated TMs strongly associate with ER lectin calnexin in transfected COS-7 cells (Figure 25). TM1,2 and TM3,4 formed a SDS resistant dimer and migrate to an added molecular weight, of a full length PLP molecule (Figure 25). Immunoprecipitations of TM1,2 (anti-myc antibody), from cells co-transfected with TM1,2 and TM3,4 encoding constructs, also shows a strong association of TMs.

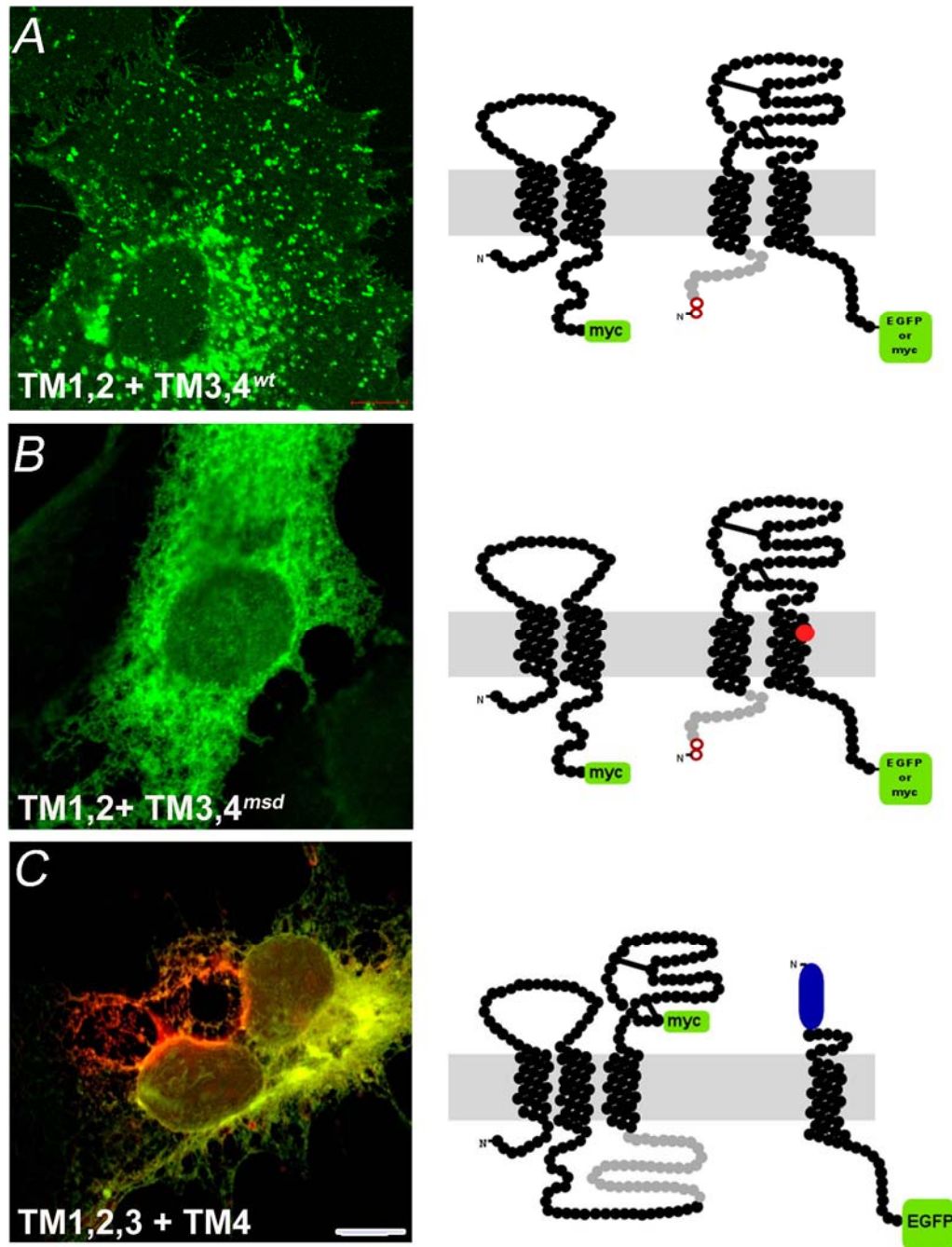


Figure 24: Prerequisite for an exit from the ER is proper alignment and masking of TMs in the bilayer

Topological models next to each representative cell show orientation of truncated PLPs in the bilayer. Scale bar annotate 10 μm . TM1,2 when co-expressed with EGFP tagged TM3,4 derived from PLP^{wt} (A) but not from PLP^{msd} (B) results in surface expression of both halves of protein, only TM3,4 is shown. In A, the endosomal accumulation is also recapitulated. C) TM1,2,3 in red when co-expressed with TM4 in green (bearing MHC I signal peptide) results in ER retention of both halves of the protein.

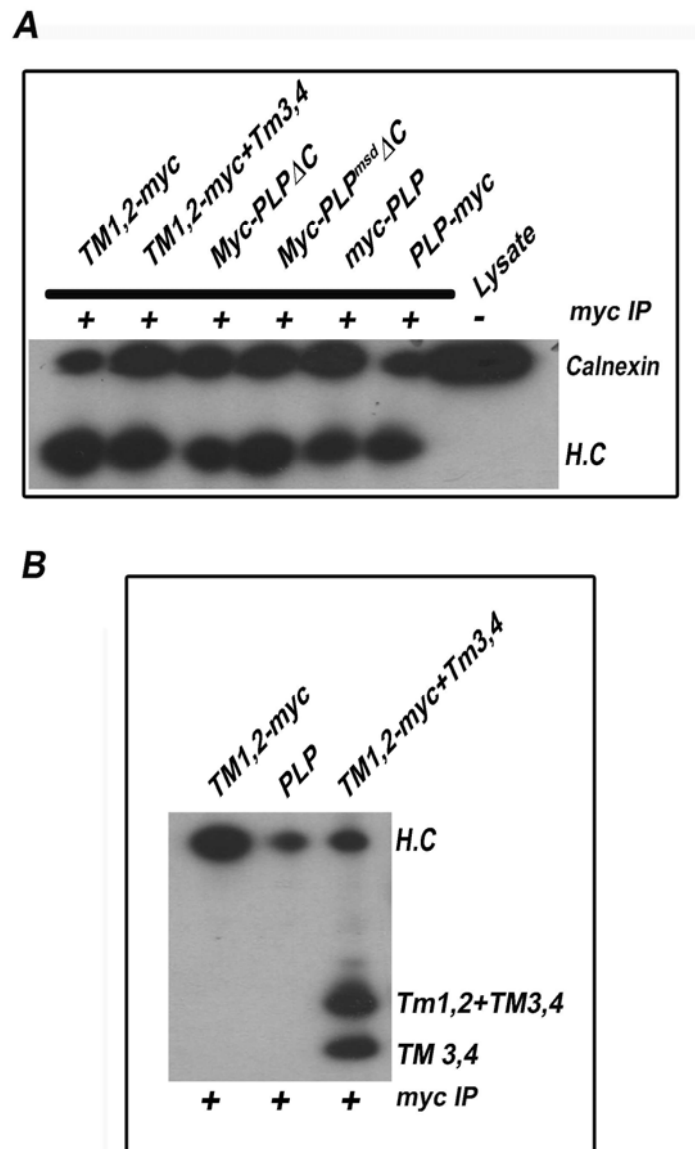


Figure 25: Truncated PLPs associate with calnexin with an equal affinity

Lysates from transfected COS-7 cells were immunoprecipitated with anti-myc antibody. Note that myc as prefix or suffix annotates the N or C terminal fusion respectively. TM3,4 (A) and PLP (B) are untagged. The immunoprecipitated material was western blotted with anti-calnexin (A) and anti-PLP antibody (B). H.C is heavy chain of myc antibody and serves as input control.

A) TM1,2-myc individually or in combination with TM3,4 (untagged) shows a strong interaction with calnexin, lane 1 and 2. Myc Δ CPLP^{wt}, myc Δ CPLP^{msd} or mycPLP^{wt} also show no difference in association to calnexin.

B) TM 3,4 associates strongly with TM1,2 and can be detected in lysate precipitated TM1,2. TM1,2 and TM3,4 form a SDS-resistant heterodimer. Note that truncated TM1,2-myc lacks last two TMs and cannot be detected anti-PLP antibody. PLP loaded in middle lane is an untagged and cannot be precipitated with myc antibody.

4.3 Conformation sensitive and compartment specific epitope: evidence that PLP matures within the ER

4.3.1 Wildtype PLP masks 3F4 epitope during its exit from ER

Lysates derived from oli-neu cells separated on SDS gels and immuno-blotted with 3F4 antibody display low levels of DM20 (Figure 18 section 4.1.6). When stained live for surface DM20, oli-neu cells show a complete lack of 3F4 reactivity (data not shown). Surprisingly, 010⁺ oli-neu cells and COS-7 transiently transfected with PLP/DM20 constructs, also show a complete absence to 3F4 avidity (Figure 26). Even more interestingly, the same antibody shows a tremendously high avidity to misfolded DM20 that traffic to the cell surface in both oli-neu (chapter 3.1) and COS-7 cells (Figure 26 E). PLP^{C200, 219S} and all rescued PMD mutants also show a high immuno-reactivity towards 3F4 antibody (Figure 26 and also Figure 16, Figure 17 section 4.1.5).

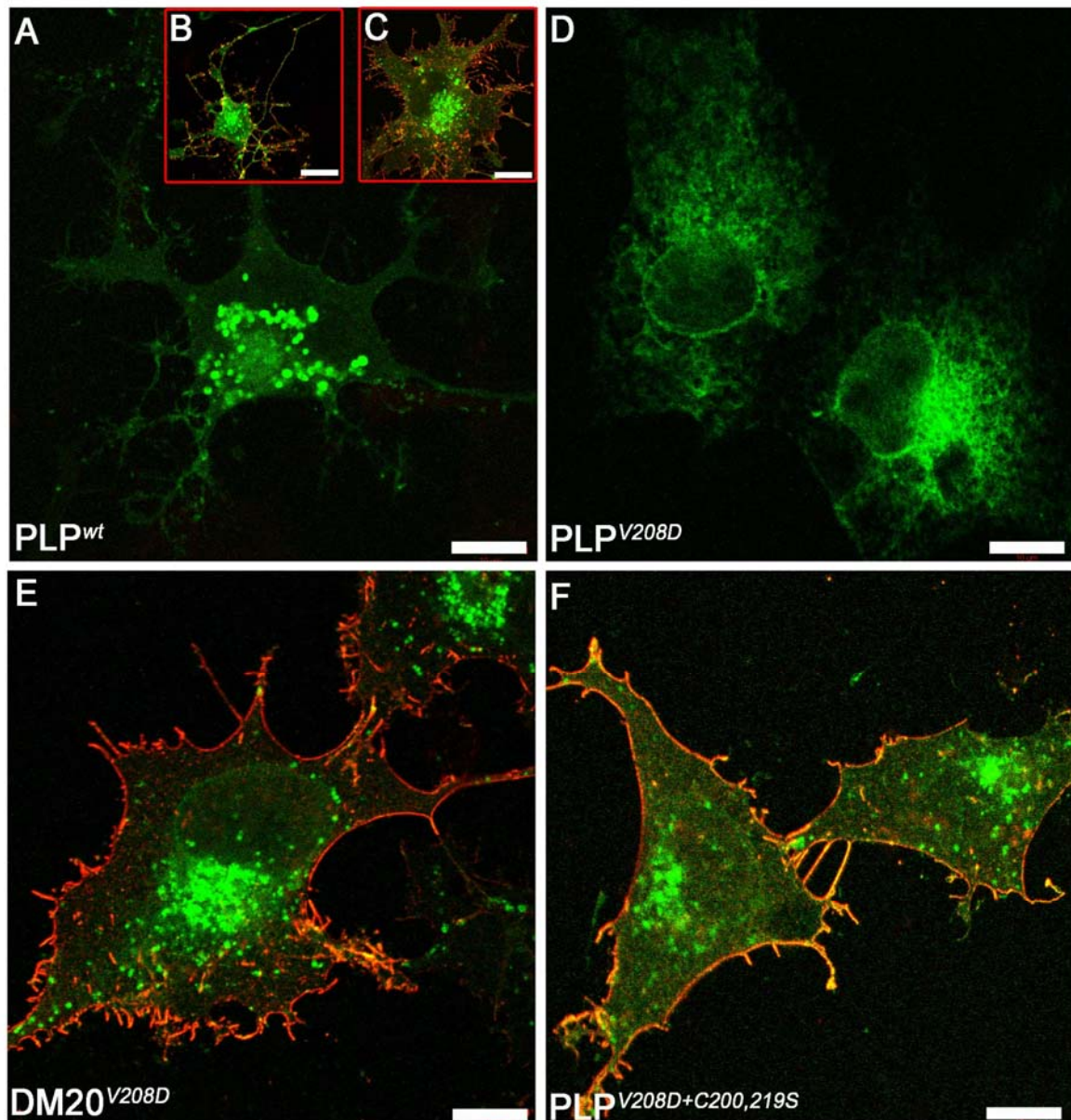


Figure 26: Oligomeric PLP masks 3F4 epitope at the cell surface

Live 3F4 staining (red) of oli-neu (**A, B**) and COS-7 (**C to F**) cells transfected with constructs encoding PLP-EGFPs (green). Only overlays are shown, scale bar annotates 10 μm . **A**) PLP^{wt} masks the 3F4 epitope and shows no reactivity at the cell surface. PLP lacking outer disulfide bond PLP^{C200S,219S} traffics to the cell surface and shows high immuno-reactivity under same conditions in both oli-neu (**B**) and COS-7 cells (**C**). PMD mutant PLP^{V208D} is strongly retained in the ER and cannot be stained live, with 3F4 antibody (**D**). DM20 bearing the same mutation DM20 is not ER retained and 3F4 antibody binds with a high avidity (**E**). PLP^{V208D} traffics exactly like DM20^{V208D} with removal of a cysteine pair, the avidity to 3F4 antibody is also restore in PLP^{V208D+C200,219S} (**F**).

To solve this puzzle, we stained permeabilized and fixed oli-neu cells transfected with constructs encoding PLP^{wt}-EGFP and PLP^{C200,219S}-EGFP. To our surprise, the antibody specifically labeled PLP^{wt}-EGFP residing only in the endo/lysosomes (E/L) (Figure 27 B) and PLP^{C200,219S}-EGFP shows an extensive labeling at the cell surface (Figure 27 E). Mutant PLP, if enriches, in E/L compartment consistently showed a low reactivity to the same antibody (Figure 27 E and Fa). In previously published report, it has been shown that 3F4 epitope emerges from oligodendrocytes cultured for 20DIV (days in vitro) (Greer et al., 1996).

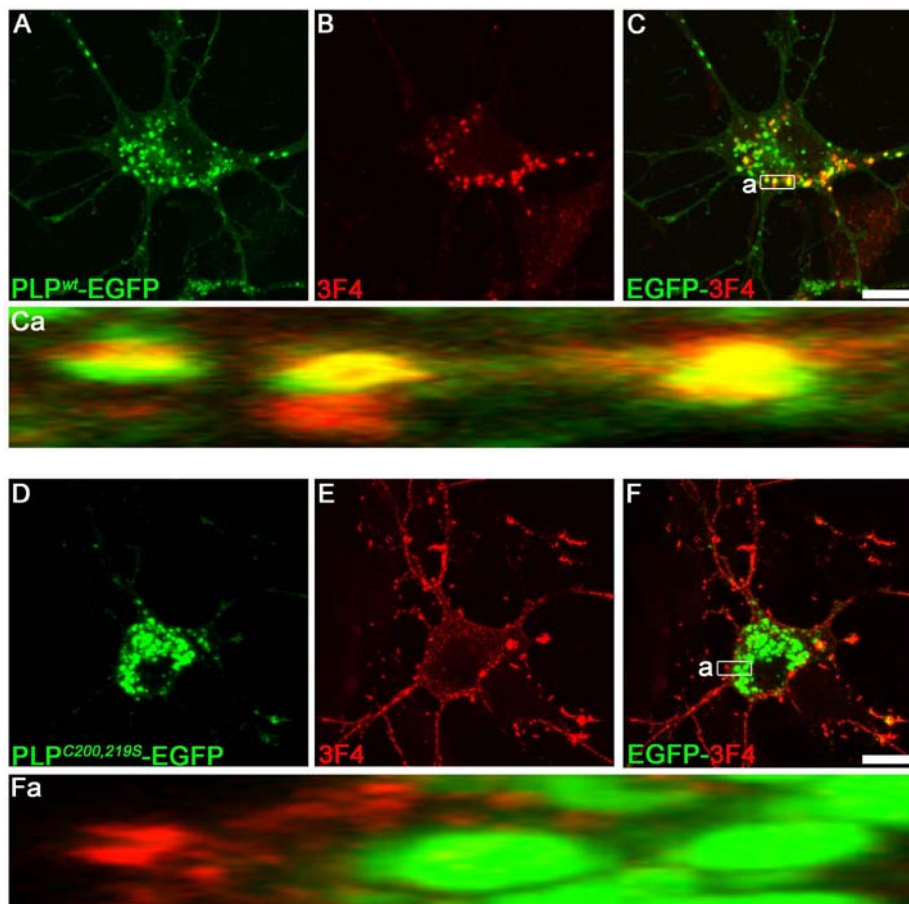


Figure 27: Maturation of PLP completes in pre-myelin E/Ls whereas PLP^{C00,219S} matures at the cell surface

oli-neu cells transfected with constructs encoding PLP^{wt}-EGFP and PLP^{C200,219S}-EGFP fixed permeabilized and stained with 3F4 antibody (red)

A) EGFP fluorescence dictates the subcellular localization PLP^{wt} and in B) only the E/L pool of PLP^{wt} shows immunoreactivity towards 3F4 antibody. Ca) show a higher magnification of boxed area in C) of the overlay. D) EGFP fluorescence dictates the sub-cellular localization of PLP^{C200,219S} and E) high avidity of 3F4 antibody towards surface PLP. Note that Fa) higher magnification of boxed area of overlay F) shows a complete lack of colocalization of 3F4 immunoreactivity in E/Ls.

4.3.2 Adult CNS myelin presents a complete overlapping avidity to 3F4 and A431

Monoclonal mouse (3F4) and polyclonal rabbit (A431) antibodies, respectively directed against EC1 and C terminus hexa-peptide of PLP, were used to detect PLP in the CNS of adult mice. Figure 28 shows an absolute overlap of PLP distribution detected with A431 (green) and 3F4 (red) antibody in the spinal cord of adult mice. Complete overlay infers that 3F4 antibody can even recognize a PLP epitope that is embedded within intraperiod lines (extracellular).

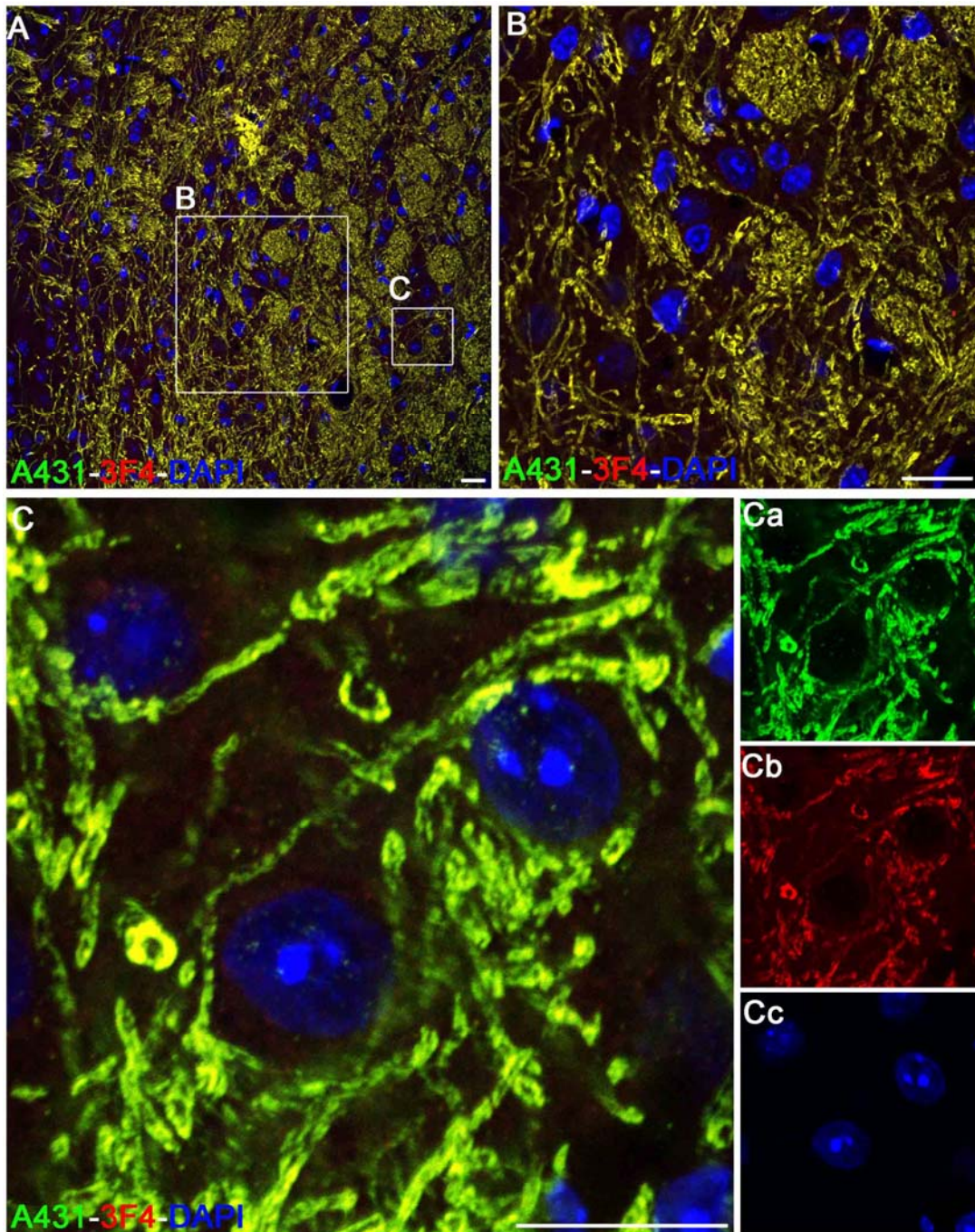


Figure 28: Identical avidity of 3F4 and A431 antibody towards MDL and IPL embedded PLP epitopes

Spinal cord from P180 mouse transversally cut and stained with A431 (green) and 3F4 (red) antibody. Nuclei are stained with DAPI (blue). The C terminus PLP epitope (A431) is embedded in the major dense layer (MDL) and the epitope displayed by extracellular loop1 (EC1) of PLP (3F4) is embedded in intra-period lines (for myelin periodicity, see Figure 2). Only overlays are shown, strikingly both antibodies show identical avidity towards PLP. Scale bar 20 μm (A , B) and 10 μm (C). B) and C) are magnifications of boxed area in A) Overlay C) is split into Ca) A431 Cb) 3F4 and Cc) dapi.

4.3.3 A novel 16 kDa PLP proteolytic cleavage product

Western blot analysis from purified CNS myelin and cultured oligodendrocytes revealed that 3F4 antibody recognizes both PLP and DM20. In addition to dominant PLP/DM20 bands (24/20 kDa), we identified a novel PLP product P16 (16 kDa). Proteolytic cleavage (PC) of PLP in EC2 gives rise two products P16 and P10. The second half of this P.C has previously been reported and speculated to exhibit neuron-protective function (McLaughlin et al., 2002; Yamada et al., 1999). McLaughlin et al (02) have shown that P10 is an abundant (comparable to full length PLP) constituent of the CNS myelin in higher mammals, equine, and have shown that this product undetectable in mouse and rat myelin. By using 3F4 antibody we have shown that the P16 protein is an abundant constituent of the adult CNS myelin of mice (Figure 29).

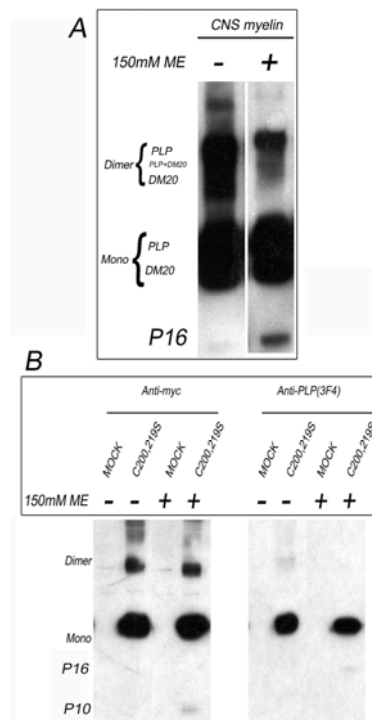


Figure 29: A novel 16 kDa myelin PLP proteolytic cleavage product

A) Purified CNS myelin (500 ng protein in each lane) from wildtype mice separated under reducing and non-reducing conditions on a 12 % SDS gel, immuno-blotted with anti-PLP (3F4) antibody. Note that a prominent 16 kDa product (PLP proteolytic product) appears under reducing conditions. Most likely, under non-reducing conditions P16 is involved in oligomer formation with PLP/DM20. Also, PLP and DM20 form homo and hetro-dimers that are largely reducible to monomers by addition of ME.

B) Lysates derived from COS-7 cells, transiently transfected with PLP-myc constructs, separated and blotted under identical conditions show that 3F4 antibody recognizes only a subpopulation of PLP. Note an emergence of P16 and P10 products only after ME addition. This finding infers that both proteins form disulfide bonds with either full-length PLP or with each other.

When used for immunoblotting on lysates derived from COS-7 or oli-neu, 3F4 seems to recognize a sub-population of PLPs in reducing and denaturing gels. The aggregated, high molecular dimers, trimers and oligomers, were specifically less intensely detected by 3F4 antibody, compared to myc antibody (Figure 29).

4.4 From transfected oligodendrocytes to PLP-EGFP expressing transgenic “knock-in” mice

4.4.1 PLP accumulates in endosomes/lysosomes (E/L)

As a first step to understand polarized morphology of oligodendrocytes, we started with a simpler system and studied trafficking of PLP in cells of oligodendrocyte lineage (oli-neu and OLN93). Wildtype PLP when transiently over-expressed in oli-neu and OLN93 readily traffics to cell surface and accumulate in endosomes within 24 hours [(section 4.1.4, Figure 13 and (Trajkovic et al., 2006)]. Stable cell line expressing PLP^{wt}-EGFP under steady state exhibited a very little PLP at the cell surface. Whether PLP exploits polarized trafficking pathways, like transcytosis or exocytosis from endo/lysosomes, hence biasing its own enrichment and trafficking to myelin compartment can only be answered by *in-vivo* tool, in which PLP/DM20 trafficking and expression are developmentally regulated.

To study trafficking of mutant PLP with a perturbed transmembrane assembly we also generated a stable cell line expressing PLP^{msd}-EGFP (Ala 242 Val in TM4). Mutant PLP is maintained at higher level compared to the wildtype PLP in stable cell line, which infers that mutant PLP is degraded poorly [Figure 31, in agreement to the previous report using COS-7 cells (Swanton et al., 2003)]. Mutant PLP is strongly retained in the ER and does not accumulate in lamp1 positive endo/lysosomal compartment (Figure 30). PLP^{msd}-EGFP is maintained at higher level compared to PLP^{wt}-EGFP in stable cell line.

4.4.2 Association of PLP with cholesterol

CNS myelin displays an unusual composition of lipids and proteins with cholesterol constituting around 40 % of all lipids. Transgenic mice lacking an ability to produce cholesterol in oligodendrocytes shows delayed myelination. The myelin still exhibits a same ratio of lipids and proteins, with PLP/DM20 still the major constituents (Saher et al., 2005). To test whether, association of PLP with cholesterol acts as a prerequisite for process outgrowth and for final delivery and ensheathment around axons, we studied cholesterol-PLP association in precursor cell-line stably expressing wt and mutant PLP. oli-neu cells expressing PLP^{wt}-EGFP and PLP^{msd}-EGFP were induced to protrude myelin like processes. Strikingly the early process outgrowth was not compromised in mutant cell line. Both cell lines protrude cholesterol rich processes (Figure 30 A and B). PLP^{wt}-EGFP expressing cells show an association with cholesterol at the cell surface and in E/L

compartment. In contrast cells expressing PLP^{msd}-EGFP, fully retain the protein in the ER and show no association at cell surface or in E/Ls (Figure 30 B). Lack of co-localization of lamp1 and PLP^{msd}-EGFP infers that mutant protein is stably retained in the ER and is not degraded via lysosomal degradation pathway (Figure 30 C and Figure 31).

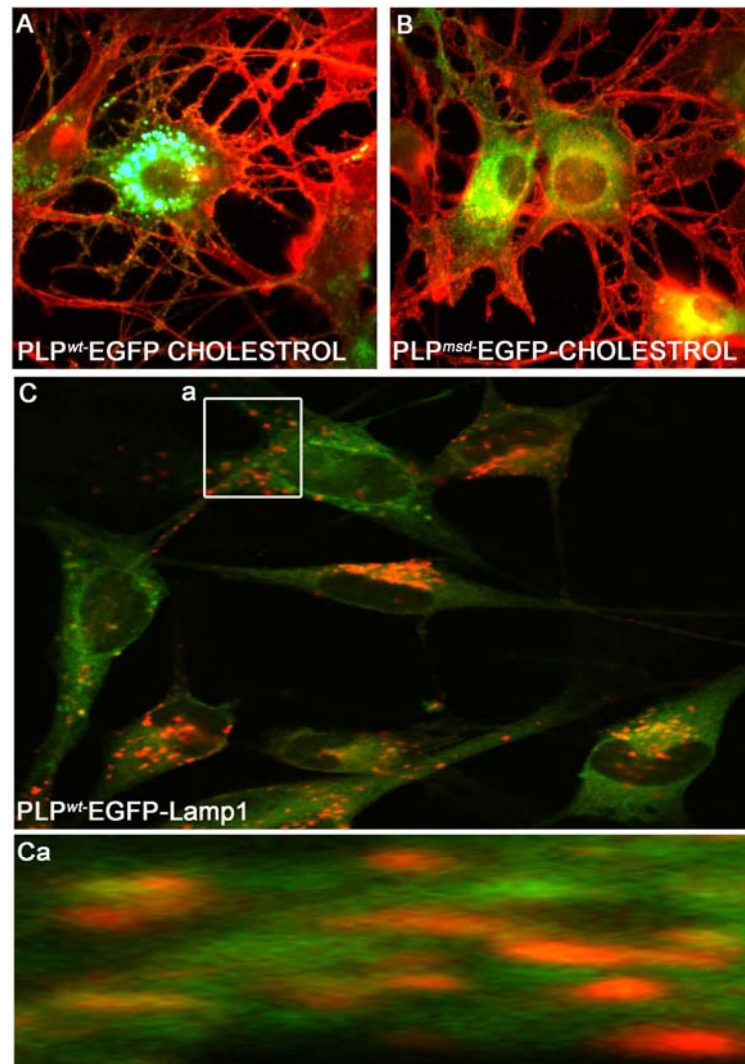


Figure 30: Association of PLP with cholesterol

PLP^{wt}-EGFP and PLP^{msd}-EGFP expressing stable cell line induced with 1 mM cAMP for 24 hours, fixed and incubated with filipin (Cholesterol) in red. A) PLP^{wt}-EGFP associates with cholesterol in E/Ls and at cell surface. PLP^{msd}-EGFP expressing cells do not show impairment in process outgrowth and cholesterol distribution (B). ER from majority of cells is virtually free from cholesterol, similar to PLP^{wt}-EGFP expressing cells. Overlay of lamp1 and EGFP fluorescence in C) and magnification Ca) shows that PLP^{msd}-EGFP is not degraded in lysosomes. Both cell lines express PLP without any observable change in growth rate or cell death compared to the *wild-type* oli-neu cells.

Due to the oligodendrocyte death the effect of this point mutation (PLP^{msd}) cannot be studied *in vivo*. By using proteomics and transcriptomics approach the expression profiles of genes differentially regulated during myelination (artificial induction with cAMP) are being investigated in both wildtype and mutant cell lines.

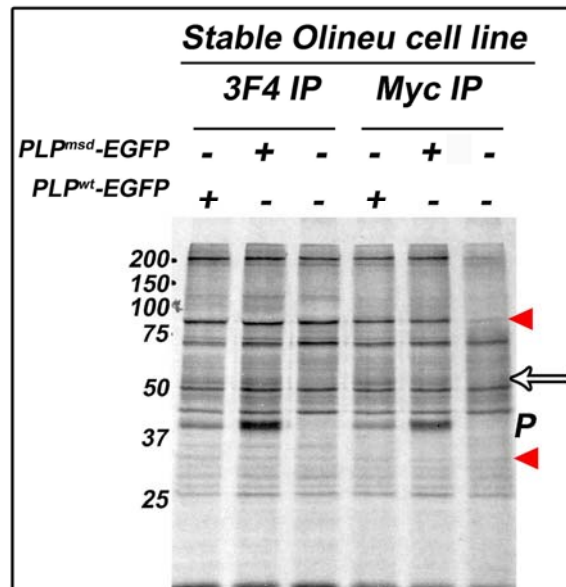


Figure 31: Co-immunoprecipitation from oli-neu stably expressing PLP^{wt}-EGFP and PLP^{msd}-EGFP

PLP^{wt}-EGFP and PLP^{msd}-EGFP expressing stable cell line were labeled for 72 hours with ³⁵S methionine-cysteine promix, harvested and incubated with c-myc and 3F4 antibodies. Immuno-precipitated lysates were separated on 10 % reducing SDS gels and exposed to radiographic films. A prominent 40 kDa band (P) shows that these cells maintain PLP^{wt}-EGFP and PLP^{msd}-EGFP are relatively low levels. Note that mutant protein is more resistant to degradation than wt. White arrow highlights a co-immunoprecipitated protein that interacts with both PLP^{wt} and PLP^{msd}. Red arrow heads highlight two more interacting proteins that are specifically precipitated with c-myc antibody from cells expressing both mutant and wild-type protein. Identity of these proteins still remains to be identified.

4.4.3 Directed trafficking of rapidly moving PLP-EGFP⁺ endo/lysosomes in primary oligodendrocytes

Primary oligodendrocytes, compared to oli-neu cell, do not show a developmental arrest at a premyelinating stage. Neither do they rely on cAMP or neuronal signal for redistribution of PLP from E/Ls storage site to the cell surface. Interestingly, PLP^{wt}-EGFP containing E/Ls structures display a directed and much faster mobility in oligodendrocytes (see attached compact disc movie 5 and 6 for comparison) compared to oli-neu cell induced

with cAMP. The E/Ls structures show a tendency to move directionally into a growing myelin process. The exact mechanism how this directional trafficking is achieved and how oligodendrocytes follow the clues to enwrap axons, *in vivo*, can be appropriately answered by generation of a tool expressing PLP^{wf}-EGFP from endogenous locus.

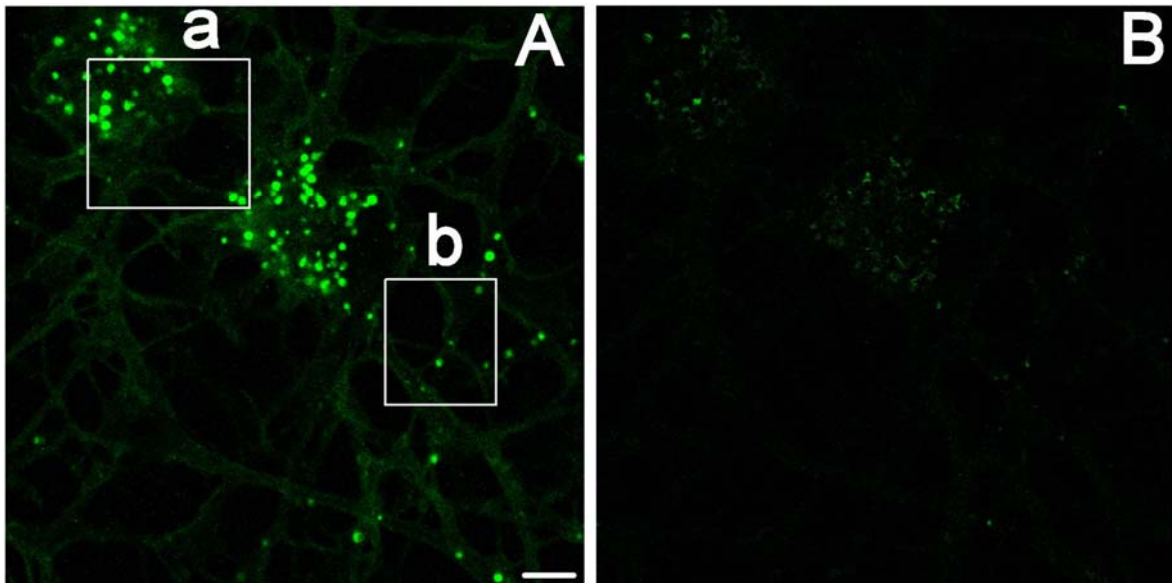


Figure 32: cAMP treatment induces process outgrowth and redistributes PLP to the cell surface

A) PLP^{wf}-EGFP expressing oli-neu cells treated with cAMP (10 nM) for 24 hours and imaged live by confocal microscopy in a low fluorescence media. Scale bar annotates 5 μm . **B)** Shows an entire mobile pool of endo/lysosomes. The net mobility was calculated by subtraction of two consecutive images interspaced by an interval of 8.9 second. Figure 32 **Aa** and **Ab** shows the mobility of endo/lysosomes an interval of 45 seconds.

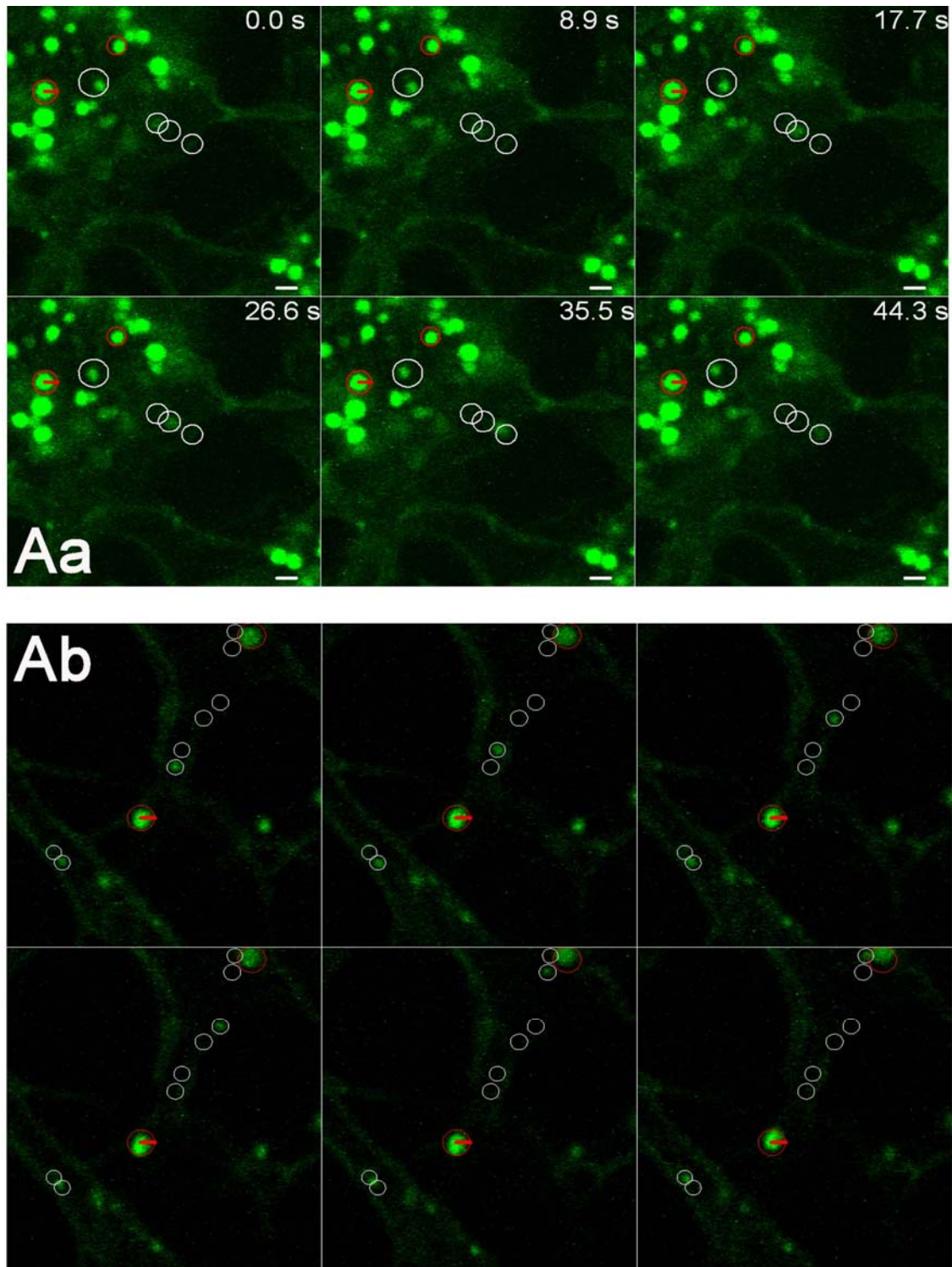


Figure 32 continued: Aa) Perinuclear and Ab) peripheral image sequences of boxed area in Figure 32 A. Scale bar is 1 μm and the radius (500 nm) of immobile endo/lysosomes (E/Ls) is marked in red. Time lapse (8.9 seconds) between consecutive scans is same from Aa and Ab. Red circles mark relatively immobile pool of large E/Ls (radius > 500 nm) with local diffusion. White circles define the path of a subset of highly mobile and small E/Ls (radius < 200 nm). Perinuclear pool of E/Ls shows relatively less mobility over long range as compared to the peripheral pool of E/Ls [approximately same size (radius 150 to 200 nm). Whereas E/Ls of a radius > 500 nm are relatively immobile in both periphery and perinuclearly (highlighted in red circles).

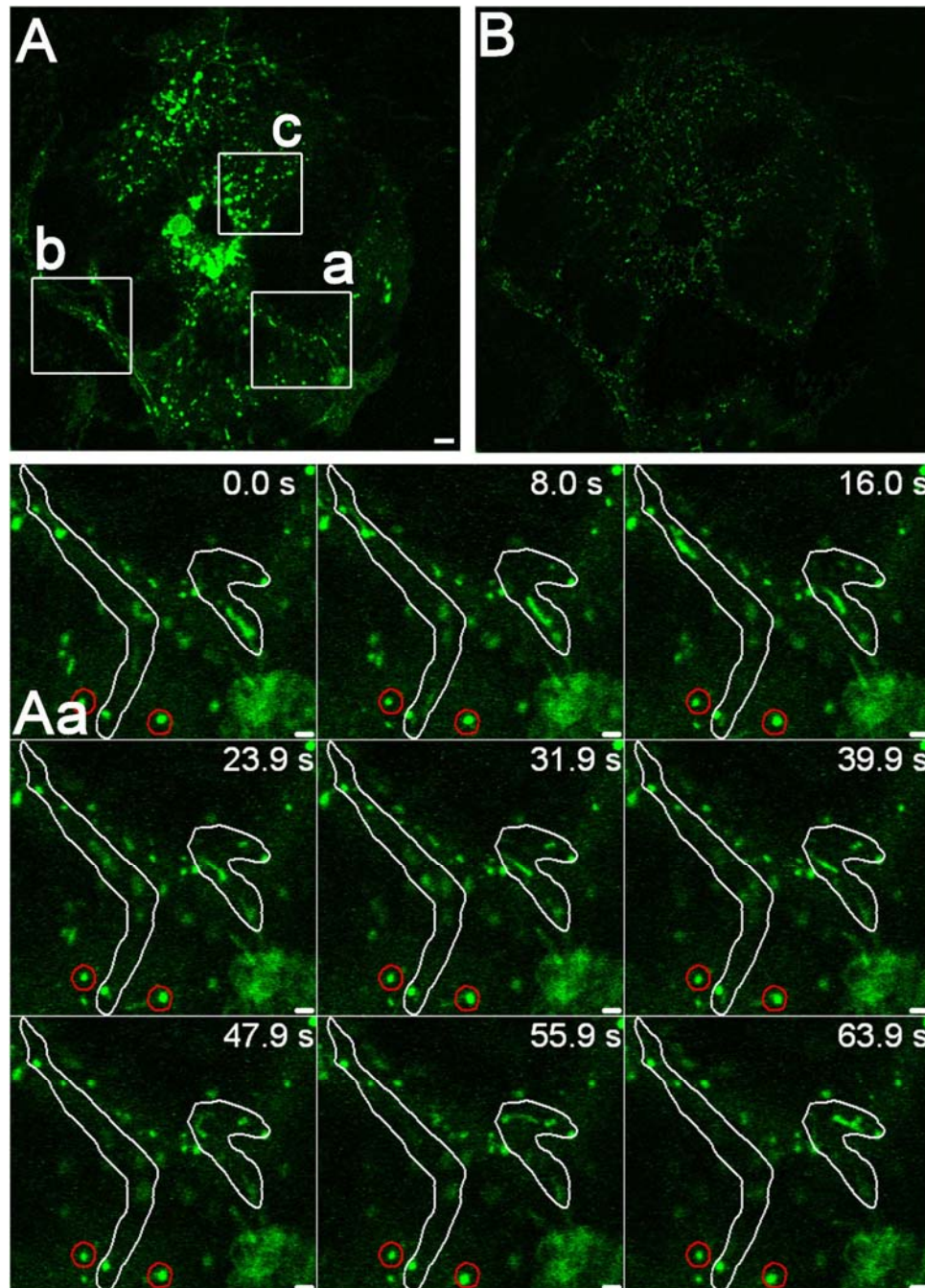


Figure 33: Highly mobile and directed endo/lysosomes in primary oligodendrocytes

Primary oligodendrocytes (OLs) transfected with PLP^{wt}-EGFP construct and imaged live. Scale bar annotates 5 μm . Note that in **A**) a single 200nm thick focal slice and **B**) an image obtained by subtraction from preceding slice, E/Ls are highly mobile in oligodendrocytes and cannot be resolved into vesicular structures. Reducing the time lapse between two scans from 8.9 to 7.9 seconds (fastest at this resolution), still gave a tubular pattern of E/Ls morphology. The endo/lysosomes (E/Ls) in OLs are highly mobile both in the periphery and perinuclearly. Either the E/Ls move much faster than their own diameter and can not be resolved or they exhibit a somewhat tubular morphology in these cells.

Aa) Peripheral pool of E/Ls is highly mobile and appears tubular. Scale bar is 1 μm . Bounded area shows a rough trajectory of highly mobile E/Ls and red marks relatively immobile E/Ls. Note time lapse between consecutive snapshots is 7.99 seconds.

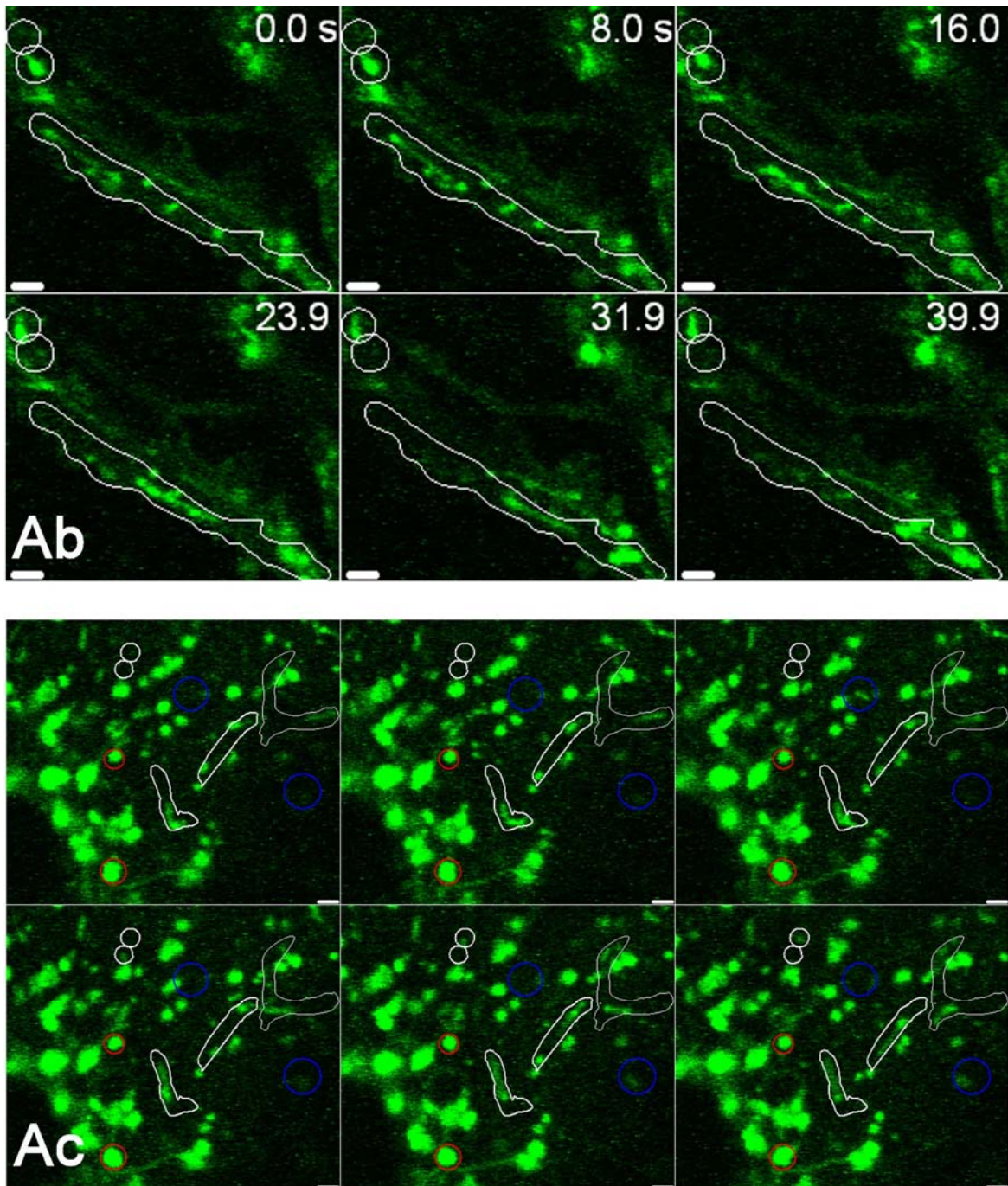


Figure 33 continued: **Ab)** and **Ac)** are time lapsed images of boxed in Figure 33 A of periphery and perinuclear areas respectively. Red circles mark relatively immobile pool with local diffusion. While the circles and the boundaries in white define the path of highly mobile E/Ls. Note that even the perinuclear E/Ls of primary oligodendrocytes show high mobility over a long range with a rod shaped morphology (see the area bounded in white boundaries **Ac**). In a growing process these E/Ls show a high mobility (**Ab**). Blue circles mark an event of appearance and disappearance of E/Ls. Relatively immobile or locally diffusing radius > 500 nm E/Ls are labeled with red boundaries. Scale bar in the image gallery annotates a length of 1 μm

4.4.4 Generation of an *in vivo* tool to study myelination, demyelination and remyelination

Several methodologies have been developed to study function of a gene *in vivo*: Generation of transgenic animals through pronuclear injection (Brinster et al., 1982; Gordon et al., 1980; McKnight et al., 1983) and targeted gene ablation in embryonic stem (ES) cells either by a loss-of-function mutation ('knock-out') or by the insertion of a reporter gene into the genetic locus of interest ('knock-in') or by conditional ablation of gene function in a specific cell type (Doetschman et al., 1987; Thomas and Capecchi, 1987) (Gu et al., 1994). In contrast to knock-in approaches, the promoters used in transgene constructs often do not provide the same pattern of expression seen for the endogenous promoter, but instead give rise to varying expression profiles. This variation in expression may be attributed to *cis*-acting regulatory elements that surround the site of transgene integration into the genome (Caroni, 1997). Thus, this technique requires a multiple founder analysis to identify an animal with a desired transgene expression profile. All seven founders screened for transgenic expression of PLP-EGFP showed no EGFP fluorescence in primary oligodendrocytes (data not shown).

As an alternative approach to label myelin *in vivo* we designed a homologous recombination (knock-in) strategy. We designed a targeting construct in which the translational termination codon of mouse *Plp* gene was replaced by in frame fusion of *Egfp* gene (Figure 34). Screening of about 500 clones ES cell clones yielded a single homologously recombined ES clone, which corresponds to a recombination efficiency of about 0.2 %. Currently, the chimeric animals obtained after the blastocysts injection are under investigation.

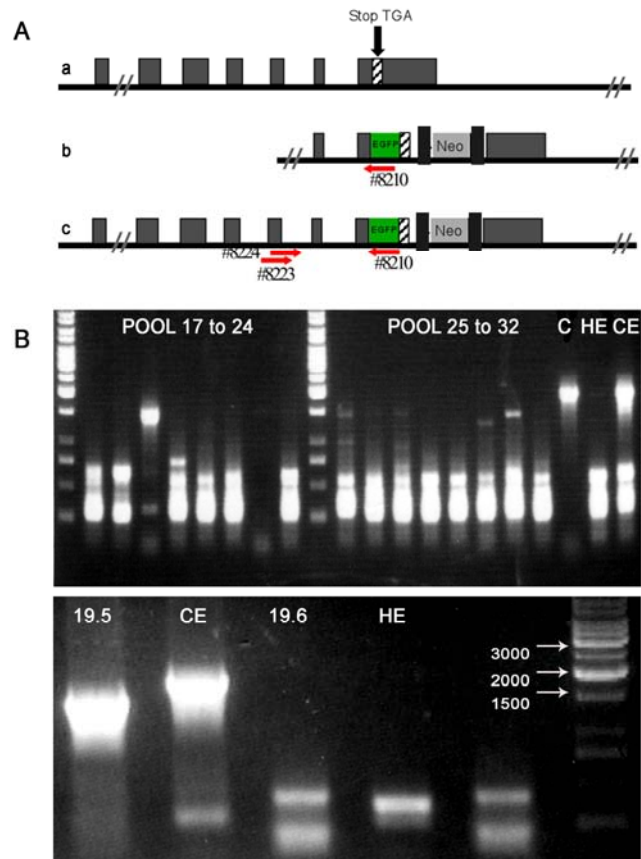


Figure 34: Strategy for targeted homologous recombination of *Plp* gene in mouse ES cells

A) Structure of the *M. musculus Plp* gene (**a**), the targeting construct (**b**) and the targeted gene (**c**). The introns and exons are not drawn to the scale. The PLP/DM20 locus comprises seven exons indicated in grey boxes. Note that after homologous recombination, only the translational termination codon (TGA) is replaced by *Egfp* and *Neo* genes.

B) R1 mouse ES cells were transfected with 50 μ g of the linearized (Sall) targeting construct. Transfected cells were selected with G418 for 8–10 days after electroporation. A fraction of a resistant colony, altogether eight, was pooled along with fractions from seven independent resistant colonies. Homologous recombinants were identified using a pool DNA as a template for PCR (pool 19 identified as positive). HE is PCR water control with ES DNA from non-transfected ES cells. The PCR amplifies a 1.4 kb genomic fragment from homologously recombined allele (clone 19.5) and 1.9 kb from the control plasmid (CE, used to monitor the PCR efficiency). The sense primers (8223 and 8224) corresponded to a PLP genomic sequence localized immediately upstream of the 5' homology region. A reverse primer (8210) was derived from the EGFP gene. Microinjection of selected ES cells into C57BL/6J blastocysts was performed by standard procedures. Currently the chimeric animals are under observation.

4.5 A therapeutic approach towards a mouse model of Pelizaeus-Merzbacher disease; treatment of rumpshaker mice with Turmeric

4.5.1 Curcumin is an active constituent of Turmeric

Curcumin, an active component of turmeric, constitutes about 0.01 to 0.1 % of its dry weight. Curcumin has been shown to resolve amyloid plaques (*in vivo*) (Lim et al., 2001; Yang et al., 2005), and to modulate and abrogate protein aggregates/retention of myelin protein zero (*in vitro*) (Khajavi et al., 2005) and other channel proteins CFTR (*in vivo* and *in vitro*) (Egan et al., 2004). Curcumin is non toxic and potent Ca^{2+} -ATPase pump inhibitor (Logan-Smith et al., 2001). Many ER luminal chaperons are Ca^{2+} binding proteins (Nigam et al., 1994; Szperl and Opas, 2005; Trombetta and Parodi, 1992). To test whether misfolded PLP is also released from ER, in agreement with above reports, we treated rumpshaker mice with turmeric rich diet. Mice under turmeric rich diet live up to three times longer than mice feed with unsupplemented jelly food. We hypothesized that the protective effect of curcumin could result from misfolded PLP to be released from the ER, potentially relieving the toxic effect associated with these mutations in cells.

4.5.2 Curcumin treatment of stable cell line expressing PLP^{msd}-EGFP

Survival of wildtype oli-neu cell was drastically compromised at a concentration $>1 \mu\text{M}$ Curcumin, whereas in above studies and other reports show a tolerance of up to $20 \mu\text{M}$ levels in various cell types. Hence, we treated wildtype and PLP^{msd}-EGFP expressing cells with Curcumin dilutions of up to $1 \mu\text{M}$. Application of $0.1 \mu\text{M}$ and $1 \mu\text{M}$ of Curcumin to cells stably expressing PLP^{msd}-EGFP resulted in a less compacted ER. The mutant PLP reaching the cell surface was not quantified, as both 3F4 and 010 antibody do not recognize PLP^{msd}-EGFP: Curcumin treated cells, displayed an elevated and homogenous distribution of PLP^{msd}-EGFP within ER as compared to the cells treated with DMSO only (Figure 35). The non compact or smoothened ER, resulting from Curcumin treatment, might also lead to a reduced toxicity in these cells. The quantification of mutant PLP^{msd}EGFP released from ER will be quantified in future experiments using biotinylation of all surface proteins and subsequent pull-down using streptavidin-agarose. Presently we are also generating a stable cell line expressing PLP^{rsh}-EGFP. PLP^{rsh} is an Ile 186 to a Thr substitution, in EC2, and is recognized by both conformation specific monoclonal antibodies; 010 and 3F4, hence is easily quantifiable by immunocytochemistry.

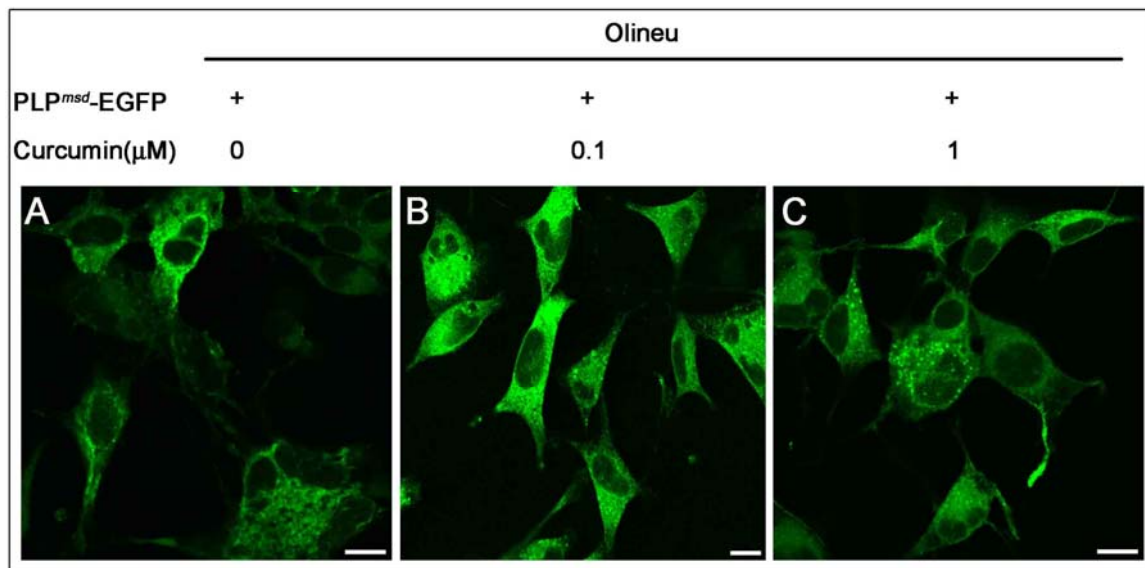


Figure 35: Treatment of PLP^{msd}-EGFP expressing cells with curcumin

Cells supplemented with 0.1 μM (B) and 1 μM curcumin (C) exhibit less compacted ER, compared to the cells treated with DMSO only (A). Due to absence of 010 and 3F4 epitopes the proportion of PLP^{msd}-EGFP at the cell surface, was not quantified (data not shown). Scale bar 10 μm.

4.5.3 Treatment of rumpshaker mice with Turmeric

Rumpshaker is a X-linked mutation in mice and associated with hypomyelination of the central nervous system. It has been shown that the phenotype of rumpshaker mouse depends critically on the genetic background (Al-Saktawi et al., 2003). Rumpshaker mice on a C3H background exhibit a normal longevity despite the impairment. After backcrossing to the inbred strain C57BL/6, the rumpshaker mice develop frequent seizures and die around postnatal day 30 (P30). The dichotomy of the phenotype probably reflects the influence of modifying loci, rather than a differential trafficking between oligodendrocytes from two different backgrounds. In our study, we maintained the mutation on C57BL/6 background. Rumpshaker mice feed on turmeric rich diet (1:10 in jelly food) from P11 onwards on an average lived about 3 times longer than the littermates kept on regular jelly food (Figure 36). This striking difference concerning the longevity, in our preliminary experiment, demonstrates that the active constituent of turmeric, most likely curcumin, can cross the blood brain barrier and modify the phenotype of rumpshaker mice. Moreover the exact molecular mechanism of turmeric action needs to be deliberated in future *in-vitro* approaches.

Rumpshaker mice

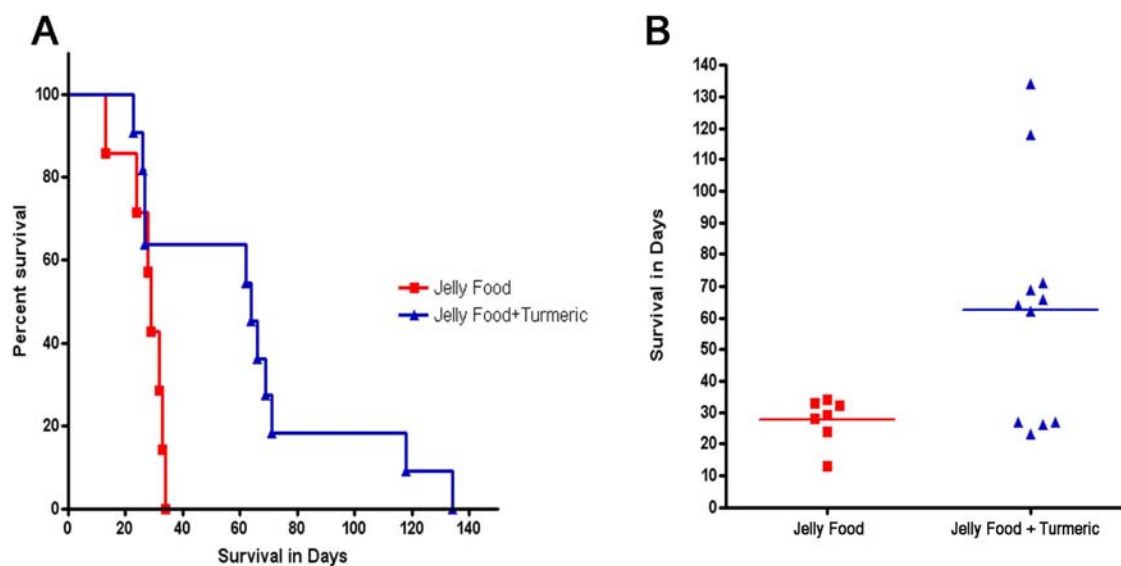


Figure 36: Survival of rumpshaker mice treated with turmeric

Kaplan-Meier and Scatter plot of rumpshaker mice fed with jelly food with (blue triangle,) or without (red square) turmeric supplement (minced roots) from P11 onwards. **A**) Kaplan-Meier plot shows a remarkably better survival of mutant mice fed on diet rich in turmeric compared to controls. All rumpshaker mice on normal diet die around P29 (median), whereas more than 60 % of rumpshaker mice live longer than P64 (median) when fed on turmeric diet from P11 onwards. **B**) Scatter plot of individual mutant animals shows a clear drift towards a prolonged longevity of mutant animals fed on turmeric rich diet.

5 DISCUSSION

5.1 Quality Control of Polytopic Membrane Proteins

5.1.1 Luminal quality control in PLP/DM20 trafficking: an implication to various membrane/secretory protein related diseases

Numerous missense mutations of the human *Plp1* gene have been identified that cause a severe neurological disorder and premature death, but the effect of these mutations is puzzling in this and other disease associated with polytopic membrane proteins. Here, we have shown that various PMD-associated point mutations, previously only predicted to alter the primary structure of the protein in an extracellular loop region, converge mechanistically by perturbing the formation of an intra-molecular disulfide bridge in the lumen of the ER. Surprisingly, this disulfide bridge itself appears dispensable for normal PLP folding and trafficking (Figure 12 and Figure 13). Moreover, in several mutant PLP isoforms derived from PMD patients, it is not the substituted amino acid itself that causes misfolding. Instead, it is an unpaired and sterically exposed cysteine that becomes critical for protein retention, as demonstrated by the rescuing effect of cysteine removal. Given that many membrane proteins harbor intramolecular disulfide bridges in their extracellular loop regions and are sensitive to point mutations in these domains, we suggest that our model is likely relevant to a broader spectrum of genetic disorders (Figure 37).

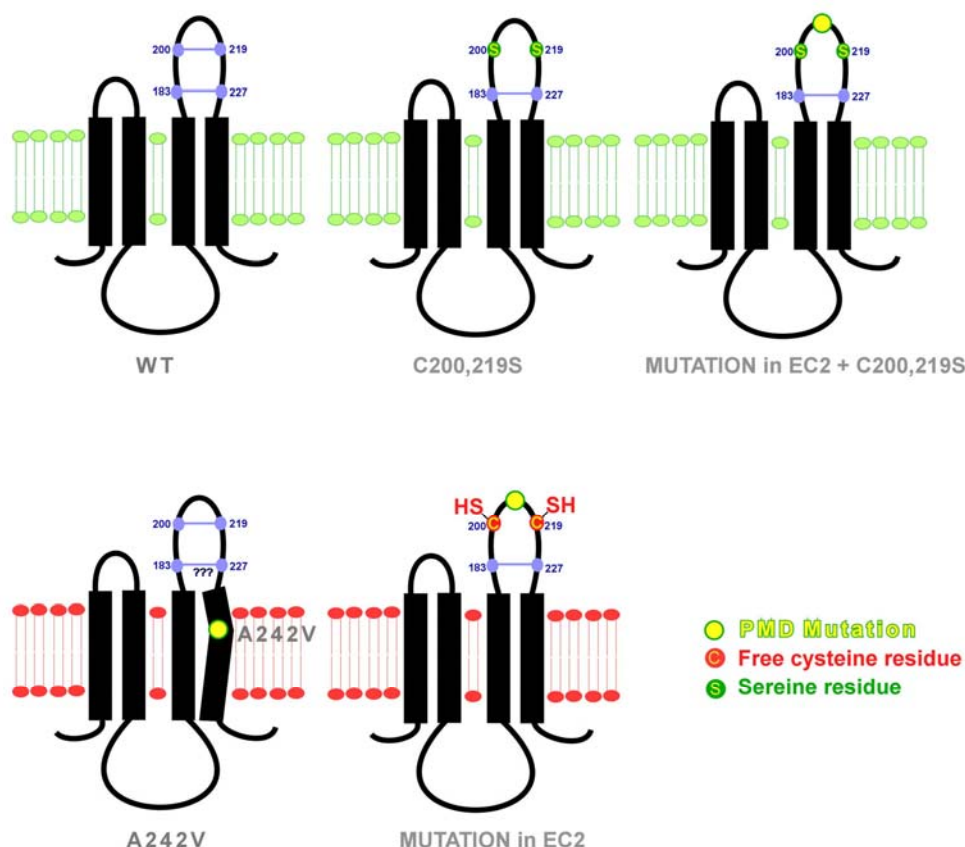


Figure 37: Proposed mechanism of ER retention

Subcellular localization of PLP: wildtype (WT), lacking the “outer” disulfide bond 200-219, *msd* (A242V), bearing a PMD causing mutation and the same PMD mutation in absence of “outer” disulfide bond. Endoplasmic reticulum membranes are drawn in red and the plasma membrane in green.

Note that mutations affecting both EC2 and the TM domain assembly retain PLP in the ER membranes (red membranes, lower panel). Mutations that destabilize globular EC domain (yellow filled circled in the last model) expose free cysteines to the oxidative environment of the ER. Under these conditions PLP forms abnormal dimers and cross links to other proteins. This ER retention of these mutants can be rescued by replacing both cysteines involved in dimerization to serines. PLP lacking outer disulfide bond and bearing a PMD causing mutation is *enrouted* to the cell surface (Green membranes, third model on top).

Mutations affecting TM assembly (A242V i.e, PLP^{*msd*}) has been shown to interact stably with ER lectins (calnexin and calreticulin) in the ER of COS-7 cells. The authenticity of such an interaction, of non glycosylated proteins, is being investigated in cells of oligodendroglial lineage.

Disulfide bridges are thought to stabilize globular domains once properly folded. It appears that for PLP not all disulfide bridges in EC2 are a prerequisite to reach the transport-competent conformation, because cell surface expression is possible in the absence of one cysteine pair (Figure 37). By introducing natural PMD mutations into PLP using site-directed mutagenesis we could show that substitutions within the extracellular loop act by preventing the intra-molecular disulfide bridge and exposing unpaired cysteines to the oxidative environment of the ER. We could also show by SDS-PAGE under non-reducing

conditions, that stable PLP dimers were generated when glial cells express PMD-causing mutants that map into EC2. These cysteine-dependent PLP dimers are novel oxidation products and fail to become O10-positive PLP (oligomers) that can exit the ER (Jung et al., 1996). Thus, abnormal cross-links are a plausible explanation for ER retention, the unfolded protein response, and apoptotic death of susceptible oligodendrocytes *in vivo*. We cannot rule out that prolonged cycles of binding and release of mutant PLP to specific chaperones, such as protein disulfide isomerase (PDI), also contributes to retention. However, attempts to chemically cross-link and immunoprecipitate PDI specifically with mutant PLP were unsuccessful. Also overexpression of mutant PDI lacking its own ER retention signal did not release PLP (data not shown). Finally, PLP interactions with still unidentified proteins in the ER cannot be excluded and could be relevant to oligodendrocyte dysfunction. However, the principle disease mechanism, i.e. the cysteine-dependent cross-linking of PLP secondary to various other mutations, has been proven by restoring normal trafficking in PLP harboring a PMD-causing substitution but lacking the responsible cysteine residues.

The present model was derived from observations with cultured glial cells, but can almost certainly be applied to mutant oligodendrocytes *in vivo*. We and others have extensively characterized the effect of mutations in the *Plp1* gene using *in vivo* systems (Edgar et al., 2004; Gow et al., 1998; Griffiths et al., 1998; Klugmann et al., 1997; Schneider et al., 1992; Schneider et al., 1995). These studies have revealed that oligodendrocytes die with typical features of apoptosis when expressing misfolded PLP/DM20 (Cerghet et al., 2001; Gow et al., 1998; Knapp et al., 1986). Thus, analysis of ER retention and trafficking requires a cellular system that is resistant to mutant PLP expression and cell death, but maintains essential features of oligodendrocytes. The cell line oli-neu, that can be fully differentiated *in vitro* (Jung et al., 1995), is thus optimally suited to study intracellular PLP/DM20 transport.

Recent studies have described the interaction of mutant PLP with calnexin, an ER-resident chaperones in COS-7 cells (Swanton et al., 2003). Whether this binding is the cause or consequence of ER retention remains to be defined. The chosen PMD mutations included substitutions within a TM domain, quite different from loop mutants. We also detected interactions between our PLP mutants in EC2 and calnexin using COS-7 cells, but observed no difference between mutant and wild-type PLP by co-immuno precipitation

(Figure 20 and section 4.1.6). Swanton et al (Swanton et al., 2005) also observed higher than normal dimerization rates of PLP, but the resulting dimers appeared stable in reducing gels, and the possible involvement of cysteines was not investigated.

Disulfide bridges play a key role in protein conformation and stabilization. A classical model system to analyze the impact of amino acid substitutions on membrane protein function is provided by rhodopsin (Khorana, 1992; Stojanovic and Hwa, 2002). Mutations of this multispan membrane protein underlies autosomal-dominant retinitis pigmentosa (ADRP)(Liu et al., 1996), and there are intriguing parallels between PLP and rhodopsin in genetic disease. It is possible that substitutions in the intradiscal/extracellular loop region of rhodopsin and local protein misfolding can prevent intramolecular disulfide bridges similar to the model that we present here.

Many human genetic diseases have been defined by missense mutations that affect polytopic membrane proteins near extracellular cysteine bridges, but exactly why even apparently minor structural changes can cause protein retention and dysfunction has not been investigated. This includes a wide spectrum of human diseases, ranging from specific forms of sensorineural deafness (connexin-26: Ref. (Thomas et al., 2004)) and diabetes insipidus (vasopressin-V2 receptor (Schulein et al., 2001)) to autoimmune disorders (TNF receptor (Galon et al., 2000; McDermott et al., 1999); HDL-deficiency (ABCA1;Ref(Albrecht et al., 2004)), X-linked Charcot-Marie-Tooth neuropathy (connexin-32: Ref.(Yum et al., 2002), and others. To what extent these missense mutation can be explained by cysteine-mediated cross-links, causing ER retention and/or protein dysfunction, can now be experimentally tested.

5.1.2 Self assembly of PLP/DM20 tetraspans

Spastic Paraplegia 2 (SPG2) is a mild form of PMD. SPG2 associated mutations of human *PLP1* gene either affect the soluble intracellular loop (IC) of PLP/DM20 or result in abnormal truncation/termination of growing polypeptide. Surprisingly, PLP/DM20 can tolerate perturbations of IC without an observable change in sub-cellular distribution of mutant PLP/DM20. Replacing a short stretch of 9 to 11 amino acids specifically in PLP or in a region common to both PLP and DM20, did not alter the trafficking of chimeric proteins. These observations explain why, the consequence of mutations affecting IC leads to a relatively mild phenotype.

We have identified a remarkable and novel property of PLP to self assemble when expressed as two independent truncated polypeptides, each exhibiting two transmembrane domains (TM). Hereby, we propose that this property is not unique to PLP but a property inspected by a bonafide quality control operated in the ER. A quality control checking proper assembly of transmembranes, and is also documented for CD82 (Cannon and Cresswell, 2001).

A surprising role of ER lectin calnexin came into limelight when the glycan independent association of calnexin but not the soluble homolog calreticulin was shown by two independent groups (Cannon and Cresswell, 2001; Swanton et al., 2003). Both groups have shown that truncated tetraspanin proteins (TM4-PLP and TM1-CD82) are retained in the ER of COS-7 cells. Interestingly TM4 (PLP) and TM1 (CD82) are both efficient in recruiting calnexin but not calreticulin to stably bind misfolded protein and inhibit the degradation in the ER (at least shown for PLP). We tested this observation further and could show that not only TM4 from PLP, but also TM1,2 (ER retained) and TM1,2 + TM3,4 (at cell surface when co-expressed) are efficient in recruiting calnexin. In addition to calnexin, we also found a strong association of PLP with calreticulin using a same system used by above groups (Figure 20 and section 4.1.6), which challenges the biological relevance of calnexin association. It is important to raise a question about authenticity of these interactions and to test whether these interactions are direct or mediated through an intermediate protein forming a multimeric complex in the ER (Ellgaard and Frickel, 2003; High et al., 2000; Kang and Cresswell, 2002)

PLP has been shown to interact with calreticulin in primary oligodendrocytes (Gudz et al., 2002). Upon stimulation of muscarinic acetylcholine receptors on oligodendrocytes induced formation of a tripartite complex containing PLP, calreticulin, and alpha(v)-integrin. Complex formation was mediated by phospholipase C and Ca^{2+} binding to the high affinity binding site on calreticulin (Gudz et al., 2002).

TM1,2 and TM3,4 derived from PLP^{wt}, when co-expressed in COS-7 and oli-neu cells, result in reconstitution of PLP^{wt} like distribution. Whereas, the same combination of TMs with an Ala242 to Val substitution in TM4 (imitating PLP^{msd} like situation), completely retains both halves of the protein in the ER. This finding strongly supports our hypothesis that all four TMs from PLP must assemble in a proper orientation to *bypass* the stringent quality control governing the assembly of TMs.

TM1,2,3 and TM4 derived from PLP^{wt}, when co-expressed can not *evade* this quality control and completely agrees with our finding that disulfide bridge 183-227 is critical for the assembly of TMs. Future studies are intended to test the authenticity of PLP interaction with various chaperons in the oli-neu cell line stably expressing PLP^{wt} and PLP^{msd}.

5.2 Conformation sensitive epitope of PLP and polarized oligodendrocytes

5.2.1 3F4 and 010 label mutually exclusive compartments of premyelinating oligodendrocytes

In the present study I have identified a conformation sensitive epitope that provides indirect evidence that myelin PLP is derived from endo/lysosomal (E/L) compartment. PLP masks the 3F4 epitope within ER during its synthesis. Strikingly, PLP remains 3F4 negative even at the cell surface, the epitope is only exposed in E/Ls compartment of transfected precursor cells. Non transfected oli-neu cells (with endogenous levels of DM20) also show a similar subcellular distribution of the protein.

In a previous study, our laboratory has identified an 010 epitope exhibited by PLP that is also conformation sensitive (Jung et al., 1996). However in distinction to 3F4, 010 stains PLP as it exits from the ER of primary oligodendrocytes and transfected COS-7 cells. It was shown that the 010 epitope emerges post-translationally. In contrast, 3F4 epitope is completely masked in the ER and at the cell surface (only in premyelinating glia). The only known co- and post-translational modification of PLP/DM20 (in addition to the formation of two disulfide bridges) is the intracellular acylation of cysteine residues (Bizzozero and Good, 1990; Shaw et al., 1989; Weimbs and Stoffel, 1992). Jung et al. (96) further speculated that the 010 epitope emerges after proper folding, i.e., when the correct disulfide bridges have formed or an oligomeric structure has formed.

The presented data strongly support Jung et al's (96) hypothesis, providing direct evidence that in these properly assembled 010⁺ PLP oligomers the 3F4 epitope is completely masked. Cell surface expressed variants of PLP and DM20, PMD causing or rescued by cysteine removal, exhibit an exposed 3F4 epitope. Strikingly, the endo/lysosomal (E/Ls) enriched mutant PLP remain negative for 3F4 to a high extent, unlike PLP^{wt} which offers a high avidity to 3F4 solely in endo/lysosomal (E/L) compartment.

5.2.2 Oligodendrocytes are polarized cells

Oli-neu cells that display a developmental arrest in pre-myelinating state are invaluable tool to study PLP trafficking and process outgrowth during myelination, as the cells are inducible with addition of cAMP to produce artificial myelin like membrane. PLP is 010⁺ throughout its subcellular trafficking pathway whereas, 3F4 epitope emerges only in endo/lysosomal (E/L) compartment of stably transfected oli-neu cells. We have shown that PLP containing E/Ls are highly mobile and fuse with the plasma membrane (Trajkovic et al., 2006). However, unlike the classical secretory lysosomes that are specialized to release luminal content in dendritic cells (Kleijmeer et al., 2001; Trombetta et al., 2003), oligodendrocytes might mainly transport membranes. For oligodendrocytes, PLP/cholesterol rich E/Ls compartments may be particularly useful as storage compartments, as they are able to harbor a large amounts membrane in a multilamellar and multivesicular fashion for myelin biogenesis. The E/Ls in oligodendrocytes are specialized and possess a low proteolytic capacity (Trajkovic et al., 2006). The interesting finding that both epitopes 010 and 3F4 co-exist at the surface of primary oligodendrocytes cultured for 20 days *in vitro* [(Greer et al., 1996) and data not shown] substantiate the findings that specialized lysosomes are docked for regulated exocytosis that may or may not rely on neuron signals.

The PLP-EGFP transgenic “knock in” mice in which, the *Plp-egfp* gene is regulated developmentally from endogenous locus is being generated. This transgene would serve as a useful tool in understanding the mechanisms underlying PMD and other dys-myelinating and de-myelinating diseases *in vivo*.

To test the biological significance of oligomerization state of PLP and compartment specific 3F4⁺ epitope exhibited by PLP. The adult murine spinal cord sections were stained for two different PLP epitopes. Interestingly, a complete overlay of PLP distribution in adult CNS myelin was observed with 3F4 and A431 antibodies, one epitope embedded in IPL and the other in MDL respectively (for myelin periodicity see section 2.2 Figure 2). Both antibodies show an extremely high avidity to PLP/DM20 in adult CNS myelin. We also identified a novel P16 proteolytic cleavage (P.C) product of PLP (P16) in purified myelin (section 4.3.3), using immuno-blot detection with 3F4 antibody. The presence of PLP P.C product (P10) was only documented in equine myelin (McLaughlin et al., 2002).

These PLP derived secretory P.C products are speculated to have an early developmental function in a premyelination state (Yamada et al., 1999).

We here propose a model in which PLP during its exit from the ER oligomerizes in cis by virtue of its TMs (similar to connexins, not necessarily hexamers) predominantly bearing intra-molecular disulfides. After and during endocytotic, PLP mature in E/Ls compartment where the TM assembly is stabilized by association with cholesterol and neighboring PLP/DM20 may or may not be further required for cis-stabilization. Now PLP docks itself for myelin compaction and it does so by forming inter-molecular disulfides in trans, which might also involve some cleavage and intercalation of proteolipid cleavage products (P.C: P10 and P16) for efficient packaging.

We have also used 3F4 as a tool to address the question of a mutation-induced misfolding of PLP and DM20 and have shown that the antibody 3F4 distinguishes between wild-type PLP/DM20 and mutant isoforms. All mutant isoforms tested in oli-neu and COS-7 cells exhibit a tremendous avidity to 3F4. Staining both live and fixed cells with 3F4 antibody we have demonstrated that in wild-type PLP the 3F4 epitope is masked after its exit from the ER and at the cell surface. The epitope is exposed only in E/Ls prior to myelination and in compact CNS myelin. Whereas mutant PLP exposes the 3F4 epitope within ER and at the cell surface, which might trigger recruitment of receptors/factors responsible for myelination prematurely and hence destabilizing ER and plasma membrane of cells expressing mutant PLP.

Taken together, in conjunction with 010 epitope, we suggest that 3F4 and 010 epitopes label PLP in mutually exclusive compartments in a premyelination state of oligodendrocytes. On receiving appropriate signals and to cope with membrane extension and surface area expansion during myelination, oligodendrocytes mature and might display exocytosis via two independently regulated pathways i.e, classical from post-golgi derived vesicles (regulated at translational level, otherwise constitutive) and the endo/lysosomal fusion for massive outbursts (Trajkovic et al., 2006). These myelinating oligodendrocytes from this stage onwards co-exhibit both 3F4 and 010.

5.3 Treatment of Rumpshaker mice with Turmeric

Turmeric has long been used in both Indian (Ayurvedic) and Chinese medicine as an anti-inflammatory, to treat digestive disorders and liver problems, and for the treatment of skin diseases and wound healing. The active ingredient in turmeric is curcumin, and it has been the subject of numerous animal studies. Recently, curcumin has been shown to resolve amyloid plaques (*in vivo*) (Lim et al., 2001; Yang et al., 2005) hence the drug is capable to cross the blood brain barrier. It also has been shown to modulate and abrogate protein aggregates/retention of myelin protein zero (*in vitro*) (Khajavi et al., 2005) and other channel proteins CFTR (*in vivo* and *in vitro*) (Egan et al., 2004). At molecular level, curcumin acts as a non toxic and potent Ca^{2+} -ATPase pump inhibitor (Logan-Smith et al., 2001). As many luminal chaperons are Ca^{2+} binding proteins (Nigam et al., 1994; Szperl and Opas, 2005; Trombetta and Parodi, 1992) here we directly tested with an *in vivo* approach whether misfolded PLP is released from the ER or not.

In our pilot experiment, rumpshaker mice (a model of PMD) were directly fed with a diet supplemented with the dried rhizome powder (turmeric) as a source of curcumin, from postnatal day 11 (P11) onwards. Turmeric supplemented food was simply kept in the cages housing mutant mice. The dosage each animal received was dictated by an urge/desire of animal to eat supplemented food (the only option in the cage). Interestingly this simple treatment course caused a remarkable increase in the life expectancy of the mutant mice. The treated mice, on an average showed longevity of 2 to 3 times (between 60 to 140 days, except few who died at same age as normal diet) as compared to control mice with an average life expectancy of between 26 to 30 days. As human studies indicate that curcumin is tolerated in extremely large oral doses without apparent toxicity (Cheng et al., 2001), our exciting data might potentially lead to a cure for Pelizaeus-Merzbacher disease.

In future studies we intend to administer curcumin (purified) doses orally, on an approximated weight per weight basis. The molecular mechanism of curcumin action in mutant oligodendrocytes is under investigation, currently.

6 REFERENCES

- Al-Saktawi, K., M. McLaughlin, M. Klugmann, A. Schneider, J.A. Barrie, M.C. McCulloch, P. Montague, D. Kirkham, K.A. Nave, and I.R. Griffiths. 2003. Genetic background determines phenotypic severity of the Plp rumpshaker mutation. *J Neurosci Res.* 72:12-24.
- Albrecht, C., K. Baynes, A. Sardini, S. Schepelmann, E.R. Eden, S.W. Davies, C.F. Higgins, M.D. Feher, J.S. Owen, and A.K. Soutar. 2004. Two novel missense mutations in ABCA1 result in altered trafficking and cause severe autosomal recessive HDL deficiency. *Biochim Biophys Acta.* 1689:47-57.
- Barres, B.A., and M.C. Raff. 1999. Axonal control of oligodendrocyte development. *J Cell Biol.* 147:1123-8.
- Birling, M.C., S. Tait, R.J. Hardy, and P.J. Brophy. 1999. A novel rat tetraspan protein in cells of the oligodendrocyte lineage. *J Neurochem.* 73:2600-8.
- Bizzozero, O.A., and L.K. Good. 1990. Myelin proteolipid protein contains thioester-linked fatty acids. *J Neurochem.* 55:1986-92.
- Boison, D., and W. Stoffel. 1994. Disruption of the compacted myelin sheath of axons of the central nervous system in proteolipid protein-deficient mice. *Proc Natl Acad Sci U S A.* 91:11709-13.
- Bond, C., X. Si, M. Crisp, P. Wong, G.W. Paulson, C.P. Boesel, S.R. Dlouhy, and M.E. Hodes. 1997. Family with Pelizaeus-Merzbacher disease/X-linked spastic paraplegia and a nonsense mutation in exon 6 of the proteolipid protein gene. *Am J Med Genet.* 71:357-60.
- Bongarzone, E.R., C.W. Campagnoni, K. Kampf, E.C. Jacobs, V.W. Handley, V. Schonmann, and A.T. Campagnoni. 1999. Identification of a new exon in the myelin proteolipid protein gene encoding novel protein isoforms that are restricted to the somata of oligodendrocytes and neurons. *J Neurosci.* 19:8349-57.
- Bongarzone, E.R., E. Jacobs, V. Schonmann, and A.T. Campagnoni. 2001. Classic and soma-restricted proteolipids are targeted to different subcellular compartments in oligodendrocytes. *J Neurosci Res.* 65:477-84.
- Brinster, R.L., H.Y. Chen, R. Warren, A. Sarthy, and R.D. Palmiter. 1982. Regulation of metallothionein--thymidine kinase fusion plasmids injected into mouse eggs. *Nature.* 296:39-42.
- Cailloux, F., F. Gauthier-Barichard, C. Mimault, V. Isabelle, V. Courtois, G. Giraud, B. Dastugue, and O. Boespflug-Tanguy. 2000. Genotype-phenotype correlation in inherited brain myelination defects due to proteolipid protein gene mutations. Clinical European Network on Brain Dysmyelinating Disease. *Eur J Hum Genet.* 8:837-45.
- Campagnoni, C.W., B. Garbay, P. Micevych, T. Pribyl, K. Kampf, V.W. Handley, and A.T. Campagnoni. 1992. DM20 mRNA splice product of the myelin proteolipid protein gene is expressed in the murine heart. *J Neurosci Res.* 33:148-55.
- Cannon, K.S., and P. Cresswell. 2001. Quality control of transmembrane domain assembly in the tetraspanin CD82. *Embo J.* 20:2443-53.
- Caroni, P. 1997. Overexpression of growth-associated proteins in the neurons of adult transgenic mice. *J Neurosci Methods.* 71:3-9.
- Cerghet, M., D.A. Bessert, K.A. Nave, and R.P. Skoff. 2001. Differential expression of apoptotic markers in jimpy and in Plp overexpressors: evidence for different apoptotic pathways. *J Neurocytol.* 30:841-55.
- Cheng, A.L., C.H. Hsu, J.K. Lin, M.M. Hsu, Y.F. Ho, T.S. Shen, J.Y. Ko, J.T. Lin, B.R. Lin, W. Ming-Shiang, H.S. Yu, S.H. Jee, G.S. Chen, T.M. Chen, C.A. Chen, M.K.

- Lai, Y.S. Pu, M.H. Pan, Y.J. Wang, C.C. Tsai, and C.Y. Hsieh. 2001. Phase I clinical trial of curcumin, a chemopreventive agent, in patients with high-risk or pre-malignant lesions. *Anticancer Res.* 21:2895-900.
- Colman, D.R., G. Kreibich, A.B. Frey, and D.D. Sabatini. 1982. Synthesis and incorporation of myelin polypeptides into CNS myelin. *J Cell Biol.* 95:598-608.
- Coman, I., G. Barbin, P. Charles, B. Zalc, and C. Lubetzki. 2005. Axonal signals in central nervous system myelination, demyelination and remyelination. *J Neurol Sci.* 233:67-71.
- Corfas, G., M.O. Velardez, C.P. Ko, N. Ratner, and E. Peles. 2004. Mechanisms and roles of axon-Schwann cell interactions. *J Neurosci.* 24:9250-60.
- Dhaunchak, A.S. 2003. Intracellular trafficking of PLP and its mutated isoforms. In Department of Neurogenetics, Max Planck Institute for Experimental Medicine. Vol. Master of Sciences. Georg August University, Goettingen.
- Doetschman, T., R.G. Gregg, N. Maeda, M.L. Hooper, D.W. Melton, S. Thompson, and O. Smithies. 1987. Targetted correction of a mutant HPRT gene in mouse embryonic stem cells. *Nature.* 330:576-8.
- Domeniconi, M., Z. Cao, T. Spencer, R. Sivasankaran, K. Wang, E. Nikulina, N. Kimura, H. Cai, K. Deng, Y. Gao, Z. He, and M. Filbin. 2002. Myelin-associated glycoprotein interacts with the Nogo66 receptor to inhibit neurite outgrowth. *Neuron.* 35:283-90.
- Edgar, J.M., M. McLaughlin, D. Yool, S.C. Zhang, J.H. Fowler, P. Montague, J.A. Barrie, M.C. McCulloch, I.D. Duncan, J. Garbern, K.A. Nave, and I.R. Griffiths. 2004. Oligodendroglial modulation of fast axonal transport in a mouse model of hereditary spastic paraplegia. *J Cell Biol.* 166:121-31.
- Egan, M.E., M. Pearson, S.A. Weiner, V. Rajendran, D. Rubin, J. Glockner-Pagel, S. Canny, K. Du, G.L. Lukacs, and M.J. Caplan. 2004. Curcumin, a major constituent of turmeric, corrects cystic fibrosis defects. *Science.* 304:600-2.
- Ellgaard, L., and E.M. Frickel. 2003. Calnexin, calreticulin, and ERp57: teammates in glycoprotein folding. *Cell Biochem Biophys.* 39:223-47.
- Ellgaard, L., and A. Helenius. 2003. Quality control in the endoplasmic reticulum. *Nat Rev Mol Cell Biol.* 4:181-91.
- Ellgaard, L., M. Molinari, and A. Helenius. 1999. Setting the standards: quality control in the secretory pathway. *Science.* 286:1882-8.
- Ever, L., and N. Gaiano. 2005. Radial 'glial' progenitors: neurogenesis and signaling. *Curr Opin Neurobiol.* 15:29-33.
- Federovitch, C.M., D. Ron, and R.Y. Hampton. 2005. The dynamic ER: experimental approaches and current questions. *Curr Opin Cell Biol.* 17:409-14.
- Feng, J.M., A.O. Fernandes, E.R. Bongarzone, C.W. Campagnoni, K. Kampf, and A.T. Campagnoni. 2003. Expression of soma-restricted proteolipid/DM20 proteins in lymphoid cells. *J Neuroimmunol.* 144:9-15.
- Fiedler, K., F. Lafont, R.G. Parton, and K. Simons. 1995. Annexin XIIIb: a novel epithelial specific annexin is implicated in vesicular traffic to the apical plasma membrane. *J Cell Biol.* 128:1043-53.
- Fiedler, K., R.G. Parton, R. Kellner, T. Etzold, and K. Simons. 1994. VIP36, a novel component of glycolipid rafts and exocytic carrier vesicles in epithelial cells. *Embo J.* 13:1729-40.

- Galon, J., I. Aksentijevich, M.F. McDermott, J.J. O'Shea, and D.L. Kastner. 2000. TNFRSF1A mutations and autoinflammatory syndromes. *Curr Opin Immunol.* 12:479-86.
- Girault, J.A., and E. Peles. 2002. Development of nodes of Ranvier. *Curr Opin Neurobiol.* 12:476-85.
- Giri, R.K., V. Rajagopal, and V.K. Kalra. 2004. Curcumin, the active constituent of turmeric, inhibits amyloid peptide-induced cytochemokine gene expression and CCR5-mediated chemotaxis of THP-1 monocytes by modulating early growth response-1 transcription factor. *J Neurochem.* 91:1199-210.
- Gordon, J.W., G.A. Scangos, D.J. Plotkin, J.A. Barbosa, and F.H. Ruddle. 1980. Genetic transformation of mouse embryos by microinjection of purified DNA. *Proc Natl Acad Sci U S A.* 77:7380-4.
- Gow, A., V.L. Friedrich, Jr., and R.A. Lazzarini. 1994. Intracellular transport and sorting of the oligodendrocyte transmembrane proteolipid protein. *J Neurosci Res.* 37:563-73.
- Gow, A., A. Gragerov, A. Gard, D.R. Colman, and R.A. Lazzarini. 1997. Conservation of topology, but not conformation, of the proteolipid proteins of the myelin sheath. *J Neurosci.* 17:181-9.
- Gow, A., and R.A. Lazzarini. 1996. A cellular mechanism governing the severity of Pelizaeus-Merzbacher disease. *Nat Genet.* 13:422-8.
- Gow, A., C.M. Southwood, and R.A. Lazzarini. 1998. Disrupted proteolipid protein trafficking results in oligodendrocyte apoptosis in an animal model of Pelizaeus-Merzbacher disease. *J Cell Biol.* 140:925-34.
- Gow, A., C.M. Southwood, J.S. Li, M. Pariali, G.P. Riordan, S.E. Brodie, J. Danias, J.M. Bronstein, B. Kachar, and R.A. Lazzarini. 1999. CNS myelin and sertoli cell tight junction strands are absent in Osp/claudin-11 null mice. *Cell.* 99:649-59.
- Greer, J.M., C.A. Dyer, M. Pakaski, C. Symonowicz, and M.B. Lees. 1996. Orientation of myelin proteolipid protein in the oligodendrocyte cell membrane. *Neurochem Res.* 21:431-40.
- Griffiths, I., M. Klugmann, T. Anderson, D. Yool, C. Thomson, M.H. Schwab, A. Schneider, F. Zimmermann, M. McCulloch, N. Nadon, and K.A. Nave. 1998. Axonal swellings and degeneration in mice lacking the major proteolipid of myelin. *Science.* 280:1610-3.
- Griffiths, I.R., I. Scott, M.C. McCulloch, J.A. Barrie, K. McPhilemy, and B.M. Cattanach. 1990. Rumpshaker mouse: a new X-linked mutation affecting myelination: evidence for a defect in PLP expression. *J Neurocytol.* 19:273-83.
- Gu, H., J.D. Marth, P.C. Orban, H. Mossmann, and K. Rajewsky. 1994. Deletion of a DNA polymerase beta gene segment in T cells using cell type-specific gene targeting. *Science.* 265:103-6.
- Gudz, T.I., T.E. Schneider, T.A. Haas, and W.B. Macklin. 2002. Myelin proteolipid protein forms a complex with integrins and may participate in integrin receptor signaling in oligodendrocytes. *J Neurosci.* 22:7398-407.
- Harding, H.P., M. Calton, F. Urano, I. Novoa, and D. Ron. 2002. Transcriptional and translational control in the Mammalian unfolded protein response. *Annu Rev Cell Dev Biol.* 18:575-99.
- High, S., F.J. Lecomte, S.J. Russell, B.M. Abell, and J.D. Oliver. 2000. Glycoprotein folding in the endoplasmic reticulum: a tale of three chaperones? *FEBS Lett.* 476:38-41.

- Horvath, L.I., P.J. Brophy, and D. Marsh. 1990. Influence of polar residue deletions on lipid-protein interactions with the myelin proteolipid protein. Spin-label ESR studies with DM-20/lipid recombinants. *Biochemistry*. 29:2635-8.
- Hurtley, S.M., and A. Helenius. 1989. Protein oligomerization in the endoplasmic reticulum. *Annu Rev Cell Biol*. 5:277-307.
- Hwang, C., A.J. Sinskey, and H.F. Lodish. 1992. Oxidized redox state of glutathione in the endoplasmic reticulum. *Science*. 257:1496-502.
- Inouye, H., and D.A. Kirschner. 1994. Membrane topology of PLP in CNS myelin: evaluation of models. *Neurochem Res*. 19:975-81.
- Ishibashi, T., L. Ding, K. Ikenaka, Y. Inoue, K. Miyado, E. Mekada, and H. Baba. 2004. Tetraspanin protein CD9 is a novel paranodal component regulating paranodal junctional formation. *J Neurosci*. 24:96-102.
- Jacobs, E.C., E.R. Bongarzone, C.W. Campagnoni, and A.T. Campagnoni. 2004. Embryonic expression of the soma-restricted products of the myelin proteolipid gene in motor neurons and muscle. *Neurochem Res*. 29:997-1002.
- Jung, M., E. Kramer, M. Grzenkowski, K. Tang, W. Blakemore, A. Aguzzi, K. Khazaie, K. Chlichlia, G. von Blankenfeld, H. Kettenmann, and et al. 1995. Lines of murine oligodendroglial precursor cells immortalized by an activated neu tyrosine kinase show distinct degrees of interaction with axons in vitro and in vivo. *Eur J Neurosci*. 7:1245-65.
- Jung, M., I. Sommer, M. Schachner, and K.A. Nave. 1996. Monoclonal antibody O10 defines a conformationally sensitive cell-surface epitope of proteolipid protein (PLP): evidence that PLP misfolding underlies dysmyelination in mutant mice. *J Neurosci*. 16:7920-9.
- Kang, S.J., and P. Cresswell. 2002. Calnexin, calreticulin, and ERp57 cooperate in disulfide bond formation in human CD1d heavy chain. *J Biol Chem*. 277:44838-44.
- Kaur, C., A.J. Hao, C.H. Wu, and E.A. Ling. 2001. Origin of microglia. *Microsc Res Tech*. 54:2-9.
- Khajavi, M., K. Inoue, W. Wiszniewski, T. Ohyama, G.J. Snipes, and J.R. Lupski. 2005. Curcumin treatment abrogates endoplasmic reticulum retention and aggregation-induced apoptosis associated with neuropathy-causing myelin protein zero-truncating mutants. *Am J Hum Genet*. 77:841-50.
- Khorana, H.G. 1992. Rhodopsin, photoreceptor of the rod cell. An emerging pattern for structure and function. *J Biol Chem*. 267:1-4.
- Kleijmeer, M., G. Ramm, D. Schuurhuis, J. Griffith, M. Rescigno, P. Ricciardi-Castagnoli, A.Y. Rudensky, F. Ossendorp, C.J. Melief, W. Stoorvogel, and H.J. Geuze. 2001. Reorganization of multivesicular bodies regulates MHC class II antigen presentation by dendritic cells. *J Cell Biol*. 155:53-63.
- Kleijnen, M.F., J.B. Huppa, P. Lucin, S. Mukherjee, H. Farrell, A.E. Campbell, U.H. Koszinowski, A.B. Hill, and H.L. Ploegh. 1997. A mouse cytomegalovirus glycoprotein, gp34, forms a complex with folded class I MHC molecules in the ER which is not retained but is transported to the cell surface. *Embo J*. 16:685-94.
- Kleizen, B., and I. Braakman. 2004. Protein folding and quality control in the endoplasmic reticulum. *Curr Opin Cell Biol*. 16:343-9.
- Klugmann, M., M.H. Schwab, A. Puhlhofer, A. Schneider, F. Zimmermann, I.R. Griffiths, and K.A. Nave. 1997. Assembly of CNS myelin in the absence of proteolipid protein. *Neuron*. 18:59-70.

- Knapp, P.E., R.P. Skoff, and D.W. Redstone. 1986. Oligodendroglial cell death in jimpy mice: an explanation for the myelin deficit. *J Neurosci.* 6:2813-22.
- Kobayashi, H., C.A. Garcia, G. Alfonso, H.G. Marks, and E.P. Hoffman. 1996. Molecular genetics of familial spastic paraplegia: a multitude of responsible genes. *J Neurol Sci.* 137:131-8.
- Konola, J.T., T. Yamamura, B. Tyler, and M.B. Lees. 1992. Orientation of the myelin proteolipid protein C-terminus in oligodendroglial membranes. *Glia.* 5:112-21.
- Kroepfl, J.F., and M.V. Gardinier. 2001. Mutually exclusive apicobasolateral sorting of two oligodendroglial membrane proteins, proteolipid protein and myelin/oligodendrocyte glycoprotein, in Madin-Darby canine kidney cells. *J Neurosci Res.* 66:1140-8.
- Lazzarini RA, G.J., Lassmann H, Nave KA, Miller R, Trapp B. 2003. Myelin Biology and Disorders. Elsevier Academic Press.
- Lees, M., and S. Brostoff. 1984. Proteins of Myelin. *Plenum, New York.*
- Lemke, G., and R. Axel. 1985. Isolation and sequence of a cDNA encoding the major structural protein of peripheral myelin. *Cell.* 40:501-8.
- Lim, G.P., T. Chu, F. Yang, W. Beech, S.A. Frautschy, and G.M. Cole. 2001. The curry spice curcumin reduces oxidative damage and amyloid pathology in an Alzheimer transgenic mouse. *J Neurosci.* 21:8370-7.
- Liu, X., P. Garriga, and H.G. Khorana. 1996. Structure and function in rhodopsin: correct folding and misfolding in two point mutants in the intradiscal domain of rhodopsin identified in retinitis pigmentosa. *Proc Natl Acad Sci U S A.* 93:4554-9.
- Logan-Smith, M.J., P.J. Lockyer, J.M. East, and A.G. Lee. 2001. Curcumin, a molecule that inhibits the Ca²⁺-ATPase of sarcoplasmic reticulum but increases the rate of accumulation of Ca²⁺. *J Biol Chem.* 276:46905-11.
- McDermott, M.F., I. Aksentjevich, J. Galon, E.M. McDermott, B.W. Ogunkolade, M. Centola, E. Mansfield, M. Gadina, L. Karenko, T. Pettersson, J. McCarthy, D.M. Frucht, M. Aringer, Y. Torosyan, A.M. Teppo, M. Wilson, H.M. Karaarslan, Y. Wan, I. Todd, G. Wood, R. Schlingens, T.R. Kumarajeewa, S.M. Cooper, J.P. Vella, C.I. Amos, J. Mulley, K.A. Quane, M.G. Molloy, A. Ranki, R.J. Powell, G.A. Hitman, J.J. O'Shea, and D.L. Kastner. 1999. Germline mutations in the extracellular domains of the 55 kDa TNF receptor, TNFR1, define a family of dominantly inherited autoinflammatory syndromes. *Cell.* 97:133-44.
- McKnight, G.S., R.E. Hammer, E.A. Kuenzel, and R.L. Brinster. 1983. Expression of the chicken transferrin gene in transgenic mice. *Cell.* 34:335-41.
- McLaughlin, M., D.J. Hunter, C.E. Thomson, D. Yool, D. Kirkham, A.A. Freer, and I.R. Griffiths. 2002. Evidence for possible interactions between PLP and DM20 within the myelin sheath. *Glia.* 39:31-6.
- Michailov, G.V., M.W. Sereda, B.G. Brinkmann, T.M. Fischer, B. Haug, C. Birchmeier, L. Role, C. Lai, M.H. Schwab, and K.A. Nave. 2004. Axonal neuregulin-1 regulates myelin sheath thickness. *Science.* 304:700-3.
- Mothes, W., S.U. Heinrich, R. Graf, I. Nilsson, G. von Heijne, J. Brunner, and T.A. Rapoport. 1997. Molecular mechanism of membrane protein integration into the endoplasmic reticulum. *Cell.* 89:523-33.
- Natarajan, C., and J.J. Bright. 2002. Curcumin inhibits experimental allergic encephalomyelitis by blocking IL-12 signaling through Janus kinase-STAT pathway in T lymphocytes. *J Immunol.* 168:6506-13.

- Nave, K., and O. Boespflug-Tanguy. 1996. X-linked developmental defects of myelination: From mouse mutants to human genetic diseases. *Neuroscientist*. 2:33–43.
- Nave, K.A., C. Lai, F.E. Bloom, and R.J. Milner. 1987. Splice site selection in the proteolipid protein (PLP) gene transcript and primary structure of the DM-20 protein of central nervous system myelin. *Proc Natl Acad Sci U S A*. 84:5665-9.
- Nedergaard, M., B. Ransom, and S.A. Goldman. 2003. New roles for astrocytes: redefining the functional architecture of the brain. *Trends Neurosci*. 26:523-30.
- Nigam, S.K., A.L. Goldberg, S. Ho, M.F. Rohde, K.T. Bush, and M. Sherman. 1994. A set of endoplasmic reticulum proteins possessing properties of molecular chaperones includes Ca(2+)-binding proteins and members of the thioredoxin superfamily. *J Biol Chem*. 269:1744-9.
- Nimmerjahn, A., F. Kirchhoff, and F. Helmchen. 2005. Resting microglial cells are highly dynamic surveillants of brain parenchyma in vivo. *Science*. 308:1314-8.
- Osaka, H., C. Kawanishi, K. Inoue, H. Onishi, T. Kobayashi, N. Sugiyama, K. Kosaka, A. Nezu, K. Fujii, K. Sugita, K. Kodama, K. Murayama, S. Murayama, I. Kanazawa, and S. Kimura. 1999. Pelizaeus-Merzbacher disease: three novel mutations and implication for locus heterogeneity. *Ann Neurol*. 45:59-64.
- Patil, C., and P. Walter. 2001. Intracellular signaling from the endoplasmic reticulum to the nucleus: the unfolded protein response in yeast and mammals. *Curr Opin Cell Biol*. 13:349-55.
- Pedraza, L., J.K. Huang, and D.R. Colman. 2001. Organizing principles of the axoglial apparatus. *Neuron*. 30:335-44.
- Pfeiffer, S.E., A.E. Warrington, and R. Bansal. 1993. The oligodendrocyte and its many cellular processes. *Trends Cell Biol*. 3:191-7.
- Pfriege, F.W. 2002. Role of glia in synapse development. *Curr Opin Neurobiol*. 12:486-90.
- Popot, J.L., D. Pham Dinh, and A. Dautigny. 1991. Major Myelin proteolipid: the 4-alpha-helix topology. *J Membr Biol*. 120:233-46.
- Pribyl, T.M., C.W. Campagnoni, K. Kampf, T. Kashima, V.W. Handley, J. McMahon, and A.T. Campagnoni. 1996. Expression of the myelin proteolipid protein gene in the human fetal thymus. *J Neuroimmunol*. 67:125-30.
- Ransom, B., T. Behar, and M. Nedergaard. 2003. New roles for astrocytes (stars at last). *Trends Neurosci*. 26:520-2.
- Readhead, C., A. Schneider, I. Griffiths, and K.A. Nave. 1994. Premature arrest of myelin formation in transgenic mice with increased proteolipid protein gene dosage. *Neuron*. 12:583-95.
- Richter-Landsberg, C., and M. Heinrich. 1996. OLN-93: a new permanent oligodendroglia cell line derived from primary rat brain glial cultures. *J Neurosci Res*. 45:161-73.
- Rosenbluth, J., W. Stoffel, and R. Schiff. 1996. Myelin structure in proteolipid protein (PLP)-null mouse spinal cord. *J Comp Neurol*. 371:336-44.
- Rutkowski, D.T., and R.J. Kaufman. 2004. A trip to the ER: coping with stress. *Trends Cell Biol*. 14:20-8.
- Saher, G., B. Brugger, C. Lappe-Siefke, W. Mobius, R. Tozawa, M.C. Wehr, F. Wieland, S. Ishibashi, and K.A. Nave. 2005. High cholesterol level is essential for myelin membrane growth. *Nat Neurosci*. 8:468-75.
- Salzer, J.L. 2003. Polarized domains of myelinated axons. *Neuron*. 40:297-318.

- Sankaram, M.B., P.J. Brophy, and D. Marsh. 1991. Lipid-protein and protein-protein interactions in double recombinants of myelin proteolipid apoprotein and myelin basic protein with dimyristoylphosphatidylglycerol. *Biochemistry*. 30:5866-73.
- Sarkar, F.H., and Y. Li. 2004. Cell signaling pathways altered by natural chemopreventive agents. *Mutat Res*. 555:53-64.
- Saugier-veber, P., A. Munnich, D. Bonneau, J.M. Rozet, M. Le Merrer, R. Gil, and O. Boespflug-Tanguy. 1994. X-linked spastic paraplegia and Pelizaeus-Merzbacher disease are allelic disorders at the proteolipid protein locus. *Nat Genet*. 6:257-62.
- Scapagnini, G., C. Colombrita, M. Amadio, V. D'Agata, E. Arcelli, M. Sapienza, A. Quattrone, and V. Calabrese. 2006. Curcumin activates defensive genes and protects neurons against oxidative stress. *Antioxid Redox Signal*. 8:395-403.
- Schneider, A., P. Montague, I. Griffiths, M. Fanarraga, P. Kennedy, P. Brophy, and K.A. Nave. 1992. Uncoupling of hypomyelination and glial cell death by a mutation in the proteolipid protein gene. *Nature*. 358:758-61.
- Schneider, A.M., I.R. Griffiths, C. Readhead, and K.A. Nave. 1995. Dominant-negative action of the jimpy mutation in mice complemented with an autosomal transgene for myelin proteolipid protein. *Proc Natl Acad Sci U S A*. 92:4447-51.
- Schulein, R., K. Zuhlke, G. Krause, and W. Rosenthal. 2001. Functional rescue of the nephrogenic diabetes insipidus-causing vasopressin V2 receptor mutants G185C and R202C by a second site suppressor mutation. *J Biol Chem*. 276:8384-92.
- Seitelberger, F. 1995. Neuropathology and genetics of Pelizaeus-Merzbacher disease. *Brain Pathol*. 5:267-73.
- Shaw, S.Y., R.A. Laursen, and M.B. Lees. 1989. Identification of thiol groups and a disulfide crosslink site in bovine myelin proteolipid protein. *FEBS Lett*. 250:306-10.
- Simons, K., and E. Ikonen. 1997. Functional rafts in cell membranes. *Nature*. 387:569-72.
- Sternberger, N.H., R.H. Quarles, Y. Itoyama, and H.D. Webster. 1979. Myelin-associated glycoprotein demonstrated immunocytochemically in myelin and myelin-forming cells of developing rat. *Proc Natl Acad Sci U S A*. 76:1510-4.
- Stevens, B., S. Porta, L.L. Haak, V. Gallo, and R.D. Fields. 2002. Adenosine: a neuron-glia transmitter promoting myelination in the CNS in response to action potentials. *Neuron*. 36:855-68.
- Stoffel, W., T. Subkowski, and S. Jander. 1989. Topology of proteolipid protein in the myelin membrane of central nervous system. A study using antipeptide antibodies. *Biol Chem Hoppe Seyler*. 370:165-76.
- Stojanovic, A., and J. Hwa. 2002. Rhodopsin and retinitis pigmentosa: shedding light on structure and function. *Receptors Channels*. 8:33-50.
- Swanton, E., S. High, and P. Woodman. 2003. Role of calnexin in the glycan-independent quality control of proteolipid protein. *Embo J*. 22:2948-58.
- Swanton, E., A. Holland, S. High, and P. Woodman. 2005. Disease-associated mutations cause premature oligomerization of myelin proteolipid protein in the endoplasmic reticulum. *Proc Natl Acad Sci U S A*. 102:4342-7.
- Szperl, M., and M. Opas. 2005. [Calreticulin, Ca²⁺-binding chaperon of the endoplasmic reticulum]. *Postepy Biochem*. 51:382-6.
- Taveggia, C., G. Zanazzi, A. Petrylak, H. Yano, J. Rosenbluth, S. Einheber, X. Xu, R.M. Esper, J.A. Loeb, P. Shrager, M.V. Chao, D.L. Falls, L. Role, and J.L. Salzer. 2005. Neuregulin-1 type III determines the ensheathment fate of axons. *Neuron*. 47:681-94.

- Thomas, K.R., and M.R. Capecchi. 1987. Site-directed mutagenesis by gene targeting in mouse embryo-derived stem cells. *Cell*. 51:503-12.
- Thomas, T., D. Telford, and D.W. Laird. 2004. Functional domain mapping and selective trans-dominant effects exhibited by Cx26 disease-causing mutations. *J Biol Chem*. 279:19157-68.
- Thomson, C.E., P. Montague, M. Jung, K.A. Nave, and I.R. Griffiths. 1997. Phenotypic severity of murine Plp mutants reflects in vivo and in vitro variations in transport of PLP isoproteins. *Glia*. 20:322-32.
- Tiwari-Woodruff, S.K., R. Kaplan, H.I. Kornblum, and J.M. Bronstein. 2004. Developmental expression of OAP-1/Tspan-3, a member of the tetraspanin superfamily. *J Neurosci Res*. 77:166-73.
- Tomita, M., B.J. Holman, C.P. Santoro, and T.J. Santoro. 2005. Astrocyte production of the chemokine macrophage inflammatory protein-2 is inhibited by the spice principle curcumin at the level of gene transcription. *J Neuroinflammation*. 2:8.
- Trajkovic, K., A.S. Dhaunchak, J.T. Goncalves, D. Wenzel, A. Schneider, G. Bunt, K.A. Nave, and M. Simons. 2006. Neuron to glia signaling triggers myelin membrane exocytosis from endosomal storage sites. *J Cell Biol*. 172:937-48.
- Trapp, B.D. 1988. Distribution of the myelin-associated glycoprotein and P0 protein during myelin compaction in quaking mouse peripheral nerve. *J Cell Biol*. 107:675-85.
- Trapp, B.D., P. Hauer, and G. Lemke. 1988. Axonal regulation of myelin protein mRNA levels in actively myelinating Schwann cells. *J Neurosci*. 8:3515-21.
- Trapp, B.D., A. Nishiyama, D. Cheng, and W. Macklin. 1997. Differentiation and death of premyelinating oligodendrocytes in developing rodent brain. *J Cell Biol*. 137:459-68.
- Trombetta, E.S., M. Ebersold, W. Garrett, M. Pypaert, and I. Mellman. 2003. Activation of lysosomal function during dendritic cell maturation. *Science*. 299:1400-3.
- Trombetta, S.E., and A.J. Parodi. 1992. Purification to apparent homogeneity and partial characterization of rat liver UDP-glucose:glycoprotein glucosyltransferase. *J Biol Chem*. 267:9236-40.
- Tsukada, Y., and H. Suda. 1980. Solubilization and purification of 2',3'-cyclic nucleotide 3'-phosphohydrolase (CNP-A) from bovine cerebral white matter--a review. *Cell Mol Biol Incl Cyto Enzymol*. 26:493-504.
- Voskuhl, R.R. 1998. Myelin protein expression in lymphoid tissues: implications for peripheral tolerance. *Immunol Rev*. 164:81-92.
- Weimbs, T., and W. Stoffel. 1992. Proteolipid protein (PLP) of CNS myelin: positions of free, disulfide-bonded, and fatty acid thioester-linked cysteine residues and implications for the membrane topology of PLP. *Biochemistry*. 31:12289-96.
- Weimbs, T., and W. Stoffel. 1994. Topology of CNS myelin proteolipid protein: evidence for the nonenzymatic glycosylation of extracytoplasmic domains in normal and diabetic animals. *Biochemistry*. 33:10408-15.
- Werner, H., M. Jung, M. Klugmann, M. Sereda, I.R. Griffiths, and K.A. Nave. 1998. Mouse models of myelin diseases. *Brain Pathol*. 8:771-93.
- Yamada, M., A. Ivanova, Y. Yamaguchi, M.B. Lees, and K. Ikenaka. 1999. Proteolipid protein gene product can be secreted and exhibit biological activity during early development. *J Neurosci*. 19:2143-51.
- Yang, F., G.P. Lim, A.N. Begum, O.J. Ubeda, M.R. Simmons, S.S. Ambegaokar, P.P. Chen, R. Kaye, C.G. Glabe, S.A. Frautschy, and G.M. Cole. 2005. Curcumin

- inhibits formation of amyloid beta oligomers and fibrils, binds plaques, and reduces amyloid in vivo. *J Biol Chem.* 280:5892-901.
- Yum, S.W., K.A. Kleopa, S. Shumas, and S.S. Scherer. 2002. Diverse trafficking abnormalities of connexin32 mutants causing CMTX. *Neurobiol Dis.* 11:43-52.

Appendix A: Abbreviations

Amino acid	Either three or single letter codes used
DM20	Splice variant of PLP
EC	Extracellular loop
E/Ls	Endosomes/lysosomes
EGFP	Enhanced green fluorescent protein
IC	Intracellular loop
Myc	EQKISEEDL (epitope with sequence, single letter code)
PLP	Proteolipid protein
<i>PLP1</i> gene	Human Proteolipid protein gene
<i>Plp1</i> or <i>Plp</i> gene	Mouse Proteolipid protein gene
PMD	Pelizaeus-Merzbacher disease
Δ	Deletion
PLP ^{wt} or wt	wildtype proteolipid protein
PLP ^{msd} or msd	Ala 242 to Val substitution
PLP ^{C200S}	cys 200 replaced to ser
TM	Transmembrane domain

In general, PLP with a superscript annotates that the superscripted amino acid residue is replaced. For numbering amino acid residue in PLP or DM20, numbering according to PLP primary structure was annotated to both PLP and DM20.

Other Abbreviation

3F4, 010, A431	anti-PLP antibodies
βME	Beta-mercaptoethanol
bp	Base pairs
BSA	Bovine serum albumin
°C	Degrees Celsius (centigrades)
CNS	Central nervous system
DMEM	Dulbecco's Modified Eagles Medium
DMSO	Dimethylsulfoxide
Kb	Kilobases
kDa	Kilodalton
M	Molar
mM	Millimolar
mA	milliAmpere

min	Minutes
ml	Milliliter
µg	Microgram
µl	Microliter
ng	Nanogram
µm	Micrometer
nm	nanometer
PAGE	Polyacrylamidgelelektrophorese
PBS	Phosphate buffered saline
PFA	Paraformaldehyde
PNS	Peripheral nervous system
Rpm	Rotations per minute
RT	Room temperature
s	Seconds
SDS	Sodium dodecyl sulfate
TBS	Tris buffered saline
TBE	Tris-Borat/EDTA
TEMED	Tetramethylendiamin
Tris/Cl	Tris-(hydroxymethyl)-aminomethan titred with HCl
U	Unit, (for enzyme activities)
V	Volt

Appendix B: Publications

Ajit Singh Dhaunchak and Klaus-Armin Nave “Rescue of mutant membrane protein from ER retention identifies a common disease mechanism” **PLOS Biology**, under review 2006 May 29. **(Results section 4.1)**

Katarina Trajkovic*, **Ajit Singh Dhaunchak***, José T Goncalves, Dirk Wenzel, Anja Schneider, Gertrude Bunt, Klaus-Armin Nave, Mikael Simons. “Neuron to glia signaling triggers myelin membrane exocytosis from endosomal storage sites”. *Journal of Cell Biology*; 2006 Mar 13;172(6):799-801,

* Equal Contribution

(Reprint enclosed)

Ajit Singh Dhaunchak and Klaus-Armin Nave “Quality control of transmembrane assembly in PLP”. **In preparation.**

Ajit Singh Dhaunchak and Klaus-Armin Nave “Conformation sensitive and compartment specific epitope of PLP: evidence that PLP matures within ER”. **In preparation.**

Neuron to glia signaling triggers myelin membrane exocytosis from endosomal storage sites

Katarina Trajkovic,^{1,2} Ajit Singh Dhaunchak,² José T. Goncalves,² Dirk Wenzel,¹ Anja Schneider,^{1,2} Gertrude Bunt,² Klaus-Armin Nave,² and Mikael Simons^{1,2}

¹Centre for Biochemistry and Molecular Cell Biology, University of Göttingen, 37073 Göttingen, Germany

²Max-Planck-Institute for Experimental Medicine, 37075 Göttingen, Germany

During vertebrate brain development, axons are enveloped by myelin, an insulating membrane produced by oligodendrocytes. Neuron-derived signaling molecules are temporally and spatially required to coordinate oligodendrocyte differentiation. In this study, we show that neurons regulate myelin membrane trafficking in oligodendrocytes. In the absence of neurons, the major myelin membrane protein, the proteolipid protein (PLP), is internalized and stored in late endosomes/lysosomes (LEs/Ls) by a cholesterol-dependent and clathrin-

independent endocytosis pathway that requires actin and the RhoA guanosine triphosphatase. Upon maturation, the rate of endocytosis is reduced, and a cAMP-dependent neuronal signal triggers the transport of PLP from LEs/Ls to the plasma membrane. These findings reveal a fundamental and novel role of LEs/Ls in oligodendrocytes: to store and release PLP in a regulated fashion. The release of myelin membrane from LEs/Ls by neuronal signals may represent a mechanism to control myelin membrane growth.

Introduction

The myelin sheath is a multilamellar, spirally wrapping extension of the plasma membrane of oligodendrocytes that is essential for rapid impulse conduction in the central nervous system. This specialized membrane exhibits a unique composition with >70% of the dry weight consisting of lipids and the remainder being comprised of a restricted set of proteins, of which most are exclusively found in myelin (Baumann and Pham-Dinh, 2001; Kramer et al., 2001). The major central nervous system myelin proteins, the myelin basic protein, and the proteolipid proteins (PLPs/DM20) are low molecular weight proteins found in compact myelin that constitute 80% of the total myelin proteins. PLP is a highly hydrophobic protein with four transmembrane domains that interact with cholesterol and galactosylceramide-enriched membranes during its biosynthetic transport in oligodendrocytes (Weimbs and Stoffel, 1992; Simons et al., 2000; Schneider et al., 2005).

To form the myelin sheath, oligodendrocytes must deliver large amounts of myelin membrane to the axons at the appropriate developmental stage of the oligodendroglial and neuronal

cell lineage (Baumann and Pham-Dinh, 2001; Kramer et al., 2001). On the other hand, axons produce signals that regulate the differentiation of oligodendrocytes (Barres and Raff, 1999; Fields and Stevens-Graham, 2002). This led us to postulate that neuronal signals could be involved in the coordination of the trafficking of myelin membrane in oligodendrocytes. In this study, we show that the transport of PLP in oligodendrocytes is under neuronal control. PLP is initially targeted to late endosomes/lysosomes (LEs/Ls) by using a cholesterol-dependent and clathrin-independent endocytosis pathway. PLP is then redistributed from LEs/Ls to the plasma membrane upon activation by neuronal cells. We provide evidence that this development-dependent regulation of PLP localization occurs by the down-regulation of endocytosis and by the stimulation of exocytosis from LE/L storage sites.

Results

PLP localizes to LEs/Ls of immature oligodendrocytes

To analyze the localization of PLP in immature oligodendrocytes, oligodendroglial precursor cells growing on top of a layer of astrocytes were shaken off and cultured for 3 d to induce the expression of PLP. By confocal immunofluorescence microscopy, extensive colocalization of PLP and Lamp-1, a marker for

K. Trajkovic and A.S. Dhaunchak contributed equally to this paper.

Correspondence to M. Simons: msimons@gwdg.de

Abbreviations used in this paper: LE/L, late endosome/lysosome; mβCD, methyl-β-cyclodextrin; MHC, major histocompatibility complex; PLP, proteolipid protein; TIRFM, total internal reflection fluorescence microscopy.

The online version of this article contains supplemental material.

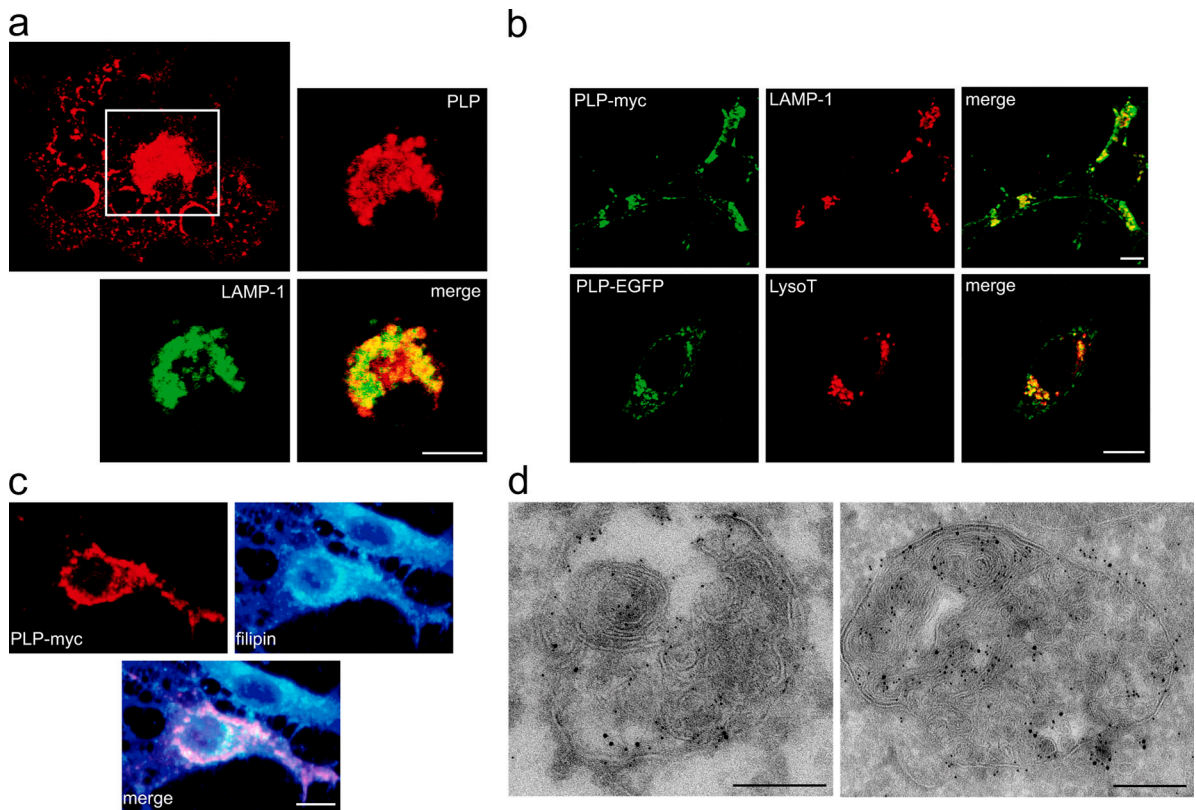


Figure 1. PLP localizes to LEs/Ls of immature oligodendrocytes. (a) Confocal immunofluorescence microscopy demonstrates the colocalization of endogenous PLP (red) with Lamp-1 (green) in primary oligodendrocytes grown for 3 d in vitro. The region in the boxed area is shown at higher magnification and lower exposure. (b) Top panels show the colocalization of PLP-myc (green) with Lamp-1 (red) in Oli-neu cells, and the bottom panels show the colocalization of PLP-EGFP (green) with LysoTracker red in living OLN-93 cells. (c) Filipin staining reveals colocalization of cholesterol (blue) and PLP (red) in OLN-93 cells. (a–c) Bars, 5 μ m. (d) Immuno-EM double labeling of primary oligodendrocytes (left) and Oli-neu cells (right) with antibodies directed against Lamp-1 (5 nm gold) and against PLP, polyclonal P6 (left), or GFP (right; both 10 nm gold) shows the localization of PLP in Lamp-1-containing multivesicular and multilamellar compartments. Bars, 200 nm.

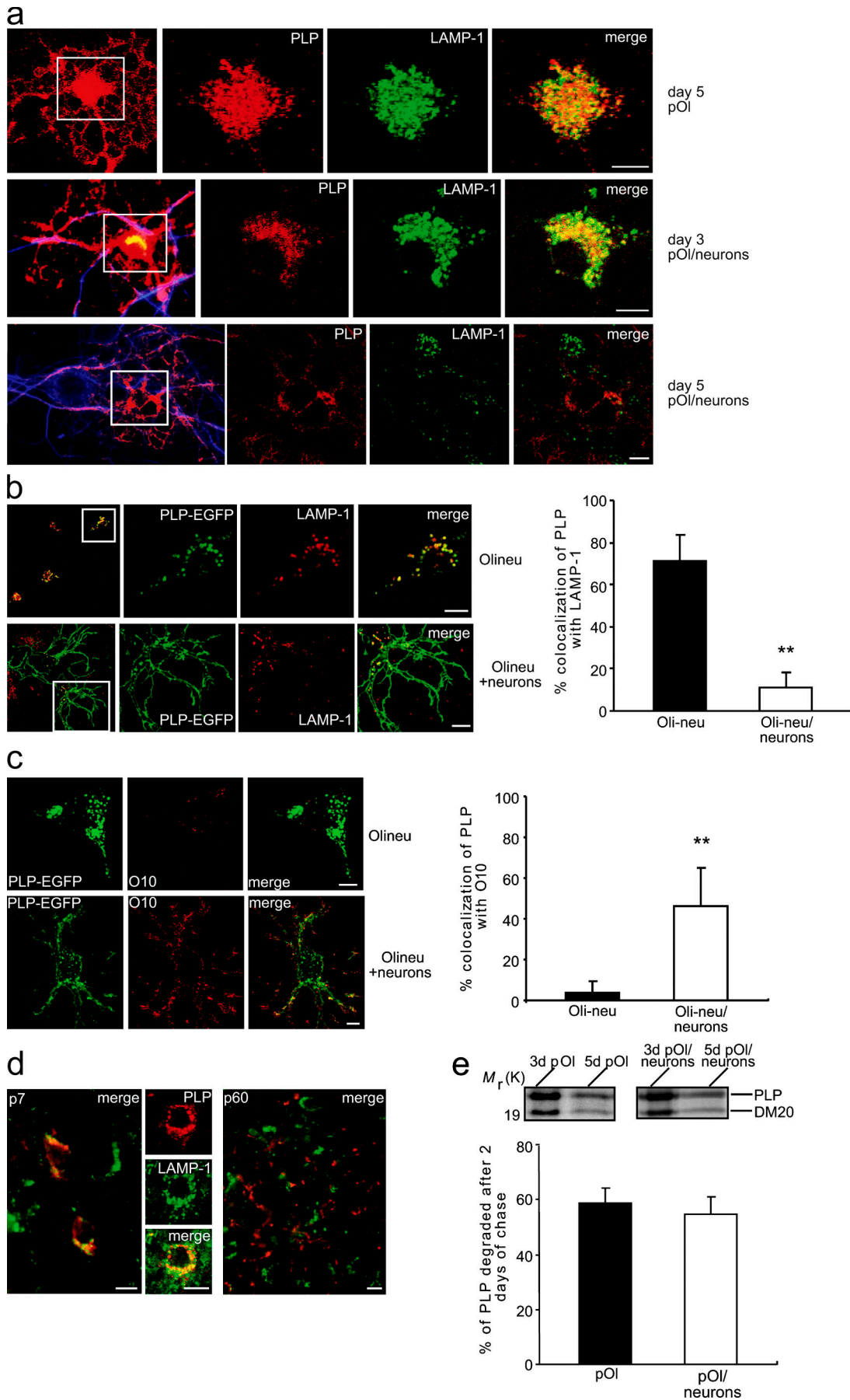
LEs/Ls, was observed (Fig. 1 a) as reported previously (Kramer et al., 2001; Simons et al., 2002). The same striking colocalization of PLP and Lamp-1 was observed in an immortalized oligodendroglial precursor cell line, Oli-neu. Fusion of either a myc tag or EGFP to PLP did not affect the LE/L targeting of PLP (Fig. 1 b). To obtain further support for the localization of PLP to LEs/Ls in immature cells, we used a spontaneously transformed oligodendroglial precursor cell line, OLN-93. When these cells were incubated for 5 h with rhodamine-dextran followed by a 2-h chase or were treated with LysoTracker red DND-99 to stain for LEs/Ls, colocalization with PLP was observed (Fig. 1 b and not depicted). Staining with filipin revealed a partial colocalization of PLP with cholesterol in LEs/Ls (Fig. 1 c).

To resolve the ultrastructure of the PLP-containing organelles, we performed immunoelectron microscopy (Fig. 1 d). Both endogenous PLP and PLP-EGFP colocalized with Lamp-1 in vacuolar structures that contained abundant luminal multilamellar and/or multivesicular membrane arrays.

PLP disappears from LEs/Ls when oligodendrocytes are cocultured with neurons

To determine whether the subcellular localization of PLP is influenced by the presence of neuronal cells, oligodendroglial progenitor cells were added to a neuronal cell culture. Similar to the cultures without neurons, oligodendrocytes started to

Figure 2. PLP disappears from LEs/Ls when oligodendrocytes are cocultured with neurons. (a) Primary oligodendrocytes were grown for 3 or 5 d with or without neurons. Confocal microscopy analysis of PLP (red) and Lamp-1 (green) demonstrates a depletion of PLP from LEs/Ls in oligodendrocytes when cultured in the presence of neurons for 5 d. Axons are visualized by β III-tubulin staining (blue). (b) Oli-neu cells were grown for 2 d with (bottom) or without (top) neurons. PLP-EGFP (green) disappears from Lamp-1-containing compartments (red) by 2 d of coculture with neurons. (a and b) The regions in the boxed areas are shown at a higher magnification and lower exposure. (c) Surface staining of living cells with O10 mAb at 4°C shows that the majority of PLP-EGFP is found at the surface of the cell in a coculturing with neurons. Quantitative analysis of the colocalization of PLP-EGFP with Lamp-1 (b) and O10 (c) are shown. Error bars represent SD ($n > 30$ cells). (a–c) Bars, 5 μ m. (d) Immunohistochemistry of brain sections of P7 and P60 adult mice for PLP (red) and Lamp-1 (green). Colocalization was observed in sections from P7 but not adult mice. Bars, 10 μ m. (e) Oligodendrocytes (for 2 d in culture) grown with or without neurons were metabolically labeled with [³⁵S]methionine/cysteine for 18 h and chased for 2 d (day 5) or not chased (day 3) before performing the PLP immunoprecipitations. Quantitative analysis of three independent experiments did not reveal any significant differences in the amount of labeled PLP and its alternatively spliced isoform DM20 (mean \pm SD). **, $P < 0.001$; † test.



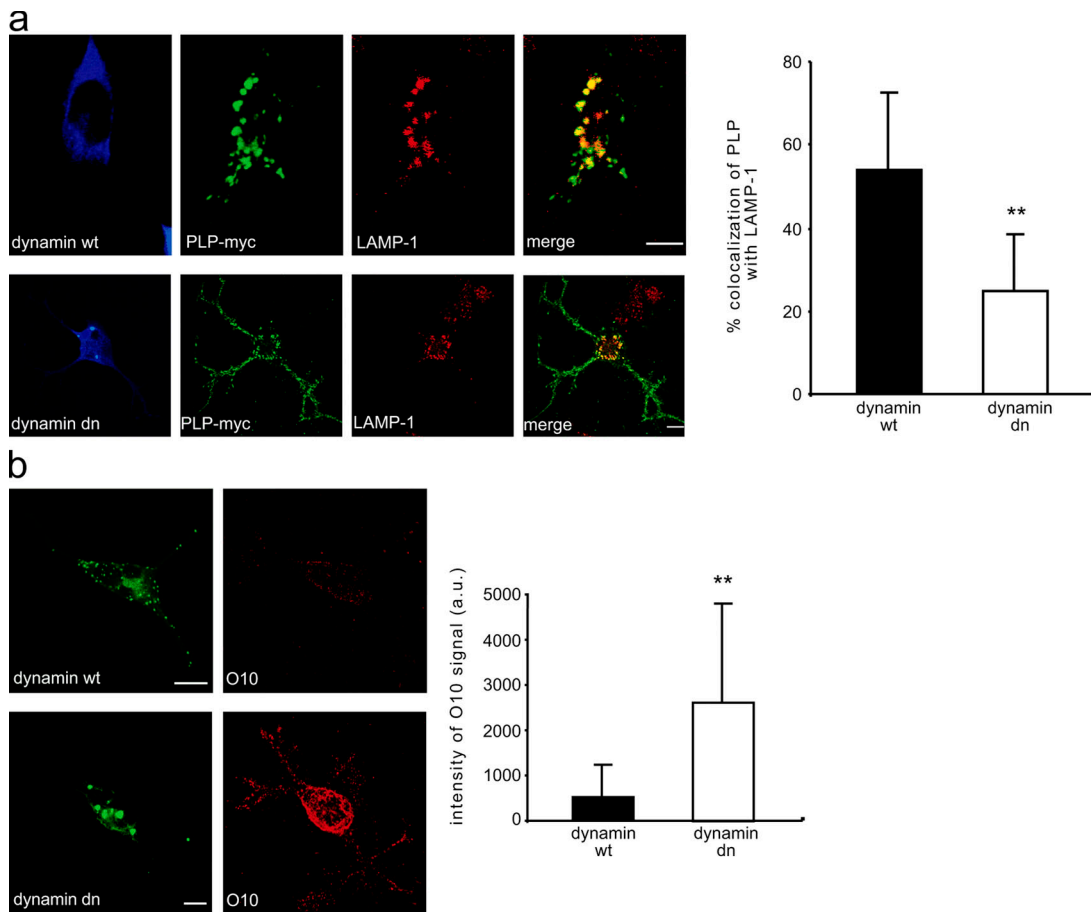


Figure 3. **PLP is routed to LEs/Ls by endocytosis.** Oli-neu cells were cotransfected with PLP-myc and wild-type or dominant-negative dynamin-II (K44A, dynamin dn), both containing an HA tag, and were stained for Lamp-1 (a) or for surface PLP (b) with O10 mAb (at 4°C on living cells). (a) Quantitative analysis of the colocalization of PLP-EGFP with Lamp-1 is shown. (b) Quantitative analysis of the fluorescence intensity of O10 signal is shown in arbitrary units (a.u.) per cell. (a and b) Values are given as the means \pm SD (error bars) of a mean of three independent experiments with >40 (a) or >30 (b) cells. **, $P < 0.001$; t test. Bars, 5 μ m.

express PLP during the first 2 d in culture, and an accumulation of PLP in LEs/Ls was observed in $\sim 90\%$ of the cells after 3 d in culture (Fig. 2 a). However, in marked contrast to cultures without neurons, we observed that PLP disappeared from LEs/Ls 2 d later (only $\sim 20\%$ of the cells showed an accumulation of PLP in LEs/Ls) in the presence of neurons (Fig. 2 a). Also, the staining of Lamp-1-containing structures decreased in intensity after PLP removal. To follow the developmental regulation of PLP trafficking in Oli-neu cells, we produced PLP-EGFP-stably expressing cell lines. Fusion of EGFP to PLP did not interfere with transport to the cell surface, as indicated by the positive staining of transfected Oli-neu cells with O10 mAb. This antibody recognizes a conformation-dependent epitope of PLP on the surface of living cells (Jung et al., 1996). In addition, transfection of primary myelinating oligodendrocytes confirmed that PLP-EGFP is transported to myelin (Fig. S1, available at <http://www.jcb.org/cgi/content/full/jcb.200509022/DC1>). When PLP-EGFP-expressing Oli-neu cells were added on top of a neuronal culture, a dramatic change in the localization of PLP was observed (Fig. 2 b). Quantitative analysis showed that 71.5% of PLP colocalized with Lamp-1 in Oli-neu cells alone, whereas only 11.5% of PLP colocalized with Lamp-1 in

cells that had been in coculture with neurons for 2 d (Fig. 2 b). Moreover, surface staining of living cells at 4°C with O10 mAb showed that the majority of PLP-EGFP was located at the plasma membrane in cells cultured with but not without neurons (Fig. 2 c). To test whether the localization of PLP shows the same developmental regulation in vivo, we performed immunohistochemistry on brain sections of young (postnatal day [P] 7) and adult mice (P60). Significant colocalization of PLP and Lamp-1 was only observed in cells of P7 mice but not in sections prepared from adult mice (Fig. 2 d). Analysis of the sections indicated that the colocalization of PLP and Lamp-1 was increased >20 -fold in P7 mice as compared with adult mice. Together, our data demonstrate that PLP disappears from LEs/Ls upon oligodendroglial maturation and emerges at the surface of the oligodendrocyte in a process that is dependent on the presence of neuronal cells.

There are several possibilities to explain our results. One possibility is that less PLP is transported into and/or more PLP is transported out of LEs/Ls in the presence of neurons. An alternative explanation is that the degradation of PLP in lysosomes increases during development. To test the latter hypothesis, we performed pulse-chase experiments. Primary oligodendrocytes

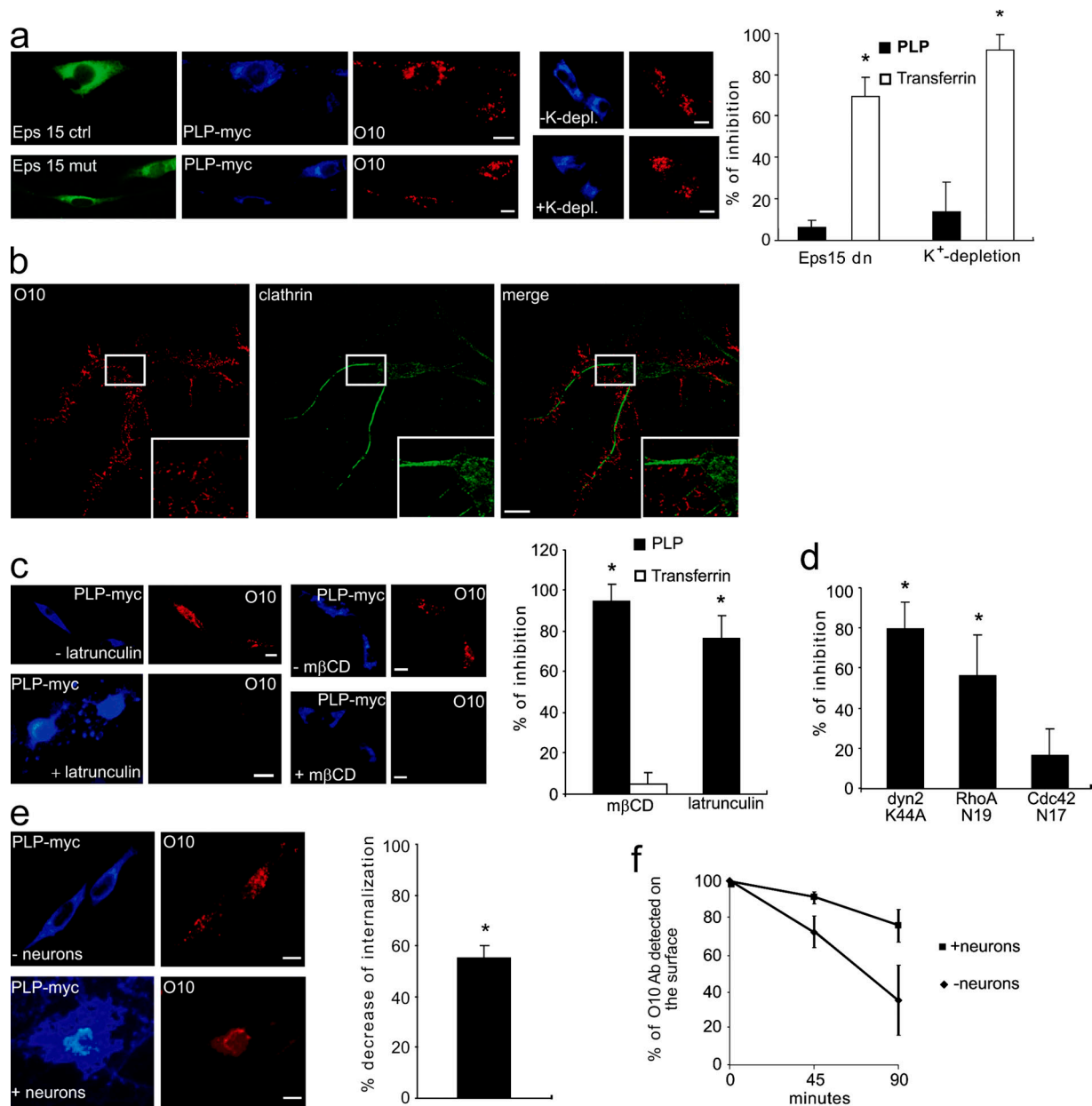


Figure 4. The cholesterol-dependent and clathrin-independent internalization of PLP is reduced after coculturing with neurons. Antibody uptake experiments were performed with the PLP antibody O10 followed by an acidic wash to remove surface-bound antibody. The internalized antibody is shown in red. (a) OLN-93 cells were cotransfected with PLP (blue) and with Eps15IIIΔ2 (Eps15 ctrl) or Eps15 EΔ95/295 (Eps15 mut; green). Potassium depletion was used as an alternative approach to interfere with clathrin function. Clathrin-mediated transferrin–rhodamine uptake served as a control. The amount of inhibition was evaluated by determining the fluorescence intensities in comparison with the control conditions. Values are given as the mean ± SD (error bars) of a mean of three independent experiments with >50 cells. (b) PLP stained with O10 (red) on the surface of OLN-93 cells does not show a significant colocalization with clathrin heavy chain (green). Insets are shown at higher magnification in the right corner of the images. (c) OLN-93 cells were transfected with PLP (blue) followed by a 30-min treatment with 1 μM latrunculin to inhibit the polymerization of the actin cytoskeleton or by a 15-min incubation with 5 mM mβCD to deplete cholesterol before performing the O10 internalization assay. Transferrin–rhodamine was used as a control for the cholesterol depletion experiments. Inhibition of the O10 uptake is shown as the mean ± SD of three independent experiments with >50 cells. (d) Cells were cotransfected with PLP and with wild type or the respective dominant-negative variants of dynamin-II, RhoA, and cdc42. The inhibition of O10 antibody uptake by the dominant-negative protein is shown in comparison with the respective wild-type construct as the mean ± SD of three independent experiments with >40 cells. The inhibition of fluid phase endocytosis (measured by dextran uptake) served as a positive control for dominant-negative cdc42 (not depicted). (e) OLN-93 cells were transfected with PLP-myc and added on top of a neuronal culture or left alone. O10 antibody uptake experiments were performed followed by an acidic wash to remove surface-bound antibody. The amount of inhibition is shown for OLN-93 cells cultured with neurons compared with cells cultured without neurons as the mean ± SD of three experiments with >40 cells. (f) The reduction of cell surface PLP was determined after various times in culture with or without neurons. Cell surface PLP was labeled with O10 mAb at 4°C, and incubation was continued at 37°C for 0, 45, and 90 min. The amount of cell surface remaining O10 mAb was analyzed by incubating cells with [¹²⁵I]-labeled secondary antibody at 4°C and subsequent determination of the radioactivity by γ counting. Quantification is shown as the mean ± SD of three experiments. *, P < 0.01; t test. Bars, 5 μm.

(for 2 d in culture) grown with or without neurons were metabolically labeled with [³⁵S]methionine/cysteine for 18 h and chased for 2 d. Hence, the metabolic labeling was performed at the stage of development (day 2–3) when PLP accumulates in LEs/Ls. The cells were chased up to the developmental stage (day 5) when PLP is almost completely removed from LEs/Ls in cells cultured with neurons but not in cells cultured without. Nevertheless, we did not observe any significant differences in the amount of labeled PLP and its alternatively spliced isoform DM20 (Fig. 2 e). Thus, differential proteolysis of PLP does not seem to be the underlying reason for the removal of PLP from LEs/Ls. Therefore, it is more likely that neuronal signals influence the transport of PLP into and/or out of LEs/Ls in oligodendrocytes.

The cholesterol-dependent and clathrin-independent internalization of PLP is reduced after coculturing with neurons

Next, we determined whether endocytosis accounts for the transport of PLP to LEs/Ls and, if so, how its endocytic trafficking is regulated. To block endocytosis, we transiently transfected Oli-neu cells with a mutant form of dynamin-II that is defective in GTP binding (K44A; Damke et al., 1994) and PLP-myc. We found that dynamin-II (K44A) reduced the colocalization of PLP with Lamp-1 and, at the same time, increased the fraction of PLP at the cell surface (Fig. 3), suggesting that endocytosis is required for the transport of PLP to LEs/Ls. A reduction of the intracellular accumulation of PLP was also observed when dynamin K44A was expressed in OLN-93 cells (not depicted).

To gain more insight into the endocytosis process of PLP, the endocytic uptake of PLP was determined by additional antibody uptake experiments using the O10 mAb. To determine whether clathrin function is involved, we either depleted cells of potassium to disrupt the formation of clathrin-coated pits or used the dominant-negative mutant of Eps15 (EΔ95/295; Benmerah et al., 1999). Despite that EΔ95/295 and K⁺ depletion had no significant effect on the uptake of O10, it led to the reduction of clathrin-mediated transferrin–rhodamine internalization (Fig. 4 a). In addition, intracellular accumulation of PLP was not reduced when EΔ95/295 was coexpressed in OLN-93 (not depicted). Furthermore, we did not detect a significant colocalization of PLP and clathrin on the surface of OLN-93 (colocalization was ~5%; Fig. 4 b) or primary oligodendroglial cells (Fig. S2; available at <http://www.jcb.org/cgi/content/full/jcb.200509022/DC1>). These results strongly suggest that the internalization of PLP occurs by a clathrin-independent endocytosis pathway.

Most clathrin-independent endocytosis pathways are sensitive to cholesterol depletion or actin depolymerization (Parton and Richards, 2003). Therefore, we used methyl-β-cyclodextrin (mβCD) to selectively extract cholesterol from the cell surface and latrunculin A to prevent actin polymerization. Treatments with either mβCD or latrunculin A led to an almost complete inhibition of O10 uptake (Fig. 4 c). The conditions of the cholesterol depletion experiments were established so that clathrin-dependent endocytosis was not affected as evaluated by the uptake of transferrin–rhodamine. Some clathrin-independent endocytosis pathways require dynamin, whereas others are

independent of dynamin function (Lamaze et al., 2001; Pelkmans et al., 2001; Sabharanjak et al., 2002; Damm et al., 2005; Kirkham et al., 2005). The uptake of O10 was clearly reduced by interfering with dynamin function (Fig. 4 d), which is consistent with the redistribution of PLP to the cell surface by dynamin-II (K44A; Fig. 3). Because both cholesterol and dynamin are essential for caveolar-dependent uptake, we compared the localization of PLP to caveolin-1 and GFP-caveolin. Caveolin-1 and GFP-caveolin were detected in punctate arrays on the plasma membrane and on intracellular compartments, but no colocalization with PLP was seen (Fig. S2 and not depicted), suggesting that caveolae are not involved in the endocytosis of PLP. The Rho family of small GTPases differentially regulate nonclathrin and noncaveolar endocytosis pathways. Although cdc42 is involved in the endocytosis of glycosyl-phosphatidylinositol-anchored proteins by a pinocytotic pathway to recycling endosomes (Sabharanjak et al., 2002), rhoA has been implicated in the dynamin-dependent uptake of interleukin 2 receptor to LEs/Ls (Lamaze et al., 2001). When O10 uptake experiments were performed with dominant-negative mutants of either cdc42 or rhoA, we observed a significant reduction of internalization when the function of rhoA but not cdc42 was inhibited (Fig. 4 d). In summary, our results show that OLN-93 cells use a clathrin-independent but cholesterol-dependent endocytosis pathway that requires a functional actin cytoskeleton and the rhoA GTPase.

To test whether the capacity for endocytosis of PLP changes after contact with neurons, we added OLN-93 cells to neuronal cultures and compared the uptake of O10 into cells that were cultured without neurons. We observed a significant reduction in the internalization of PLP in cells in coculture as compared with cells cultured without neurons (Fig. 4 e). We also analyzed the reduction of cell surface PLP upon various times in culture with or without neurons using the O10 mAb internalization assay. The amount of O10 mAb remaining at the cell surface was analyzed by incubating cells with [¹²⁵I]-labeled secondary antibody at 4°C. We found that PLP was cleared more efficiently over time from the surface of OLN-93 cells that were cultured without neurons as compared with cells in coculture. Together, these results indicate that neurons reduce the endocytosis of PLP (Fig. 4 f).

Neurons trigger the retrograde transport of PLP from LEs/Ls to the surface of oligodendrocytes

Reduction of endocytosis appears to be one reason why PLP disappears from LEs/Ls after contact with neurons. Another event that could simultaneously contribute is the increased resorting of PLP to the plasma membrane by retrograde transport from LEs/Ls. There are many examples (e.g., wound healing, cytotoxic lymphocyte killing, major histocompatibility complex [MHC]–II processing, and melanin secretion) that show that lysosomes are not merely degradative dead ends but are able to store and release proteins in a regulated fashion (Blott and Griffiths, 2002).

To analyze the putative exocytic trafficking of PLP from LEs/Ls, we performed live cell imaging experiments with

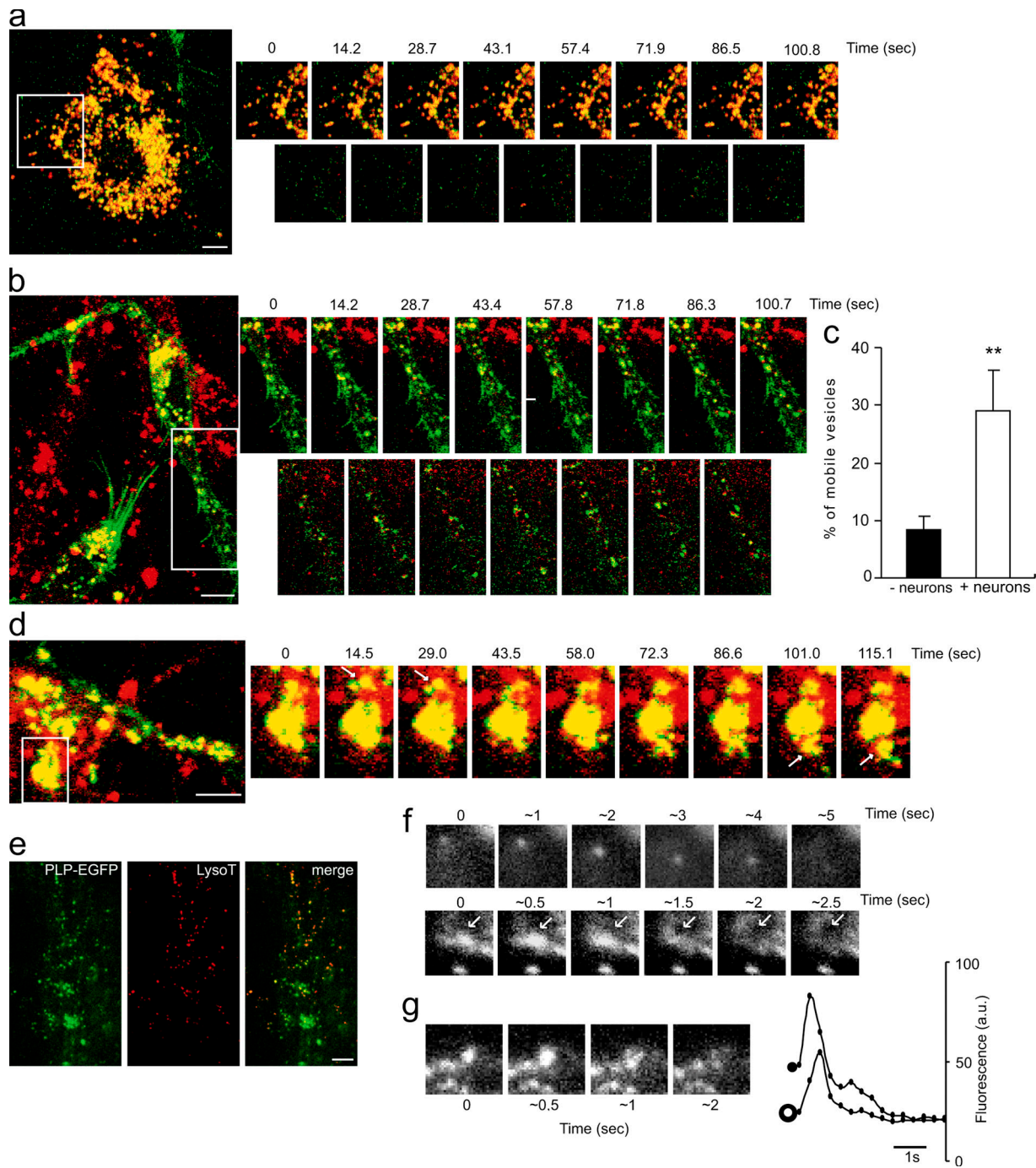


Figure 5. Neurons trigger the retrograde transport of PLP from LEs/Ls to the surface of oligodendrocytes. (a) Living PLP-EGFP-expressing Oli-neu cells were labeled with LysoTracker red and observed by confocal microscopy. Images were collected every ~ 15 s. The image sequences of the boxed areas (a, b, and d) are shown. Representative examples of a time stack are shown in the top panels. The images in the bottom panels were obtained by subtracting from each image in the top panels. The absence of signal in the subtractions demonstrates the immobility of vesicles. (b) Cells were added onto a neuronal culture and imaged ~ 8 h later. The subtractions (bottom) of consecutive frames (top) demonstrate the mobility of PLP and LysoTracker-containing vesicles. (c) The mean fraction of mobile vesicles calculated by the subtraction of consecutive frames (mean \pm SD [error bars] of 15 cells; 26 consecutive time frames were analyzed for each cell). **, $P < 0.001$; t test. (d) Individual frames from a video of a cell prepared as in b. Images were taken every ~ 15 s. The frame sequence illustrates the exit (indicated by arrows) of PLP and LysoTracker-containing vesicles from perinuclear LEs/Ls. (e) The TIRFM image demonstrates the colocalization of PLP-EGFP and LysoTracker within 100 nm of the plasma membrane in Oli-neu cells in coculture with neurons. (f and g) Exocytic fusion of vesicles was visualized by time-lapse TIRFM of Oli-neu cells in coculture with neurons. (f) The vesicles that lost their fluorescence during the time of observation fell into two groups. An example of vesicles moving in and out of the evanescent field without fusing is shown in the top panels. Vesicles fusing with the plasma membrane are shown in the bottom panels (indicated by arrows) and in g. Increase in brightness, lateral spread, and disappearance of vesicular fluorescence indicates fusions. (g) The fluorescence intensity changes (in arbitrary units) were determined in a small circle enclosing the vesicle (closed symbol) and in a concentric ring around the circle (open symbol). Other examples of fusions are shown as a flash of fluorescence (LysoTracker channel; Video 3, available at <http://www.jcb.org/cgi/content/full/jcb.200509022/DC1>). Bars, 5 μ m.

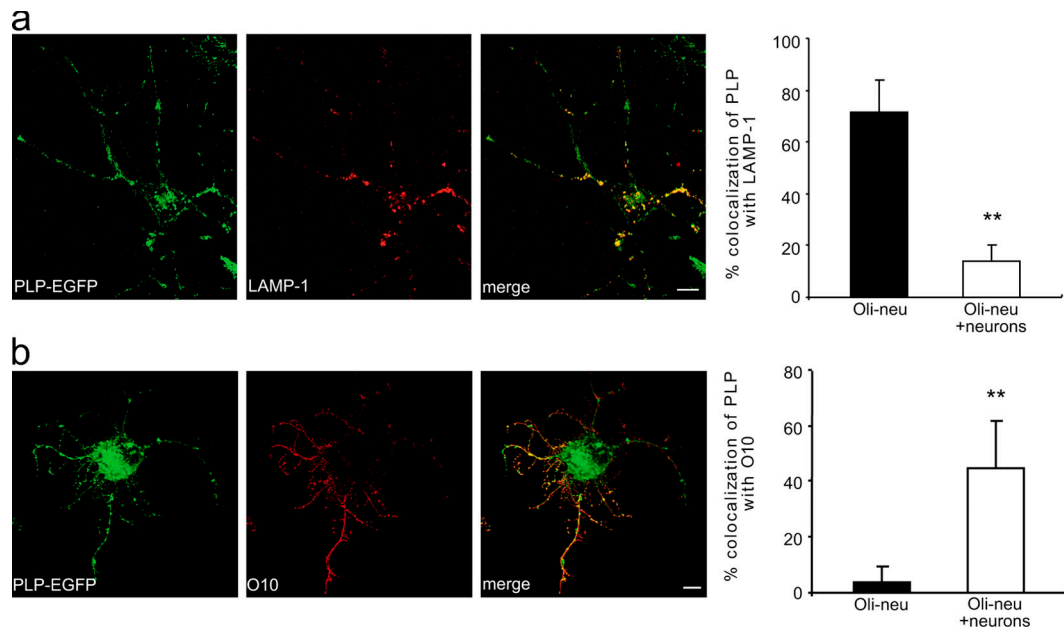


Figure 6. **A soluble factor is sufficient for redistributing PLP from LEs/Ls to the cell surface.** Oli-neu cells expressing PLP-EGFP were added to a neuronal culture on a separate coverslip to prevent cell contact allowing diffusible factors to reach the cells. After 1 d, cells were stained for Lamp-1 (a) or for surface PLP with O10 mAb (b) on living cells at 4°C. Quantitative analysis of the colocalization of PLP-EGFP with Lamp-1 and O10 are shown. Error bars represent SD ($n > 60$ cells). **, $P < 0.001$; t test. Bars, 5 μm .

LysoTracker in PLP-EGFP-expressing Oli-neu cells. There was an almost complete colocalization of PLP-EGFP and LysoTracker (Fig. 5 a) similar to the observation in OLN-93 cells. Analysis of the dynamics of PLP-EGFP/LysoTracker vesicles in Oli-neu cells revealed that most vesicles were clustered perinuclearly and did not show any significant movement (Fig. 5 a and Video 1, available at <http://www.jcb.org/cgi/content/full/jcb.200509022/DC1>). Next, we investigated whether the movement of the vesicles changes as a result of the presence of neurons. When live cell imaging experiments were performed shortly (6–12 h) after the addition of Oli-neu cells to neuronal cultures, an extensive colocalization of PLP-EGFP and LysoTracker (Fig. 5 b) was still observed. However, the movement of these vesicles was markedly increased. Two pools of vesicles could be distinguished: a perinuclear, immobile pool and a peripheral pool of highly mobile vesicles (Fig. 5 b and Video 2). Both pools of vesicles colocalized with Lamp-1. Quantitative analysis revealed that $\sim 29\%$ of the vesicles were mobile and exhibited a mean speed of $\sim 0.56 \mu\text{m/s}$ (Fig. 5 c). The pool of perinuclear vesicles not only decreased in size (Fig. 2), but the individual vesicles also became smaller with increasing time in coculture ($\sim 33\%$ decrease after 16 h of coculture; reduction from $0.96 \pm 0.2 \mu\text{m}$ to $0.63 \pm 0.19 \mu\text{m}$; $n = 96$). In several cases, PLP-EGFP and LysoTracker-filled vesicles emanated from larger perinuclear vesicles and moved radially toward the plasma membrane at the cell periphery (Fig. 5 d).

To analyze the behavior of the peripheral vesicle pool, we used total internal reflection fluorescence microscopy (TIRFM). TIRFM allows the selective illumination of a region within a 70–120-nm distance of the plasma membrane as the excitatory evanescent field decays exponentially from the interface of the cell membrane with the coverslip. We observed PLP-EGFP and

LysoTracker-containing vesicles within the 100-nm vicinity of the plasma membrane in living Oli-neu cells that were cocultured with neurons (Fig. 5 e). In contrast, no PLP-EGFP and LysoTracker-containing vesicles were observed in the proximity of the plasma membrane when cells were cultured without neurons.

To determine whether the acidic vesicles fuse with the plasma membrane, we used time-lapse TIRFM imaging. The cells we studied contained 6 ± 2.4 vesicles per $100\text{-}\mu\text{m}^2$ area of the plasma membrane. The vesicles that lost their fluorescence during the time of observation fell into two groups. We found vesicles moving in and out of the evanescent field without fusing and vesicles fusing with the plasma membrane (Fig. 5 f, top). Fusion was defined by the loss of vesicular fluorescence and the concurrent lateral spread of the released dye into the medium (Fig. 5 g). We detected one to two fusion events/minute per cell at the plasma membrane. When Oli-neu cells were cultured without neurons, we did not observe any fusions in agreement with the absence of PLP-EGFP and LysoTracker-containing vesicles at the plasma membrane.

A cAMP-dependent neuronal signal regulates the trafficking of PLP

Because the redistribution of PLP from LEs/Ls to the surface of the plasma membrane was only observed in Oli-neu cells grown in the presence of neurons, neuronal signals are likely to activate this pathway. We wanted to determine whether this neuronal signaling is transferred as a soluble factor or is a consequence of direct cell-to-cell contact. Oli-neu cells were either directly added on top of a neuronal culture or placed on a separate coverslip to prevent cell contact, allowing diffusible factors to reach the cells. We found that diffusible factors were sufficient to redistribute PLP from LEs/Ls to the surface of the cell (Fig. 6).

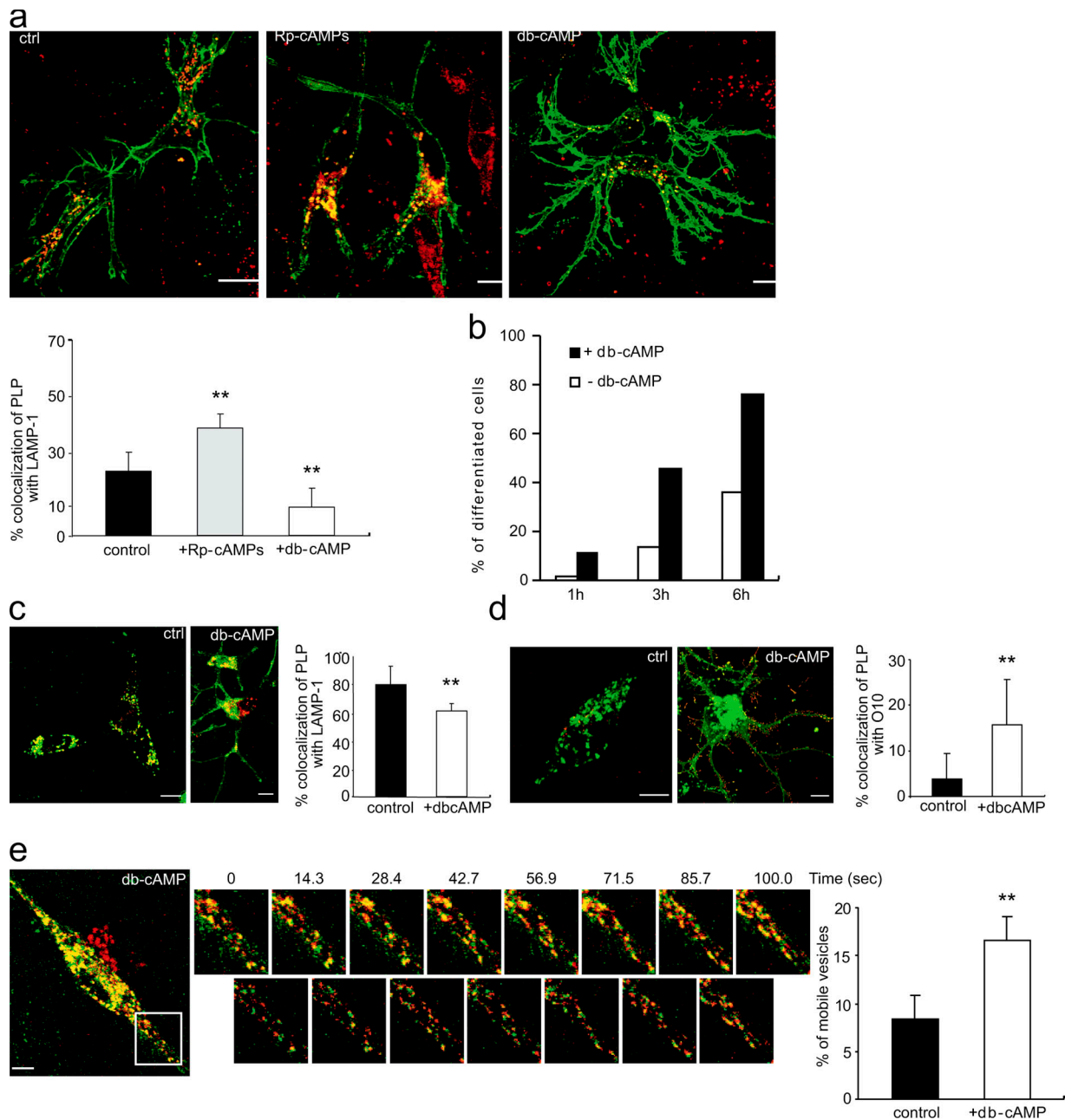


Figure 7. A cAMP-dependent neuronal signal regulates the release of PLP from LEs/Ls in Oli-neu cells. (a) Oli-neu cells were cocultured with neurons for 1 d in the presence or absence of 100 μ M Rp-cAMPs or 1 mM db-cAMP. Quantitative analysis of the colocalization of PLP-EGFP with Lamp-1 is shown as the mean \pm SD of >30 cells. (b) Time-course experiments demonstrate that treatment of Oli-neu cells in the presence of neurons with 1 mM db-cAMP accelerates the removal of PLP-EGFP from Lamp-1–positive compartments. The quantitative analysis of one representative experiment (out of three independent experiments) is shown. Analysis was performed by classifying cells into two categories according to the extent of the colocalization of PLP-EGFP with Lamp-1. (c and d) Oli-neu cells were grown without neurons and treated with 1 mM db-cAMP for 1 d and stained for Lamp-1 (c) or for surface-PLP with O10 mAb (d) on living cells at 4°C. Quantitative analysis of the colocalization of PLP-EGFP with Lamp-1 and O10 are shown. Error bars represent SD ($n = 30$ cells). (e) Oli-neu cells grown without neurons were treated for 1 d with 1 mM db-cAMP and imaged as in Fig. 5 a. An image sequence of the boxed area is shown. The images in the bottom panels represent subtractions of the consecutive frames in the top panels. The analysis demonstrates a significant increase in the mobility of PLP and LysoTracker-containing vesicles by treatment with db-cAMP as compared with the control condition. **, $P < 0.001$; t test. Bars, 5 μ m.

To analyze the signals involved, we treated Oli-neu cells cultured in the presence of neurons with various pharmacological kinase inhibitors. Colocalization of PLP-EGFP and Lamp-1 increased markedly when cocultures were treated for 1 d with Rp-cAMPs to inhibit protein kinase A (Fig. 7 A). In contrast, treatment of cocultures with db-cAMP, a protein

kinase A agonist, promoted the localization of PLP to the plasma membrane (Fig. 7 A). Quantitative analysis of time-course experiments showed that db-cAMP accelerated the redistribution of PLP to the surface of the cell (Fig. 7 B). To test whether similar effects were observed in Oli-neu cells cultured without neurons, we treated Oli-neu cells for 1 d with db-cAMP

and quantified the amount of PLP-EGFP in LEs/Ls and on the surface of the cell. In cells treated with db-cAMP, more PLP was found on the surface of the cell, whereas, at the same time, the fraction within LEs/Ls decreased (Fig. 7, C and D). Furthermore, a peripheral pool of highly mobile PLP-EGFP/LysoTracker-containing vesicles was observed by live cell imaging (Fig. 7 E). These data suggest that cAMP-dependent signaling is part of the developmental switch that is triggered by neurons, leading to the redistribution of PLP from LEs/Ls to the surface of the plasma membrane.

Discussion

Our data demonstrate that the trafficking of PLP in oligodendrocytes is under neuronal control. PLP is initially targeted to LEs/Ls by using a cholesterol-dependent and clathrin-independent endocytosis pathway. The situation changes dramatically upon receiving maturation signals from neurons. PLP is then redistributed from LEs/Ls to the plasma membrane. We provide evidence that the developmental regulation of PLP localization occurs by the down-regulation of endocytosis and by the transport from LEs/Ls to the cell surface.

The regulation of the transport of PLP is strikingly similar to the trafficking of MHC-II in dendritic cells (Mellman and Steinman, 2001). Immature dendritic cells have a high rate of endocytosis and target MHC-II to lysosomes (Pierre et al., 1997). After exposure to inflammatory mediators, the endocytosis of MHC-II is reduced, and the transport of MHC-II from lysosomes to the cell surface is triggered (Kleijmeer et al., 2001; Boes et al., 2002; Chow et al., 2002). The transport pathway of PLP from LEs/Ls can also be related to the release of secretory lysosomes from hematopoietic cells. However, unlike the classic secretory lysosomes that are specialized to release luminal content, oligodendrocytes mainly transport membrane, and this may occur without significant extracellular release of lysosomal content, as is the case for dendritic cells (Kleijmeer et al., 2001; Trombetta et al., 2003). For oligodendrocytes, LE/L compartments may be particularly useful as storage compartments, as they are able to harbor large amounts of membrane in a multilamellar and multivesicular fashion for myelin biogenesis. In most cells, however, the majority of molecules that localizes to internal vesicles of the endosomal system are destined for lysosomal degradation. This raises the question of how PLP survives in an environment where protein degradation usually occurs. One possibility is that immature oligodendrocytes have specialized LEs/Ls with low proteolytic capacity. Our unpublished observation that the vesicular stomatitis virus glycoprotein accumulates undegraded in LEs/Ls of Oli-neu cells supports this notion. In dendritic cells, for example, lysosomal proteolysis is regulated in a developmentally linked fashion (Trombetta et al., 2003; Delamarre et al., 2005). Another possibility is that PLP is poorly degradable and, therefore, accumulates within LEs/Ls. A second issue is how PLP escapes from a compartment associated with the limited capacity for membrane recycling. Previous work has provided evidence that not all intraluminal membranes of LEs/Ls are destined for lysosomal degradation. It has been suggested that some vesicles may undergo back

fusion with the limiting membrane, and, in some instances, this membrane is sorted via tubulovesicles to the plasma membrane (Kleijmeer et al., 2001; Boes et al., 2002; Chow et al., 2002; Abrami et al., 2004; Le Blanc et al., 2005). Whether PLP is sorted by back fusion and tubules to the surface of oligodendrocytes are issues that have to be addressed in future studies. It is important to note that the accumulation of PLP at the surface of the plasma membrane after the receipt of maturation signals most likely reflects the contribution of multiple factors. Our finding that the endocytosis of PLP is reduced after receiving signals from neuronal cells suggests that the regulation of endocytosis may play an essential role in this process. It will be interesting to elucidate the molecular mechanisms of how neurons control the rate of endocytosis in oligodendrocytes. One attractive possibility is that the endocytic activity is controlled by the RhoA GTPase.

Importantly, not all myelin components were found to be internalized into LEs/Ls. Although PLP and cholesterol resided in LEs/Ls, myelin basic protein and galactosylceramide were mainly found in or at the plasma membrane (unpublished data). The differential compartmentalization of myelin components before the onset of myelination might be a mechanism to prevent premature and inappropriate assembly. Our results suggest that an external soluble factor regulates myelin membrane assembly by controlling the trafficking of PLP to and from the surface of the cell. Among the many potential candidates are soluble mediators such as neurotrophins, neuregulin, or adenosine that can now be tested with the described experimental system (Barres and Raff, 1999; Fields and Stevens-Graham, 2002).

Together, our findings reveal an unexpected and novel role of LEs/Ls in oligodendrocytes. It provides a striking example of how cell-to-cell communication regulates trafficking to and from a cellular compartment to guide the development of a multicellular tissue. The proposed role of LEs/Ls in myelin biogenesis may help to explain the cellular mechanisms of dysmyelination that is observed in many lysosomal storage diseases.

Materials and methods

Antibodies, plasmids, and other reagents

The mutant and wild-type cDNAs of GFP-Eps15 and GFP-dynamin-II were provided by A. Benmerah (Institut Pasteur, Paris, France) and S. Schmid (Scripps Research Institute, La Jolla, CA), respectively. The following primary antibodies were used: myelin basic protein (monoclonal IgG; Sternberger, Inc.), PLP (polyclonal, P6; Lington and Waehnel, 1990), O10 (monoclonal mouse IgM), β III-tubulin (Promega), neurofilament (monoclonal IgM; Qbiogene), τ (polyclonal; DakoCytomation), myc tag (monoclonal IgG; Cell Signaling), clathrin heavy chain (monoclonal IgG; BD Transduction Laboratories), GFP (Synaptic Systems GmbH), caveolin-1 (monoclonal IgM; BD Biosciences), and Lamp-1 (CD107a, rat monoclonal; BD Biosciences). Secondary antibodies were obtained from Dianova and GE Healthcare.

Cell culture, cloning, and transfections

Primary cultures of mouse oligodendrocytes were prepared as described previously (Simons et al., 2000). After shaking, cells were plated in MEM containing B27 supplement, 1% horse serum, L-thyroxine, tri-iodo-L-thyronine, glucose, glutamine, gentamycin, pyruvate, and bicarbonate on poly-L-lysine-coated dishes or glass coverslips. Cocultures of neurons and oligodendrocytes were produced by preparing mixed brain cultures from 16-d-old fetal mice that were cultivated for 2 wk, to which the primary oligodendrocytes or Oli-neu cells were added. The mixed brain cultures were

prepared at a density of $\sim 50,000$ cells/cm². Cocultures without direct neuron–glia contact were prepared by growing neuronal cultures on glass coverslips, which were placed upside down on a metal ring positioned in a culture dish. Oligodendrocytes were added on an additional coverslip facing upwards. The oligodendroglial precursor cell line, Oli-neu (provided by J. Trotter, University of Mainz, Mainz, Germany), and OLN-93 cells (provided by C. Richter-Landsberg, University of Oldenburg, Oldenburg, Germany) were cultured as described previously (Jung et al., 1995; Richter-Landsberg and Heinrich, 1996). Transient transfections were performed using FuGENE transfection reagent (Roche) according to the manufacturer's protocol. PLP-EGFP was generated by fusing EGFP to the COOH terminus of PLP by gene fusion PCR. The fusion product was cloned into pEGFPN1 vector using the EcoRI–NotI site. Stable cell lines were obtained by the cotransfection of PLP-EGFPN1 and pMSCV-hygro (CLONTECH Laboratories, Inc.) followed by the selection of clones by incubation with hygromycin.

Immunofluorescence and endocytosis assays

Immunofluorescence and immunohistochemistry were performed as described previously (Simons et al., 2002). For assaying endocytosis, living cells were incubated with O10 antibody in medium for 30 min at 4°C, washed, and incubated in medium at 37°C for 60 min. The antibody remaining on the surface was removed under low pH conditions in 0.2 M glycine and 0.5 M NaCl, pH 4.5, for 30 min at 4°C. Cells were washed three times in PBS, fixed, and stained by immunofluorescence. Additionally, OLN-93 cells were transiently transfected with PLP and added on a neuronal culture or left alone. Cells were incubated at 4°C for 30 min with O10 antibody in binding medium consisting of HBSS and 10 mM Hepes supplemented with 0.2% BSA 16 h after transfection. After washing, O10 internalization was allowed to continue for 0, 45, and 90 min. O10 antibody remaining at the cell surface was detected with 5–20 $\mu\text{Ci}/\mu\text{g}$ [¹²⁵I]-labeled mouse secondary antibody in binding medium for 30 min at 4°C. Next, the cells were washed five times, lysed in 0.2 M NaOH, and the amount of radioactivity was determined by γ counting.

Microscopy and analysis

Fluorescence images were acquired on a microscope (DMRXA; Leica) or a confocal microscope (LSM 510; Carl Zeiss MicroImaging, Inc.) with a 63 \times oil plan-Apochromat objective (NA 1.4; Carl Zeiss MicroImaging, Inc.). For live cell imaging, coverslips containing the cells were mounted in a live cell imaging chamber and observed in low fluorescence imaging medium (HBSS, 10 mM Hepes, and 1% horse serum, pH 7.4) at 37°C. Temperature was controlled by means of a digital system (Tempcontrol 37-2; PeCon) or a custom-built perfusion system. Time-lapse imaging was performed on a confocal laser scanning microscope (LSM 510; Carl Zeiss MicroImaging, Inc.). Images were acquired at ~ 15 -s intervals for the indicated time periods using sequential line excitation at 488 and 543 nm and appropriate band pass emission filters.

Image processing and analysis were performed using Meta Imaging Series 6.1 software (Universal Imaging Corp.). Quantification of colocalization was performed with the colocalization module of the software. Vesicle movement was analyzed by subtracting from each image in a time stack preceding its image. The different image stack thus generated was used to identify vesicle motility events. The velocity of individual vesicles was determined using the Manual Tracking plug-in for ImageJ software (National Institutes of Health). Statistical differences were determined with a *t* test. TIRFM was performed on a custom-built prism-based evanescent field microscope using an HCX Apo L 63 \times water immersion objective (NA 0.90; Leica; Oheim et al., 1998). Evanescent field excitation was obtained by focusing 488- and 568-nm laser light onto a hemicylindrical prism at 68 and 71° incidence angles, respectively, leading to a field depth of ~ 80 –100 nm. Images were acquired with a back-illuminated 16-bit CCD camera (Cascade 512B; Roper Scientific) with on-chip charge multiplication. Each pixel corresponded to 0.25 μm in the specimen plane. For analysis of individual fusion events, a small circle was positioned on the vesicular fluorescence, a concentric ring was placed around the circle, and fluorescence intensity was plotted against time. Fusion events were identified by the increase of fluorescence in the central region that spread into the surrounding annulus followed by a sudden decline (Schmoranz et al., 2000; Zenisek et al., 2000; Becherer et al., 2003; Bezzi et al., 2004). Immuno-EM was performed as described previously (Wenzel et al., 2005).

Metabolic labeling and immunoprecipitations

For metabolic labeling, cells were pulsed with 265 μCi [³⁵S]methionine (1 Ci = 37 GBq; GE Healthcare) in methionine and cysteine-free DME for 18 h, and chase was performed for 0 or 48 h. Immunoprecipitation was

performed as described previously (Simons et al., 2000). Autoradiographs were scanned and quantified with ScionImage software (Scion Corp.). Values are shown as means \pm SD. Statistical differences were determined with a *t* test.

Online supplemental material

Fig. S1 shows that EGFP-tagged PLP is sorted to myelin. Fig. S2 shows the absence of PLP colocalization with clathrin heavy chain or caveolin-1. Video 1 shows the movement of LEs/Ls in Oli-neu cells, whereas Video 2 shows this in Oli-neu cells cultured with neurons. Video 3 shows the fusion of vesicles with the plasma membrane. Online supplemental material is available at <http://www.jcb.org/cgi/content/full/jcb.200509022/DC1>.

We are grateful to G. Schulz for excellent technical assistance. We thank C. Richter-Landsberg and J. Trotter for providing reagents, J. Landgrebe for help with iodine-125 experiments, and W. Stühmer for support.

This work was supported by the Deutsche Forschungsgemeinschaft (SFB 523 to M. Simons and K.-A. Nave and SFB 406 to G. Bunt).

Submitted: 6 September 2005

Accepted: 26 January 2006

References

- Abrami, L., M. Lindsay, R.G. Parton, S.H. Leppla, and F.G. van der Goot. 2004. Membrane insertion of anthrax protective antigen and cytoplasmic delivery of lethal factor occur at different stages of the endocytic pathway. *J. Cell Biol.* 166:645–651.
- Barres, B.A., and M.C. Raff. 1999. Axonal control of oligodendrocyte development. *J. Cell Biol.* 147:1123–1128.
- Baumann, N., and D. Pham-Dinh. 2001. Biology of oligodendrocyte and myelin in the mammalian central nervous system. *Physiol. Rev.* 81:871–927.
- Becherer, U., T. Moser, W. Stühmer, and M. Oheim. 2003. Calcium regulates exocytosis at the level of single vesicles. *Nat. Neurosci.* 6:846–853.
- Benmerah, A., M. Bayrou, N. Cerf-Bensussan, and A. Dautry-Varsat. 1999. Inhibition of clathrin-coated pit assembly by an Eps15 mutant. *J. Cell Sci.* 112:1303–1311.
- Bezzi, P., V. Gunderson, J.L. Galbete, G. Seifert, C. Steinhäuser, E. Pilati, and A. Volterra. 2004. Astrocytes contain a vesicular compartment that is competent for regulated exocytosis of glutamate. *Nat. Neurosci.* 7:613–620.
- Blott, E.J., and G.M. Griffiths. 2002. Secretory lysosomes. *Nat. Rev. Mol. Cell Biol.* 3:122–131.
- Boes, M., J. Cerny, R. Massol, M. Op den Brouw, T. Kirchhausen, J. Chen, and H.L. Ploegh. 2002. T-cell engagement of dendritic cells rapidly rearranges MHC class II transport. *Nature.* 418:983–988.
- Chow, A., D. Toomre, W. Garrett, and I. Mellman. 2002. Dendritic cell maturation triggers retrograde MHC class II transport from lysosomes to the plasma membrane. *Nature.* 418:988–994.
- Damke, H., T. Baba, D.E. Warnock, and S.L. Schmid. 1994. Induction of mutant dynamin specifically blocks endocytic coated vesicle formation. *J. Cell Biol.* 127:915–934.
- Damm, E.M., L. Pelkmans, J. Kartenbeck, A. Mezzacasa, T. Kurzchalia, and A. Helenius. 2005. Clathrin- and caveolin-1-independent endocytosis: entry of simian virus 40 into cells devoid of caveolae. *J. Cell Biol.* 168:477–488.
- Delamarre, L., M. Pack, H. Chang, I. Mellman, and E.S. Trombetta. 2005. Differential lysosomal proteolysis in antigen-presenting cells determines antigen fate. *Science.* 307:1630–1634.
- Fields, R.D., and B. Stevens-Graham. 2002. New insights into neuron–glia communication. *Science.* 298:556–562.
- Jung, M., E. Kramer, M. Grzenkowski, K. Tang, W. Blakemore, A. Aguzzi, K. Khazaie, K. Chlichlia, G. von Blankenfeld, H. Kettenmann, et al. 1995. Lines of murine oligodendroglial precursor cells immortalized by an activated neu tyrosine kinase show distinct degrees of interaction with axons in vitro and in vivo. *Eur. J. Neurosci.* 7:1245–1265.
- Jung, M., I. Sommer, M. Schachner, and K.A. Nave. 1996. Monoclonal antibody O10 defines a conformationally sensitive cell-surface epitope of proteolipid protein (PLP): evidence that PLP misfolding underlies dysmyelination in mutant mice. *J. Neurosci.* 16:7920–7929.
- Kirkham, M., A. Fujita, R. Chadda, S.J. Nixon, T.V. Kurzchalia, D.K. Sharma, R.E. Pagano, J.F. Hancock, S. Mayor, and R.G. Parton. 2005. Ultrastructural identification of uncoated caveolin-independent early endocytic vesicles. *J. Cell Biol.* 168:465–476.

- Kleijmeer, M., G. Ramm, D. Schuurhuis, J. Griffith, M. Rescigno, P. Ricciardi-Castagnoli, A.Y. Rudensky, F. Ossendorp, C.J. Melief, W. Stoorvogel, and H.J. Geuze. 2001. Reorganization of multivesicular bodies regulates MHC class II antigen presentation by dendritic cells. *J. Cell Biol.* 155:53–63.
- Kramer, E.M., A. Schardt, and K.A. Nave. 2001. Membrane traffic in myelinating oligodendrocytes. *Microsc. Res. Tech.* 52:656–671.
- Lamazze, C., A. Dujeancourt, T. Baba, C.G. Lo, A. Benmerah, and A. Dautry-Varsat. 2001. Interleukin 2 receptors and detergent-resistant membrane domains define a clathrin-independent endocytic pathway. *Mol. Cell.* 7:661–671.
- Le Blanc, I., P.P. Luyet, V. Pons, C. Ferguson, N. Emans, A. Petiot, N. Mayran, N. Demareux, J. Faure, R. Sadoul, et al. 2005. Endosome-to-cytosol transport of viral nucleocapsids. *Nat. Cell Biol.* 7:653–664.
- Linnington, C., and T.V. Waehneltd. 1990. Conservation of the carboxyl terminal epitope of myelin proteolipid protein in the tetrapods and lobe-finned fish. *J. Neurochem.* 54:1354–1359.
- Mellman, I., and R.M. Steinman. 2001. Dendritic cells: specialized and regulated antigen processing machines. *Cell.* 106:255–258.
- Oheim, M., D. Loerke, W. Stuhmer, and R.H. Chow. 1998. The last few milliseconds in the life of a secretory granule. Docking, dynamics and fusion visualized by total internal reflection fluorescence microscopy (TIRFM). *Eur. Biophys. J.* 27:83–98.
- Parton, R.G., and A.A. Richards. 2003. Lipid rafts and caveolae as portals for endocytosis: new insights and common mechanisms. *Traffic.* 4:724–738.
- Pelkmans, L., J. Kartenbeck, and A. Helenius. 2001. Caveolar endocytosis of simian virus 40 reveals a new two-step vesicular-transport pathway to the ER. *Nat. Cell Biol.* 3:473–483.
- Pierre, P., S.J. Turley, E. Gatti, M. Hull, J. Meltzer, A. Mirza, K. Inaba, R.M. Steinman, and I. Mellman. 1997. Developmental regulation of MHC class II transport in mouse dendritic cells. *Nature.* 388:787–792.
- Richter-Landsberg, C., and M. Heinrich. 1996. OLN-93: a new permanent oligodendroglia cell line derived from primary rat brain glial cultures. *J. Neurosci. Res.* 45:161–173.
- Sabharanjak, S., P. Sharma, R.G. Parton, and S. Mayor. 2002. GPI-anchored proteins are delivered to recycling endosomes via a distinct cdc42-regulated, clathrin-independent pinocytotic pathway. *Dev. Cell.* 2:411–423.
- Schmoranzler, J., M. Goulian, D. Axelrod, and S.M. Simon. 2000. Imaging constitutive exocytosis with total internal reflection fluorescence microscopy. *J. Cell Biol.* 149:23–32.
- Schneider, A., H. Lander, G. Schulz, H. Wolburg, K.A. Nave, J.B. Schulz, and M. Simons. 2005. Palmitoylation is a sorting determinant for transport to the myelin membrane. *J. Cell Sci.* 118:2415–2423.
- Simons, M., E.M. Kramer, C. Thiele, W. Stoffel, and J. Trotter. 2000. Assembly of myelin by association of proteolipid protein with cholesterol- and galactosylceramide-rich membrane domains. *J. Cell Biol.* 151:143–154.
- Simons, M., E.M. Kramer, P. Macchi, S. Rathke-Hartlieb, J. Trotter, K.A. Nave, and J.B. Schulz. 2002. Overexpression of the myelin proteolipid protein leads to accumulation of cholesterol and proteolipid protein in endosomes/lysosomes: implications for Pelizaeus-Merzbacher disease. *J. Cell Biol.* 157:327–336.
- Trombetta, E.S., M. Ebersold, W. Garrett, M. Pypaert, and I. Mellman. 2003. Activation of lysosomal function during dendritic cell maturation. *Science.* 299:1400–1403.
- Weimbs, T., and W. Stoffel. 1992. Proteolipid protein (PLP) of CNS myelin: positions of free, disulfide-bonded, and fatty acid thioester-linked cysteine residues and implications for the membrane topology of PLP. *Biochemistry.* 31:12289–12296.
- Wenzel, D., G. Schaueremann, A. von Lupke, and G. Hinz. 2005. The cargo in vacuolar storage protein transport vesicles is stratified. *Traffic.* 6:45–55.
- Zenisek, D., J.A. Steyer, and W. Almers. 2000. Transport, capture and exocytosis of single synaptic vesicles at active zones. *Nature.* 406:849–854.

Ajit Singh Dhaunchak

Date and Place of Birth	Sex
01 Aug 1979, Chandigarh, INDIA	Male

Qualifications and Degrees Achieved

April 2003-May 2006 PhD in Neurosciences	Max Planck Institute of Experimental Medicine
Sep 2001- April 2003 Master of Sciences in Neuroscience	Max Planck Institute of Experimental Medicine
Aug 1997- July 2000 Bachelor of Sciences (Honors)	Panjab University

Research Interests

Protein Trafficking, in-vivo and in-vitro Live-Imaging, protein oxidation and reduction states under native and perturbed conditions. Understand and improve the way of remyelination after de/dysmyelination. To work on a project with future clinical application.

Conference and Symposia Attended

Society for Neuroscience Meeting, Washington D.C, USA, Nov 11-16 2005.

30th International Goettingen Neuroscience Conference, Goettingen, Germany Feb 17-20, 2005.

ELSO 2003, Dresden, Germany, Sep 20-24 2003.

VI European Meeting in Glial Cell Function in Health and Disease, Berlin, Germany Sep 3 - 6, 2003

29th International Goettingen Neuroscience Meeting, June 12-15, 2003.

Talks and Posters

Talks

An essential role of disulfide bridges in PLP; implications for protein Misfolding in PMD. 30th International Goettingen neuroscience conference, Goettingen, Germany, Feb 12-16, 2005.

An essential role of disulfide bridges in PLP; implications for protein Misfolding in PMD. Neurizons- Interdisciplinary PhD Student Symposium on Current Topics in the Neurosciences. Goettingen, Germany, November 12 - 14, 2004.

Posters

Ajit Singh Dhaunchak and Klaus Armin Nave. An essential role of disulfide bridges in PLP; implications for protein Misfolding in PMD. Society for

Neuroscience Meeting, Washington D.C, USA, Nov 11-16 2005.

Ajit Singh Dhaunchak and Klaus Armin Nave. An essential role of disulfide bridges in PLP; implications for protein Misfolding in PMD. 30th International Goettingen Neuroscience conference, Goettingen, Germany.

Research and Experimental Experience

Molecular/Cell Biology and Protein Biochemistry; Including site directed mutagenesis, transgenic and Knock-in/out technology, stable cell line, pulse chase, CoIPs and other protein-protein interaction assays. Special interest; In-vitro and in-vivo imaging i.e, FRAP, FRET (Acceptor photo-bleaching). I really enjoy time lapse imaging and movies.

Education Details

Apr 2003-**Expected 06** Georg-August University, Goettingen, Germany.
PhD in Neurosciences (Expected in April 2006)
Department of Neurogenetics, Max Planck Institute of Experimental Medicine,
Hermann Rein Strasse-3, Goettingen-37075, Germany.

Sep 2001-Apr 2003 Georg-August University, Goettingen, Germany.
Masters of Sciences (M.Sc) in Neurosciences
Department of Neurogenetics, Max Planck Institute of Experimental Medicine,
Hermann Rein Strasse-3, Goettingen-37075, Germany.

Aug 2000-Sep 2001 Panjab University, Chandigarh, India.
M.Sc-Honors in Biophysics (Completed only the 1st year).
Department of Biophysics, Panjab University, Chandigarh.

Aug 1997-Jul 2001 Panjab University, Chandigarh, India.
B.Sc-Honors in Biophysics.
Department of Biophysics, Panjab University, Chandigarh

Languages

English (fluent), Hindi, Punjabi, German (advanced beginner).

Hobbies

Chess, Movies, Cricket (active) and other outdoor sports.

(Ajit Singh Dhaunchak)